UNIVERSITY OF SOUTHERN CALIFORNIA

DEPARTMENT OF CIVIL ENGINEERING

SCATTERING OF ELASTIC WAVES BY AN ALLUVIAL VALLEY OF ARBITRARY SHAPE

by

M. Dravinski

Report No. CE 80-06

A Report on Research Conducted Under a Contract
from the U.S. Nuclear Regulatory Commission

Los Angeles, California

September, 1980

ABSTRACT

Reduction of earthquake hazards calls for the development of design criteria which ensure the safety of structures subjected to strong earthquake ground motion. Recent developments in seismic risk analysis suggest a refinement of such criteria by taking into account the available knowledge on soil and geologic properties in the area of investigation. Much work has been undertaken, for instance, in the analysis and mapping of the amplification effects of the wave motion which results from local soil and geological configuration. Summaries of such studies are sometimes presented in the form of microzonation maps with some amplification factors being evaluated for an entire region, or a site.

Some procedures for evaluation of these amplification factors are inadequate for a number of reasons. For example:

(1) there is no uniform theoretical basis for many procedures used in the evaluation of the strong ground motion amplification factors;

(2) there is lack of thorough analysis or use of recently developed techniques which provide the results needed for engineering purposes; and

(3) the validity of the desired risk maps or amplification maps has not been tested systematically by repeated earthquake recordings.

The purpose of this paper is to develop a method for studying strong ground motion amplification by near surface inhomogeneities. In particular, diffraction of elastic waves by an alluvial valley of an arbitrary shape will be considered.

Much has been developed in various scientific and engineering disciplines, in the way of solution techniques to analyze complex wave propagation phenomena. However, little has been done to introduce these techniques into engineering applications and to further develop solution methods to a point where a typical applied engineering problem can be routinely analyzed. The aim of this paper is to attempt to bridge this gap. This can be done first by detailed consideration of the complete physical nature of the wave propagation through a homogeneous medium and second by development of physical models which consider the most important governing phenomena and do not violate or eliminate some of them by a brute-force oversimplification.

I. INTRODUCTION

The study of diffraction of elastic waves arose as a result of research into the nature of light. The expression diffraction is attributed to Francisco Maria Grimaldi (1665). He used the word diffraction to describe the phenomenon of the bending of the light beam when it passes the edge of an aperture. Presently, the same term is used to denote the phenomenon of wave propagation when the rays of the waves do not follow rectilinear paths.

The British scientists, James Clark Maxwell, in his memoir, "A Dynamic Theory of Electromagnetic Field" (1865), showed that "...light itself is an electromagnetic disturbance in the form of waves propagated through the electromagetic field according to electromagnetic laws." Subsequently, the elastic theory of light was replaced by the electromagnetic theory. As a consequence, interest in diffraction of elastic waves (excluding sound waves) diminished for some time.

It is believed that the earliest mathematical treatment of the diffraction of elastic waves by a bounded obstacle is due to Alfred Clebsch (1863). Using the equations of elasticity, Clebsch studied the reflection and transmission of light by lenses. He also studied the diffraction of elastic waves by a rigid sphere. Although he could not obtain any conclusions from his complex solution, Clebsch's contribution is important because he was the first to publish a complete formulation of a boundary value problem for the diffraction of elastic waves by an obstacle.

As an extension of Clebsch's work, Sezawa (1927) considered

diffraction of elastic waves by a rigid, circular (and elliptic) cylinder embedded in an elastic full-space. The contribution of Sezawa is considered to be the first formulation of the scattering of elastic waves by an inclusion applicable to seismology.

Following Sezawa's paper, numerous attempts have been made to study the diffraction of elastic waves by an obstacle and the corresponding stress concentrations (see the review by Miklowitz, 1966).

For the design of earthquake resistant structures, it is essential to understand in detail the nature of amplification of the strong ground motion during large earthquakes. Observations from some recent earthquakes (e.g., Sozen, et. al., 1968; Jennings, 1971) indicate that the areas of intense damage can be highly localized. The intensity of ground shaking can change significantly within a short distance (Gutenberg, 1957; Hudson, 1972; Esteva, 1977). It is believed that the inhomogeneity of the soil and the surface topographies are the cause of localized amplification effects (e.g., Kanai, et. al., 1953; Duke, 1958; Kanai, 1957; Kanai and Tanaka, 1961; Boore, 1973; Griffiths, et. al., 1979). As pointed out by Trifunac (1971) and Wong and Trifunac (1974b), the irregular distribution of strong ground motion may result from constructive and destructive interferences between the incident and diffracted waves at the site.

The amplification of strong ground motion due to the diffraction of waves by subsurface irregularities has not yet been fully resolved because the problem is characterized by some complexity. Therefore, it is not only necessary to understand the basic phenomena that occur in soil amplification, but it is also necessary to develop

methods capable of predicting surface amplitudes at certain sites for a given wave input.

The purpose of this paper is to study the amplification effects caused by scattering, refraction and diffraction of elastic waves by inhomogeneities of arbitrary shape in an elastic soil medium. Basic aspects of ground motion amplification and the literature review are given in Section II. The proposed method and its application are described in Section III.

II. LITERATURE REVIEW

In this section, the literature pertaining to diffraction of elastic waves by obstacles and strong ground motion seismology is presented for two and three dimensional models. Two methods emerge for analyzing soil amplification problems: (1) numerical methods (such as finite element and finite difference methods), and (2) analytical methods (which rely upon the solution of the equations of elastodynamics by analytical means). Each of these methods has limitations. The analytical methods are applied mainly to linear, isotropic and homogeneous materials and simple geometries. The numerical methods, on the other hand, are often inapplicable to geophysical problems which involve large dimensions.

Numerical Methods

Two-Dimensional Models:

For the finite difference method, Alterman and Karal (1968), and Boore (1969; 1972; 1973) formulated the scheme for general wave propagation problems. Cherry (1973) applied the method to fault rupture problems. Cole, et. al. (1978) formulated the boundary initial value problems of elastodynamics in terms of boundary integral equations. They can be solved by time-stepping numerical methods for the unknown boundary values. Using the finite difference schemes, Ilan, et. al. (1979) studied the diffraction of a compressional pulse by a slot in a half-space.

Both the finite difference and finite element methods are ideal for analyzing finite bodies with inhomogeneous material properties.

However, there is one serious restriction caused by the limited core size of present day computers; i.e., the total number of nodal points in the discrete network is limited. This problem reduces the effectiveness of these methods for geotechnical problems because of the large dimensions of the earth as compared to most other models. Introduction of a model with limited dimensions reduces the time for which the analysis is valid, i.e., before the arrival of reflected fields from introduced model boundaries. An attempt was made (Lysmer and Waas, 1972) to absorb the wave energy at, and to introduce, transparent boundaries, but these energy absorption models are not applicable for all circumstances. Superimposing the difference boundary conditions, Smith (1974) devised transparent boundaries which can extend the analysis for longer durations, but the solution for a model with N unwanted reflective boundaries requires as much as 2^N times more computer time than the standard analysis.

Three-Dimensional Models:

The restriction caused by limited core size of computers is even more pronounced in three dimensions. Consequently, the spatial dimensions of the model must be reduced even further compared to the two-dimensional models. Therefore, most three-dimensional analyses have been done for special cases only, e.g., models with an axis of symmetry where the reduction of spatial coordinates is possible. A model by Reimer, et. al. (1974) is an attempt to model the topographic effects of the Pacoima Canyon. Although the top surface of the model resembles the canyon, the sides and bottom of the model trap the energy inside to create the resonance behavior that should be absent. Thus, the amplification

predictions made by these "box-like" models are generally not valid. A similar "box" model was used by Schlue (1979) to study the Love waves when material properties vary in two dimensions.

Analytical Methods

Two-Dimensional Models:

For a two-dimensional elastodynamic boundary value problem, there is only a limited number of coordinate systems which allow exact series solutions to be developed. In particular, the anti-plane strain problems (SH waves) is considered simple, compared to the plane strain models. This follows because no mode conversions between SH, P or SV waves take place and the mathematical formulation is very similar to that of acoustic wave problems.

Anti-Plane Strain Model:

Trifunac (1973) presented an exact solution for scattering of plane SH waves by a canyon of semi-cylindrical shape. His results indicate that the wave amplification patterns are influenced by the angle of incidence as well as the frequency excitation. For a semi-elliptical canyon and an anti-plane strain model, an exact solution is presented by Wong and Trifunac (1974a). They showed that the depth of the canyon can play an important role in diffraction. An exact, short-time solution for diffraction of a plane SH-wave by a rigid rectangular obstacle embedded in an elastic half-space studied by Thau and Umek (1975) and Dravinski and Thau (1976a), showed that the embedded depth of the obstacle is important for the resultant diffracted field. Wong and Jennings (1975) generalized the geometry of the topography to include

arbitrary shaped canyons, and concluded that topographic effects are important for very steep slopes and for wavelengths shorter than or comparable to the dimensions of the canyon. Sabina and Willis (1975) also presented an approximate method for calculating topographic effects caused by canyons with constant slopes. This method can be extended to the plane strain model as well. Singh and Sabina (1977) studied ground motion amplification by topographic depressions for incident P waves but under acoustic approximation. Wong, et. al. (1977) compared the analytical results for the effects of surface and subsurface irregularities upon ground amplification with experimental results: they found the effects of the dipping layer to play a more important role compared to the canyon. Sills (1978) studied scattering of SH waves by general topographies such as hills and/or depressions. A singular Fredholm integral equation is developed and solved numerically. The results indicate strong amplification due to topographic irregularities. Sanchez-Sesma and Rosenblueth (1979) considered ground motions at canyons of arbitrary shapes by using essentially the method developed by Wong (Wong and Jennings, 1975; Wong, et. al., 1977).

A limited amount of work has been done for diffraction of elastic waves involving the contrasting material properties. Aki and Larner (1970) considered the problem of a horizontal layer bonded to a half-space and having small interface irregularities (comparable to the incident wavelength). Focusing effects were observed at the layer surface. These focusing phenomena, often observed in strong earthquakes,

also appeared in exact solutions for diffraction of plane SH waves by semi-cylindrical and semi-elliptical alluvial valleys bonded to an elastic half-space (Trifunac, 1971; Wong and Trifunac, 1974b). Recently, Sanchez-Sesma and Esquivel (1979) studied diffraction of plane elastic SH waves by an alluvial valley of arbitrary shape. Their results demonstrate significant ground motion amplification to be present in the problem.

Dravinski and Udwadia (1980) considered the influence of the so called Rayleigh assumption in solving the ground amplification due to surface topography. Comparison with the exact solutions indicate significant difference in amplification factors for periodically corrugated surface.

Plane Strain Model:

In this model, the longitudinal and shear waves are coupled at the stress-free surface and the boundary conditions are much more complex compared to the anti-plane strain model.

Mal and Knopoff (1965) examined the case of Rayleigh waves propagating past the vertical change in elevation. Asano (1966) and McIvor (1969) studied effects of shallow topography by perturbation methods. However, these methods are not practical for engineering purposes due to the complexity of the mathematical analysis involved. Bouchon (1973) studied the effect of topography on surface motion for incident P, SV and SH waves. Several types of topography ranging from a ridge to a valley are used. The computation is made by using the method due to Aki and Larner (1970) in order to get results in the time domain. The results show that the surface displacement is very much influenced by

surface irregularities. Thau and Umek (1974) and Dravinski and Thau (1976b) studied diffraction of waves by a rigid rectangular obstacle using the so-called "relaxed" boundary conditions in which the longitudinal and shear waves are separable along the boundaries. Bouchon and Aki (1977) considered the near-field of a seismic source for layered medium with irregular interfaces. By adopting the Rayleigh's approach, they evaluated the scattered wave field and presented numerical examples of the results and studied the error due to Rayleigh's assumption on the scattered wave field. Their results show that large amplification of horizontal motions can occur for wavelengths of the order of the dimension of the imperfection.

Wong (1979) studied diffraction of P, SV and Rayleigh waves by the surface topography of arbitrary shape. A diffraction by an elliptical canyon is presented in detail for illustration. His results can be summarized as follows: (1) the amplitude of waves near an elliptical canyon are less than two times the free-field amplitude; (2) for P and SV incidence, larger amplification does not always occur in front of the canyon; (3) standing wave phenomena caused by interference of waves occur only in front of the canyon. Large amplitudes at the rear of the canyon are caused by mode conversion; and (4) Rayleigh waves with wavelengths at most the width of the canyon can be blocked effectively by the canyon.

Three-Dimensional Models:

There are very few solutions for scattering of elastic waves by three-dimensional irregularities. Wong (1975) and Wong and Luco (1976) studied wave scattering problems involving surface objects.

Lee (1978) presented a solution for the problem of diffraction of elastic plane waves (P, SV, and SH) by a hemispherical canyon. He used the method of series expansion in devising the total wave field and the corresponding amplification factors. He found that the displacement amplitudes and phases of the surface ground motions near the canyon are significantly different from the uniform half-space motions. Furthermore, the angle of incidence determines the overall trends of motion amplitudes. For oblique incidence, considerable amplification is observed in front of the canyon, with a shadow zone behind the canyon.

Although not many solutions of three-dimensional problems are available, it is not difficult to extend some of the approximate methods from two-dimensional to three-dimensional models. For example, the study by Lee (1978) suggests another method for scattering of elastic waves by a three-dimensional elastic obstacle, i.e., alluvial valley, bonded to an elastic half-space. The technical background required for the source method is reviewed next.

III. TECHNICAL BACKGROUND AND THE SOURCE METHOD

There are two approaches which lead to the source method. Oshaki (1973) used one approach in the study of static loading of a rigid foundation embedded in an elastic half-space. Wong, et. al. (1977) applied the same idea to study the diffraction of monochromatic waves by surface irregularities. Recently, Wong (1979) used this method in the analysis of diffraction of P, SV and Rayleigh waves by ground surface topographies. The second approach originated by Copley (1967). In plane elastostatics, this approach has been used by Heise (1978). Applications to the wave propagation problems are due to Sanchez-Sesma and Rosenblueth (1979) and Sanchez-Sesma and Esquivel (1979).

First, the scattering of an elastic plane SH wave by an alluvial valley is presented in detail. The geometry of the problem is depicted by Figure 1; the valley is assumed to be perfectly bonded to the elastic half-space. The equation of motion for steady-state wave propagation is given by

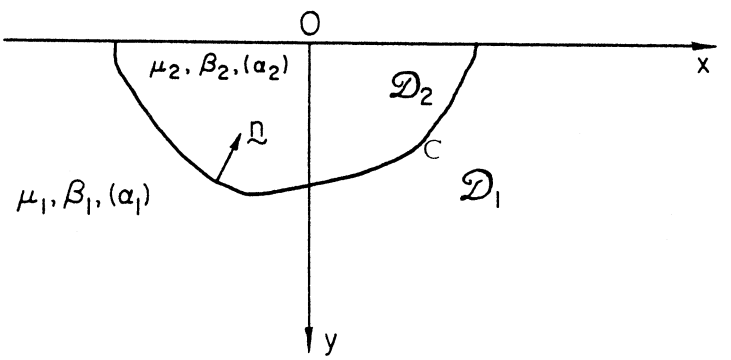

Figure 1

$$\left(\nabla^2 + k_j^2\right) w_j(x,y) = 0 \qquad j=1,2; \qquad \nabla^2 \equiv \frac{\partial^2}{\partial x^2} + \frac{\partial^2}{\partial y^2} \quad , \tag{1}$$

where the subscripts 1 and 2 denote the half-space and the inclusion, respectively, k represents the wave number, and w represents the only non-zero component of the displacement field acting along the z-axis. Throughout the analysis, the factor $e^{+i\omega t}$ is understood. The velocity of the shear wave is denoted by β.

Boundary conditions are specified by

$$\frac{\partial w_j}{\partial y} = 0 \quad , \quad \text{at } y=0 \text{ and } \underset{\sim}{r} \in \mathscr{D}_j \ , \ j=1,2, \tag{2}$$

where $\underset{\sim}{r}$ represents a position vector, $\mathscr{D}_1$ and $\mathscr{D}_2$ denote the region of elastic half-space and inclusion, respectively (Figure 1). Perfect bonding along the interface C requires

$$w_1 = w_2 \tag{3.1}$$

$$\mu_1 \frac{\partial w_1}{\partial n} = \mu_2 \frac{\partial w_2}{\partial n} \qquad \underset{\sim}{r} \in C \ , \tag{3.2}$$

with μ and $\underset{\sim}{n}$ denoting the shear modulus and unit normal to the C, respectively. The total wave field in the half-space, w_1, and the elastic inclusion, w_2, are given by

$$w_1 = w^i + w_1^s \tag{4.1}$$

$$w_2 = w_2^s \quad , \tag{4.2}$$

where w_j^s, j=1,2, denotes the scattered wave field and w^i is the incident wave motion. It is assumed that the scattered wave field can be expressed in terms of single layer potentials (Ursell, 1973),

$$w_1^s(r) = \int_{C_1} g_1(\underset{\sim}{r}_o) G_1(\underset{\sim}{r}, \underset{\sim}{r}_o) ds_o \tag{5.1}$$

$$w_2^s(r) = \int_{C_2} g_2(\underset{\sim}{r}_o) G_2(\underset{\sim}{r}, \underset{\sim}{r}_o) ds_o \quad . \tag{5.2}$$

The C_1 and C_2 are the curves defined in the half-space inside and outside of the interface C, respectively (see Figures 2a, b) and the density

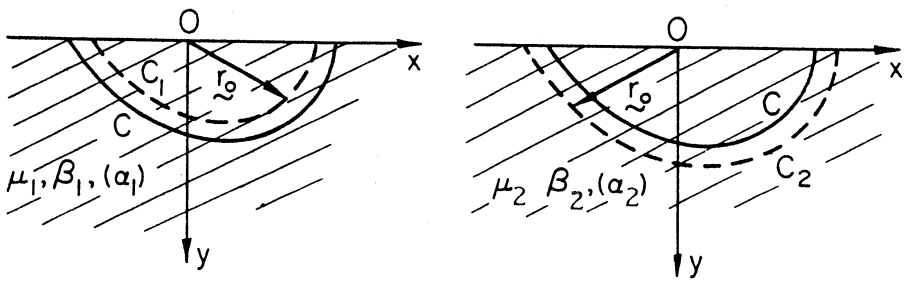

(a) (b)

Figure 2

functions g_1 and g_2 are yet to be determined. The Green's functions G_1 and G_2 are the solutions of the equations

$$\left(\nabla^2 + k_j^2\right) G_j(\underset{\sim}{r},\underset{\sim}{r}_o) = -\delta(|\underset{\sim}{r} - \underset{\sim}{r}_o|) \qquad , \; j=1,2; \tag{6.1}$$

$$\left.\frac{\partial G_j}{\partial n}\right|_{y=0} = 0 \tag{6.2}$$

with $\delta(\cdot)$ being the Dirac delta function.

The Green's functions in this problem are

$$G_j(\underset{\sim}{r},\underset{\sim}{r}_o) = \frac{i}{4}\left\{ H_o^{(2)}(k_j\sigma_1) + H_o^{(2)}(k_j\sigma_2) \right\} \; ; \quad \sigma_1 = \sqrt{(x-x_o)^2 + (y-y_o)^2}$$

$$\sigma_2 = \sqrt{(x-x_o)^2 + (y+y_o)^2}$$

$$j=1,2, \tag{7}$$

where $H_o^{(2)}(\cdot)$ denotes the Hankel function of the second kind and order zero.

Assuming that the density functions g_1 and g_2 represent systems of discrete line sources along the C_1 and C_2, respectively, i.e.,

$$g_1(\underset{\sim}{r}_o) = \sum_{m=1}^{M} a_m \delta(|\underset{\sim}{r}_o - \underset{\sim}{r}_m|) \tag{8.1}$$

$$g_2(\underset{\sim}{r}_o) = \sum_{\ell=0}^{L} b_\ell \delta(|\underset{\sim}{r}_o - \underset{\sim}{r}_\ell|), \tag{8.2}$$

equations (5) imply the scattered field to be

$$w_1^s(\underset{\sim}{r}) = \sum_{m=1}^{M} a_m G_1(\underset{\sim}{r},\underset{\sim}{r}_m) \; , \quad \underset{\sim}{r}_m \varepsilon C_1 \tag{9.1}$$

$$w_2^s(\underset{\sim}{r}) = \sum_{\ell=1}^{L} b_\ell G_2(\underset{\sim}{r},\underset{\sim}{r}_\ell) \; , \quad \underset{\sim}{r}_\ell \varepsilon C_2 \; . \tag{9.2}$$

The continuity conditions (3) then imply

$$\sum_{m=1}^{M} a_m G_1(\underset{\sim}{r},\underset{\sim}{r}_m) - \sum_{\ell=1}^{L} b_\ell G_2(\underset{\sim}{r},\underset{\sim}{r}_\ell) = -w^i(\underset{\sim}{r}) \tag{10.1}$$

$$\sum_{m=1}^{M} a_m \frac{\partial G_1(\underset{\sim}{r},\underset{\sim}{r}_m)}{\partial n} - \frac{\mu_2}{\mu_1} \sum_{\ell=1}^{L} b_\ell \frac{\partial G_2(\underset{\sim}{r},\underset{\sim}{r}_\ell)}{\partial n} = - \frac{\partial w^i(\underset{\sim}{r})}{\partial n} \; . \tag{10.2}$$

Choosing the N observation points $\underset{\sim}{r} = \underset{\sim}{r}_i$, i=1,2,...,N along the interface C, the continuity conditions (10) are written in the following form

$$\underset{\sim\sim}{A}\underset{\sim}{a} = \underset{\sim}{f} \quad , \tag{11}$$

where the matrix $\underset{\sim}{A}$ of order 2N x (M+L) is defined through

$$\underset{\sim}{A} = \begin{bmatrix} \underset{\sim}{G}_1 & -\underset{\sim}{G}_2 \\ \\ \underset{\sim}{G}_{1n} & -\frac{\mu_2}{\mu_1}\underset{\sim}{G}_{2n} \end{bmatrix} \tag{11.1}$$

where

$$[G_{ij}]_1 = G_1(\underset{\sim}{r}_i, \underset{\sim}{r}_j) \qquad \begin{matrix} i=1,2,\ldots,N \\ j=1,2,\ldots,M \end{matrix} \tag{11.2}$$

$$[G_{ij}]_{1n} = \frac{\partial G_1(\underset{\sim}{r}_i, \underset{\sim}{r}_j)}{\partial n} \qquad \ell=1,2,\ldots,L \tag{11.3}$$

$$[G_{i\ell}]_2 = G_2(\underset{\sim}{r}_i, \underset{\sim}{r}_\ell) \tag{11.4}$$

$$[G_{i\ell}]_{2n} = \frac{\partial G_2(\underset{\sim}{r}_i, \underset{\sim}{r}_\ell)}{\partial n} \quad . \tag{11.5}$$

The forcing vector $\underset{\sim}{f}$ in (11) is of order 2N x 1 and is defined by

$$\underset{\sim}{f} = \begin{bmatrix} -\underset{\sim}{w}^i \\ -\underset{\sim}{w}_n \end{bmatrix} \quad , \tag{11.6}$$

where

$$[w_j]^i = w^i(\underset{\sim}{r}_j) \tag{11.7}$$

$$[w_j]^i_n = \frac{\partial w^i(\underset{\sim}{r}_j)}{\partial n} \qquad j=1,2,\ldots,N \tag{11.8}$$

The unknown intensities of the discrete sources are incorporated in vector $\underset{\sim}{a}$ through

$$[a_j] = a_j \quad , \qquad j=1,2,\ldots,M \tag{11.9}$$

$$[a_j] = b_{j-M} \quad , \qquad j=M+1,M+2,\ldots,M+L \quad . \tag{11.10}$$

Equation (11) is solved for the unknown coefficient vector $\underset{\sim}{a}$ so that the mean square error of (11) is minimized (Noble, 1969)

$$\underset{\sim}{a} = (\underset{\sim}{A}^{*}\underset{\sim}{A})^{-1}\underset{\sim}{A}^{*}\underset{\sim}{f} \ . \tag{12}$$

Here, $\underset{\sim}{A}^{*}$ denotes the transpose complex conjugate of $\underset{\sim}{A}$.

To test the accuracy of the method, the source method results for diffraction of a plane SH wave by a semi-circular cylindrical alluvial valley are compared with the exact solution. Therefore, one considers an incident wave

$$w^{i} = e^{-i(k_1 x - \omega t)} \tag{13}$$

which propagates in an elastic half-space, strikes a semi-cylindrical elastic inclusion, partly scatters back into the half-space and partly transmits into the inclusion. The radius of the semi-cylindrical inclusion R, the shear modulus μ_1 and the shear wave velocity β_1 of the half-space are all taken to be equal to one so that the results are in dimensionless form.

The exact solution for the total wave field is given by (Pao and Mow, 1973)

$$w_1 = w^{i} + w_1^{s} \tag{14.1}$$

$$w_2 = w_2^{s} \quad , \tag{14.2}$$

where the scattered wave field is defined through

$$w_1^{s} = \sum_{n=0}^{\infty} A_n H_n^{(2)}(k_1 r)\cos n\theta \quad , \quad r \in \mathscr{D}_1 \tag{14.3}$$

$$w_2^{s} = \sum_{n=0}^{\infty} B_n J_n(k_2 r)\cos n\theta \quad , \quad r \in \mathscr{D}_2 \tag{14.4}$$

and θ is measured positive, clockwise from the positive x axis (Figure 1).

As defined earlier, $\mathscr{D}_1$ and $\mathscr{D}_2$ represent the domain of the half-space and the inclusion, respectively. The expansion coefficients are given by

$$A_n = \frac{\Delta_1}{\Delta} \tag{14.5}$$

$$B_n = \frac{\Delta_2}{\Delta} \tag{14.6}$$

$$\Delta_1 = -\varepsilon_n(-i)^n\left[\mu_2 k_2 J_n(k_1R)J_n'(k_2R) - \mu_1 k_1 J_n'(k_1R)J_n(k_2R)\right] \tag{14.7}$$

$$\Delta_2 = -\varepsilon_n(-i)^n\mu_1 k_1\left[J_n'(k_1R)\cdot H_n^{(2)}(k_1R) - J_n(k_1R)\cdot H_n'(k_1R)\right] \tag{14.8}$$

$$\Delta = \mu_2 k_2 H_n^{(2)}(k_1R)\cdot J_n'(k_2R) - \mu_1 k_1 H_n^{(2)\prime}(k_1R)\cdot J_n(k_2R) \quad , \tag{14.9}$$

where prime denotes differentiation with respect to the argument and

$$\varepsilon_n = \begin{cases} 1 & , n=0 \\ 2 & , n=1,2,\ldots \end{cases} \quad . \tag{14.10}$$

For the source method, the curves C_1 and C_2 introduced by equation (5) are chosen to be semicircles $r = R_I$ and $r = R_o$, respectively, with $0 < R_I < R < R_o < \infty$. Five sources are equally spaced along each C_1 and C_2 ($M = 5$, $L = 5$; see eq. (3)). The number of 'observation points,' equally spaced along the C, is chosen to be, say, eleven ($N = 11$; see eqn. (11)).

Distribution of the sources and the observation points is depicted by Figure 3. The total wave fields in the half-space and in the alluvial valley are evaluated at the N observation points by the exact method and the source method. To present the results in a more compact form, an error is defined to be

$$e(Z) \equiv \frac{\sum_{i=1}^{N}\left[Z_{exact}(\underset{\sim}{R}_i) - Z(\underset{\sim}{R}_i)\right]^2}{\sum_{i=1}^{N}\left[Z_{exact}(\underset{\sim}{R}_i)\right]^2} \quad , \tag{15}$$

where Z represents $R_e w_1$, $I_m w_1$, $R_e w_2$, or $I_m w_2$.

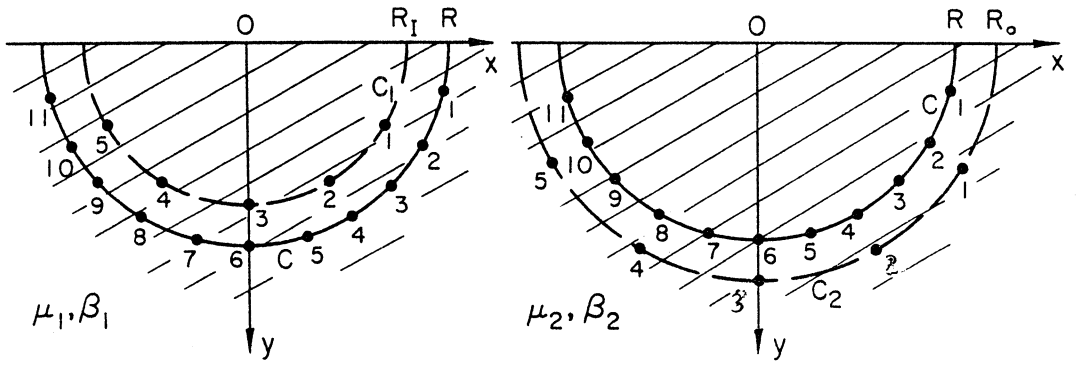

(a) (b)

Figure 3

The R_i, i=1,2,...,N denotes the observation points along the C.

For the frequency of the incident field, $\omega = 0.1\pi$, and the material properties of the alluvial valley, $\mu_2 = 2$, $\beta_2 = 2$, the results of error for different values of R_I and R_o (see Fig. 3) are given in Table I.

TABLE I -- Error Analysis Results at $\omega = 0.1\pi$

$\mu_1 = \beta_1 = 1$ $\mu_2 = \beta_2 = 2$		$R = 1$ $\omega = 0.1\pi$		$M = L = 5$ $N = 11$	
R_I	R_o	$e(R_e w_1)$	$e(I_m w_1)$	$e(R_e w_2)$	$e(I_m w_2)$
0.05	1.95	0.011082	0.000916	0.000012	0.000533
0.10	1.90	0.015151	0.001622	0.000017	0.000712
0.20	1.80	0.008088	0.005513	0.000008	0.001156
0.30	1.70	0.027094	0.007015	0.000029	0.001837
0.40	1.60	0.070120	0.009837	0.000078	0.002972
0.50	1.50	0.191873	0.012619	0.000220	0.004791
0.60	1.40	0.550260	0.014484	0.000666	0.007775
0.70	1.30	1.92053	0.016684	0.002471	0.013705
0.80	1.20	11.8644	0.040384	0.016188	0.0316807
0.90	1.10	98.1315	0.259476	0.135341	0.105225
0.95	1.05	191.972	0.541028	0.260099	0.183345

To illustrate the physical meaning of the error results, the total wave fields w_1 and w_2 are plotted at N observation points and are shown by Figures 4 through 9. Exact results are presented by symbols connected with straight lines. The source method results are presented by corresponding symbols not connected.

Results of Table I and Figures 4 through 9 indicate a wide range of R_I and R_o for which the source method provides excellent results. As frequency ω is increased to $\omega=\pi$, the errors are presented in Table II.

TABLE II -- Error Analysis Results at $\omega=\pi$

$\mu_1 = \beta_1 = 1$		$R = 1$		$M = L = 5$	
$\mu_2 = \beta_2 = 2$		$\omega = \pi$		$N = 11$	
R_I	R_o	$e(R_e w_1)$	$e(I_m w_1)$	$e(R_e w_2)$	$e(I_m w_2)$
0.05	1.95	0.019946	0.022991	0.007377	0.011392
0.10	1.90	0.020403	0.007298	0.005334	0.007089
0.20	1.80	0.004546	0.019804	0.006898	0.011043
0.30	1.70	0.005934	0.02652	0.009666	0.015969
0.40	1.60	0.0078465	0.031017	0.014208	0.025274
0.50	1.50	0.013328	0.034968	0.024262	0.041885
0.60	1.40	0.025810	0.049931	0.050910	0.075462
0.70	1.30	0.075697	0.178820	0.140602	0.227945
0.80	1.20	0.154763	0.219877	0.269653	0.299975
0.90	1.10	0.156622	0.316306	0.484507	0.404402
0.95	1.05	0.259892	0.496948	0.505733	0.725041

The results of Table II are graphically presented by Figure 10. It is seen again that there is a wide range of parameters R_o and R_I for which the source method provides excellent results. Analysis of the results of Tables I and II implies that for the fixed number of sources, the accuracy of the source method is better at lower frequencies which is in agreement with the physical interpretation of the method.

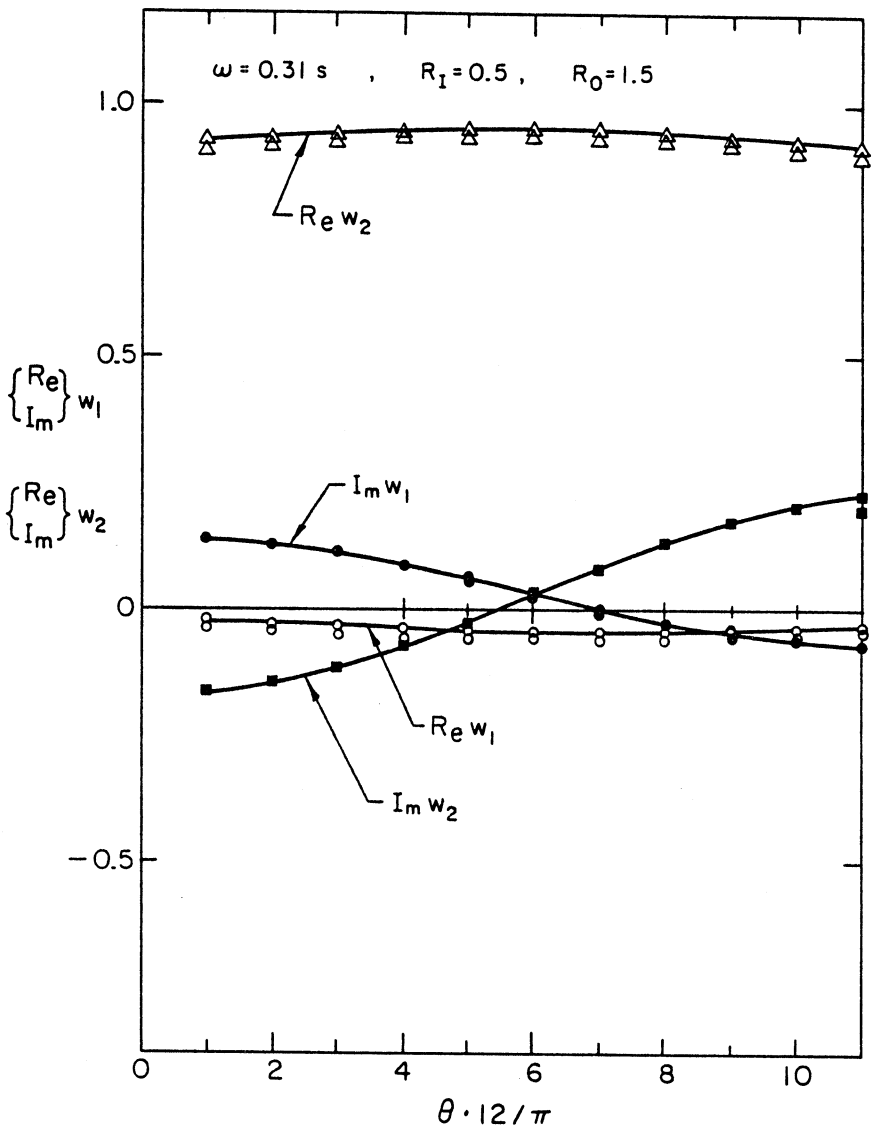

Fig. 4 Scattering of a plane SH-wave by a Semicylindrical Elastic Inclusion. Error as a Function of Position of Sources.
a) Exact Solution: Connected Symbols
b) Approximate Solution: Symbols not Connected
($\mu_1 = \beta_1 = R = 1$; $\mu_2 = \beta_2 = 2$, $M = L = 5$, $N = 11$)

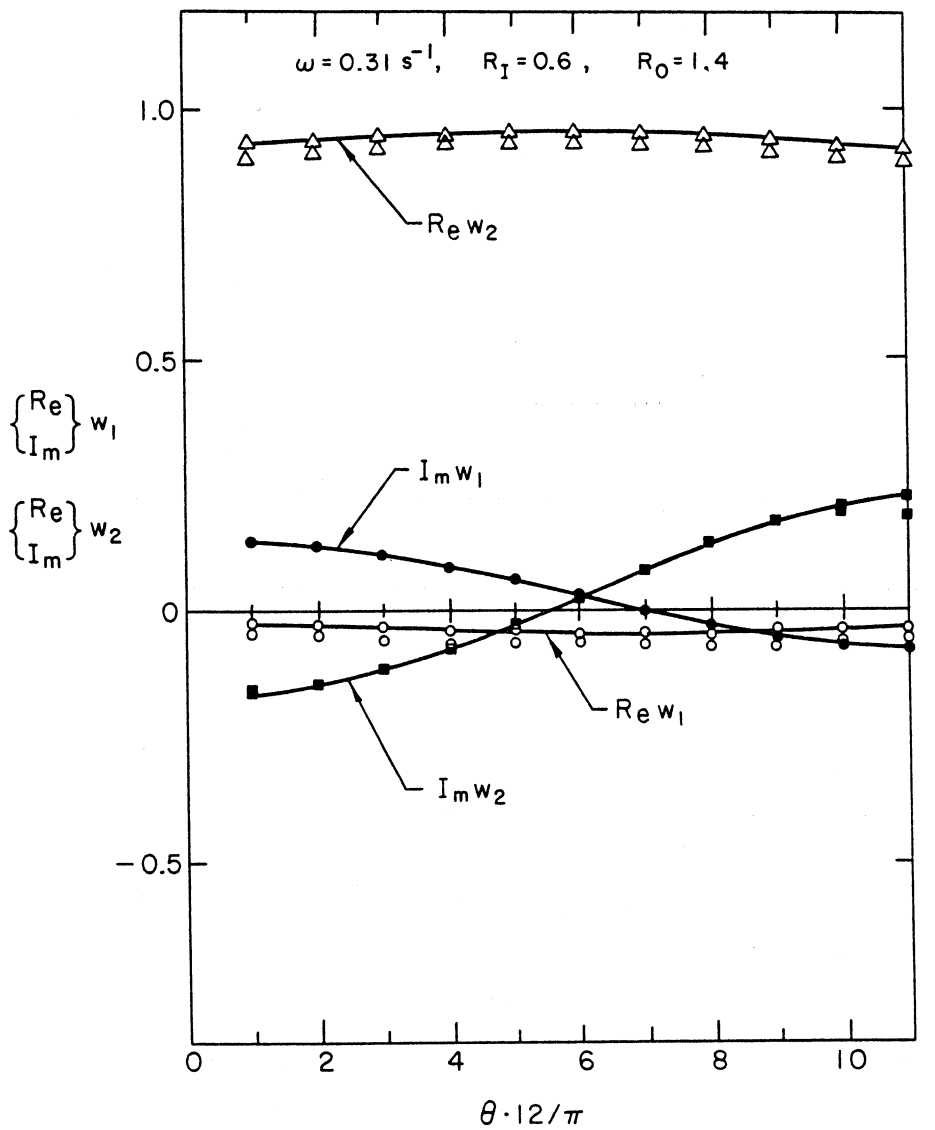

Fig. 5 Scattering of a plane SH-wave by a Semicyclindrical Elastic Inclusion. Error as a Function of Position of Sources.
a) Exact Solution: Connected Symbols
b) Approximate Solution: Symbols not Connected
($\mu_1 = \beta_1 = R = 1$; $\mu_2 = \beta_2 = 2$, $M = L = 5$, $N = 11$)

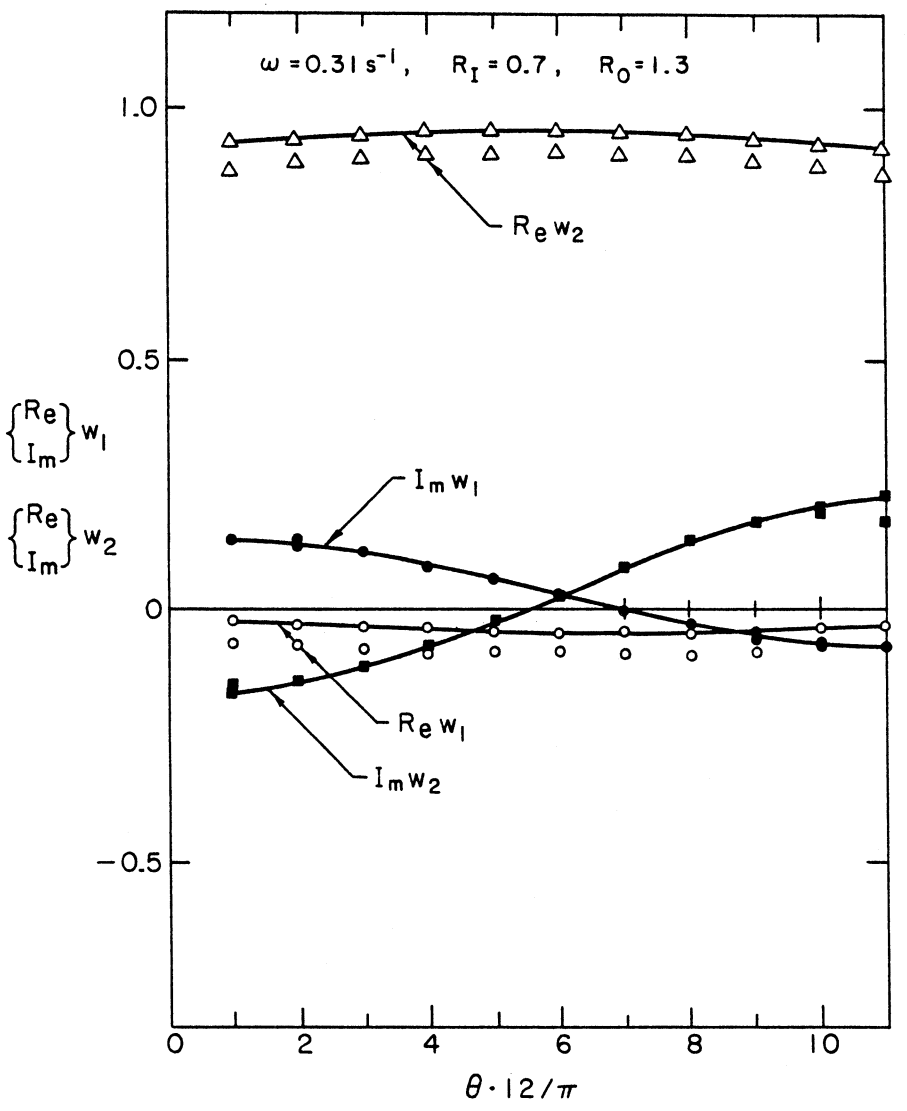

Fig. 6 Scattering of a plane SH-wave by a Semicylindrical Elastic Inclusion. Error as a Function of Position of Sources.
a) Exact Solution: Connected Symbols
b) Approximate Solution: Symbols not Connected
($\mu_1 = \beta_1 = R = 1$; $\mu_2 = \beta_2 = 2$, $M = L = 5$, $N = 11$)

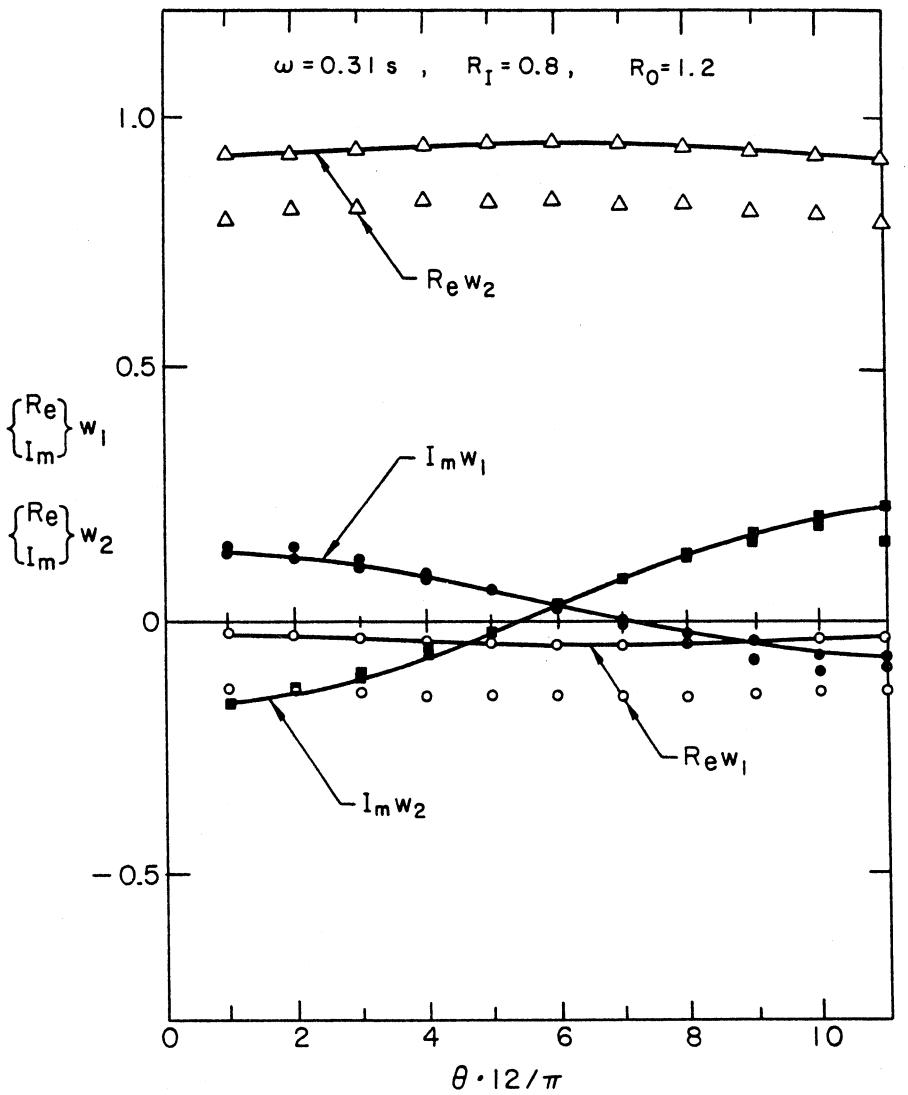

Fig. 7 Scattering of a plane SH-wave by a Semicylindrical Elastic Inclusion. Error as a Function of Position of Sources.
a) Exact Solution: Connected Symbols
b) Approximate Solution: Symbols not Connected
($\mu_1 = \beta_1 = R = 1$; $\mu_2 = \beta_2 = 2$, M = L = 5, N = 11)

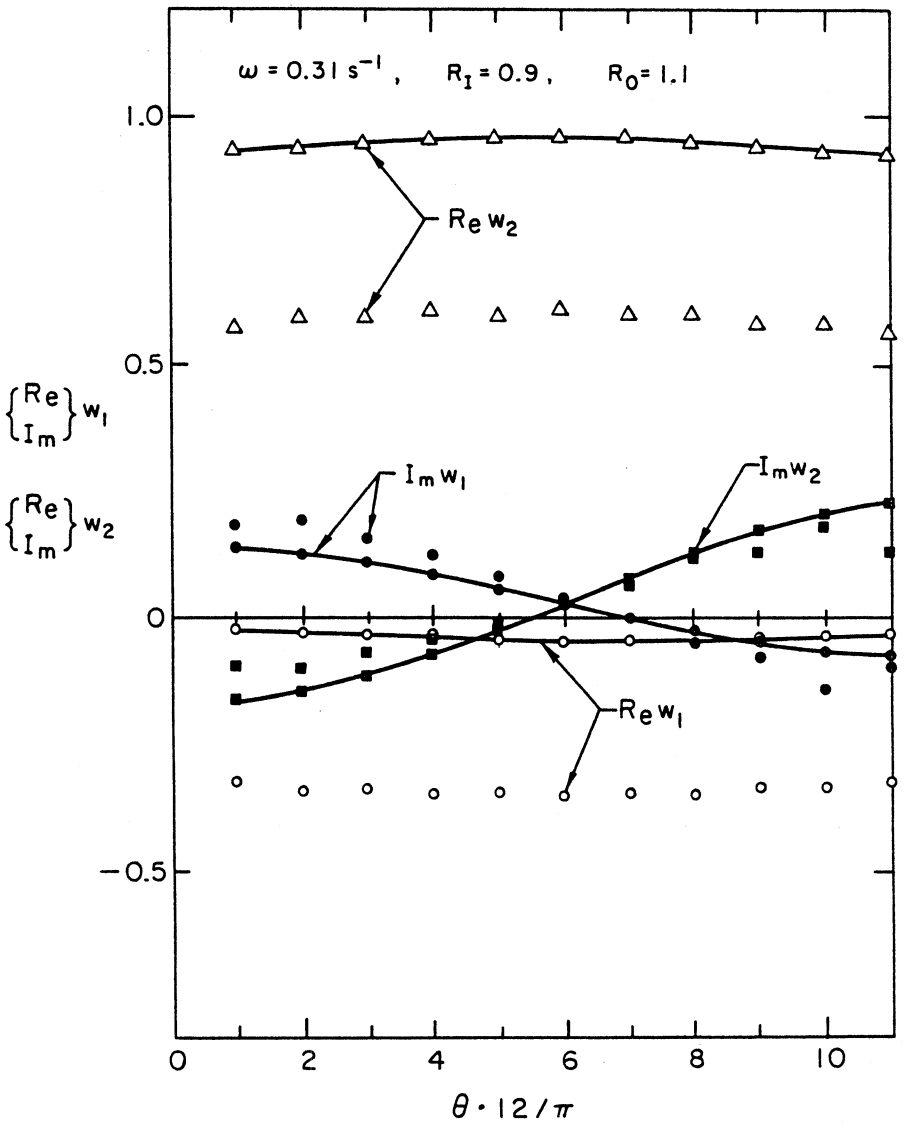

Fig. 8 Scattering of a plane SH-wave by a Semicylindrical Elastic Inclusion. Error as a Function of Position of Sources.
a) Exact Solution: Connected Symbols
b) Approximate Solution: Symbols not Connected
($\mu_1 = \beta_1 = R = 1$; $\mu_2 = \beta_2 = 2$, $M = L = 5$, $N = 11$)

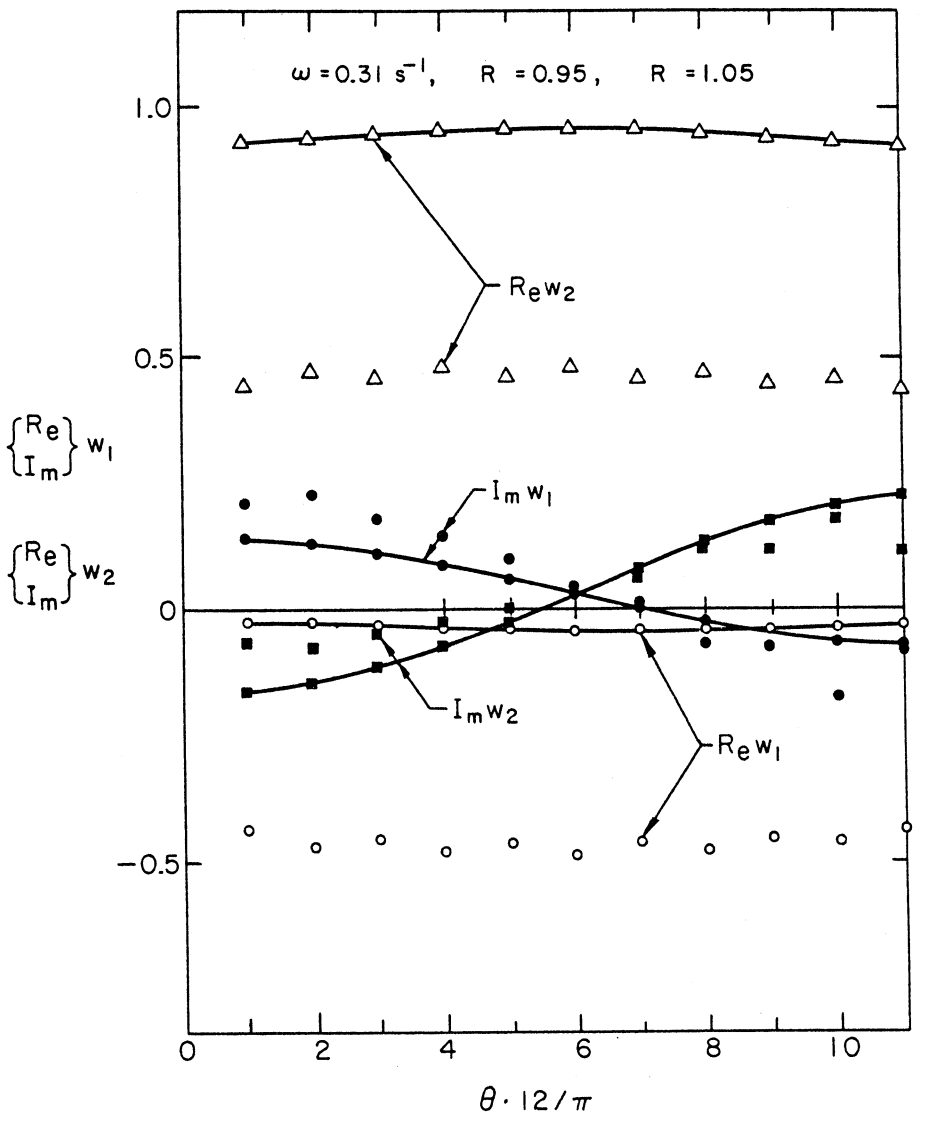

Fig. 9 Scattering of a plane SH-wave by a Semicylindrical Elastic Inclusion. Error as a Function of Position of Sources.
a) Exact Solution: Connected Symbols
b) Approsimate Solution: Symbols not Connected
($\mu_1 = \beta_1 = R = 1$; $\mu_2 = \beta_2 = 2$, M = L = 5, N = 11)

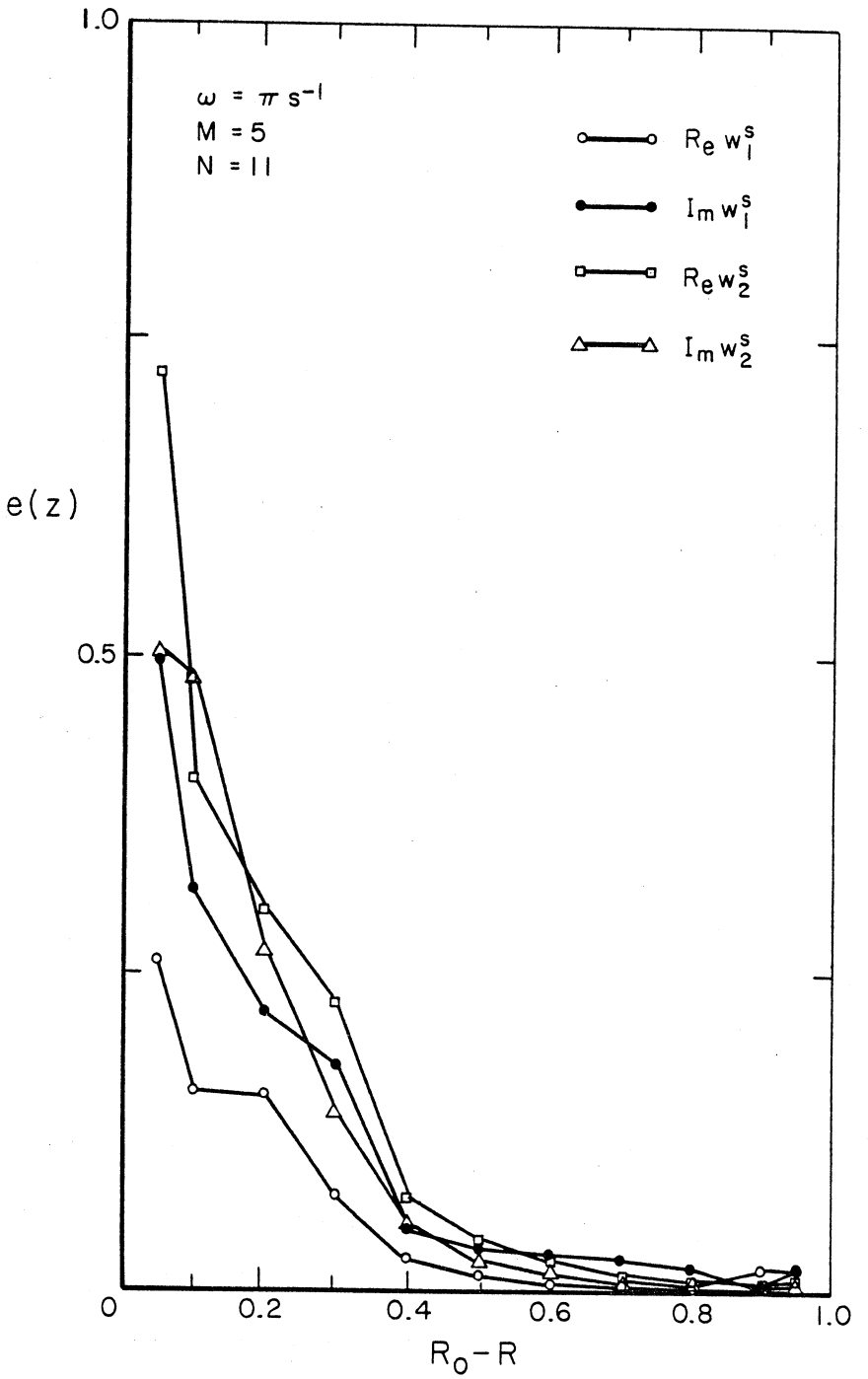

Fig. 10 Error as a Function of Position of Sources ($\mu_1 = \beta_1 = R = 1$, $\mu_2 = \beta_2 = 2$, M = L = 5, N = 11)

At this point a question arises about the influence of the number of sources upon the accuracy of the method. Therefore, the error analysis is repeated for eleven sources (M = L = 11) and twenty-three observation points (N = 23), both equally spaced in the manner indicated by Figure 3. The results are presented by Tables III and IV. Comparison of Tables I-IV implies that as the number of sources increase, the accuracy of the source method improves.

TABLE III -- Error Analysis results at $\omega = 0.1\pi$

$\mu_1 = \beta_1 = 1$		$R = 1$	$M = L = 11$		
$\mu_2 = \beta_2 = 2$		$\omega = 0.1\pi$	$N = 23$		
R_I	R_o	$e(R_e w_1)$	$e(I_m w_1)$	$e(R_e w_2)$	$e(I_m w_2)$
0.05	1.95	0.000013	0.000014	0.000000	0.000000
0.10	1.90	0.000003	0.000000	0.000000	0.000000
0.20	1.80	0.000010	0.000000	0.000000	0.000000
0.30	1.70	0.000096	0.000011	0.000000	0.000002
0.40	1.60	0.000186	0.000042	0.000000	0.000006
0.50	1.50	0.000723	0.000284	0.000000	0.000029
0.60	1.40	0.001709	0.000788	0.000002	0.000082
0.70	1.30	0.013000	0.002137	0.000013	0.000312
0.80	1.20	0.110289	0.003886	0.000126	0.001004
0.90	1.10	5.20772	0.014701	0.006913	0.007279
0.95	1.05	78.9799	0.190455	0.106095	0.060798

TABLE IV -- Error Analysis Results at $\omega = \pi$

$\mu_1 = \beta_1 = 1$		$R = 1$	$M = L = 11$		
$\mu_2 = \beta_2 = 2$		$\omega = \pi$	$N = 23$		
R_I	R_o	$e(R_e w_1)$	$e(I_m w_1)$	$e(R_e w_2)$	$e(I_m w_2)$
0.05	1.95	0.084933	2.26812	0.192501	0.295296
0.10	1.90	0.004632	0.06638	0.000360	0.001183
0.20	1.80	0.013472	0.004160	0.001739	0.000651
0.30	1.70	0.000182	0.000557	0.000052	0.000134
0.40	1.60	0.000031	0.000251	0.000011	0.000057
0.50	1.50	0.000061	0.000163	0.000025	0.000051
0.60	1.40	0.000119	0.000678	0.000063	0.000232
0.70	1.30	0.000215	0.003445	0.000345	0.001477
0.80	1.20	0.001967	0.006242	0.002414	0.004235
0.90	1.10	0.013704	0.012274	0.047018	0.040577
0.95	1.05	0.083886	0.129421	0.265477	0.372792

Analysis of the results for scattering of plane SH-waves by a semicylindrical alluvial valley in terms of the source method indicate that the accuracy of the displacement field along the interface increases as the sources along the inner source surface C_1 (see Fig.3) converge to the origin,while the sources along the outer source surface C_2 are placed away from the interface.It follows that the distribution of the sources and the accuracy of approximation are related to the assumption about the nature of the scattered wave field (see Eqn.9). The scattered field is represented by superposition of Green's functions which become singular as the "observation" points approach the "source" points. Consequently,the best results are achived with the "observation" points away from the "source" points.

SEMI-CYLINDRICAL ALLUVIAL VALLEY:SURFACE DISPLACEMENT FIELD

The exact surface displacement field is compared with the source method results by using the relative error functional (15).The relative error is evaluated for different inner and outer surfaces C_i and C_o which are assumed to be of semi-cylindrical form (see Fig. 3) with $R_i \leq R \leq R_o$. Using the same number of sources (eleven) along the source surfaces C_i and C_o, with twenty-three observation points along the interface r=R,the surface displacement field is evaluated along $y=0,-2R \leq x \leq 2R$, at forty-six equally spaced points. The relative error is determined for real and imaginary parts of the surface displacement field W for different placement of the source surfaces. Those results

are depicted by Fig. 11. It can be seen from the graphic error display that the average relative error remains unchanged for a wide range of positions of the source surfaces C_1 and C_2. However, the significant increase in the error is found if the sources approach the interface C (not shown since it is out of scale of Fig. 11). The contribution to the error arises due to singularities of the Green's functions in continuity condition (10) as the "source" points approach the "observation" points.

So far the analysis has been concerned with the circular shape of the alluvial valley. To explore the source method in more detail, it is necessary to investigate the noncircular type of the interface. Therefore, scattering of a plane SH-wave by a semi-elliptical alluvial valley is considered next.

SCATTERING OF PLANE SH-WAVES BY SEMI-ELLIPTICAL ALLUVIAL VALLEY

The alluvial valley is specified by

$$C: \quad x = R_1\cos\theta; \quad y = R_2\sin\theta; \quad 0 \le \theta \le \pi, \tag{16.1}$$

where the principal axis R_1 and R_2 are known. The inner and outer sources are placed along the surfaces C_1 and C_2, respectively defined by

$$C_1: \quad x = R_{1i}\cos\theta; \; y = R_{2i}\sin\theta \tag{16.2}$$

$$0 \le \theta \le \pi,$$

$$C_2: \quad x = R_{1o}\cos\theta; \; y = R_{2o}\sin\theta; \tag{16.3}$$

with the principal axis $R_{1i,o}$ and $R_{2i,o}$ defined through

$$R_{1,2i} = \xi R_{1,2};\ R_{1,2o} = \eta R_{1,2};\ 0 < \xi < 1;\ 1 < \eta. \tag{16.4}$$

An incident wave is given by

$$w^i(x,y,t) = 1/2\ e^{-i[k(x\sin\theta_o - y\cos\theta_o - \omega t]}, \tag{16.5}$$

where θ_o is the angle of incidence and k is the wave number. The free fild associated with the incident wave (16.5) follows to be

$$w^{ff}(x,y,t,) = e^{-i[k\,x\sin\theta_o - \omega t]} \cos(ky\cos\theta_o), \tag{16.6}$$

thus, the vector $\underset{\sim}{f}$ in Eq. (11) should be replaced by

$$\underset{\sim}{f} \equiv \begin{bmatrix} -\underset{\sim}{w}^{ff} \\ \\ -w^{ff}_{\sim n} \end{bmatrix}$$

$$[w_j]^{ff} \equiv w^{ff}(\underset{\sim}{r}_j)$$

$$[w_j]^{ff}_n \equiv \frac{\partial w^{ff}(\underset{\sim}{r}_j)}{\partial n}, \quad \underset{\sim}{r}_j \in C,\ j=1,2,\ldots,N. \tag{16.7}$$

where $\underset{\sim}{r}_j$ represents the "observation" points along the interface C. The N "observation" points are chosen to be at values of $\theta = \frac{\pi}{N+1} n$, n=1,2,..., N=23. The source points along C_1 and C_2 are taken to be at angles $\theta = \frac{\pi}{M+1} m$, m=1,2,...,M=11 (=L). For angle of incidence $\theta_o = 30^o$, frequency $\omega = 0.79\ s^{-1}$ and for various choices of the $C_{1,2}$ interfaces (i.e. for different values of the parameters ξ and η in 16.4) the absolute value of surface displacement field is presented by Fig. 12. Comparison with the exact solution (represented by solid circles) of the problem under consideration given by Wong and Trifunac, (1974b) indicates excellent agreement between the two solutions for a wide range of the parameters ξ and η. Case of vertical incidence is depicted by Fig. 13. Again, agreement between the approximate and the exact solution is excellent. To test the accuracy of the source method solution at higher frequencies, the

surface displacement amplitude is evaluated for circular frequency 1.57 s^{-1} and angle of incidence 30° and 0° (Fig. 14 and 15, respectively). The case of vertical incidence and ciruclar frequency 2.36 s^{-1} is depicted by Fig. 16. Figures 12-16 demonstrate high accuracy with which the source method predicts the amplitude of the surface displacement field for a wide range of frequencies of the incident wave field.

Similarly to the results derived for semi-cylindrical alluvial valley, the surface displacement field in present model is accurate for a wide range of source locations, provided the sources are not placed in immediate vicinity of the interface.

It should be pointed out that the accuracy of the surface displacement field is excellent not only inside the alluvial valley but along the surface of the half-space as well.

To summarize, the analysis of the anti-plane strain model leads to the following conclusions:

1. The source method appears to provide very good results for a wide range of frequencies.
2. Approximate results are more accurate at lower frequencies for a given number of sources.
3. As the number of sources increases, the error decreases.
4. Singularities in the Green's functions of the scattered wave field prohibit the placing the source surfaces very close to the interface.

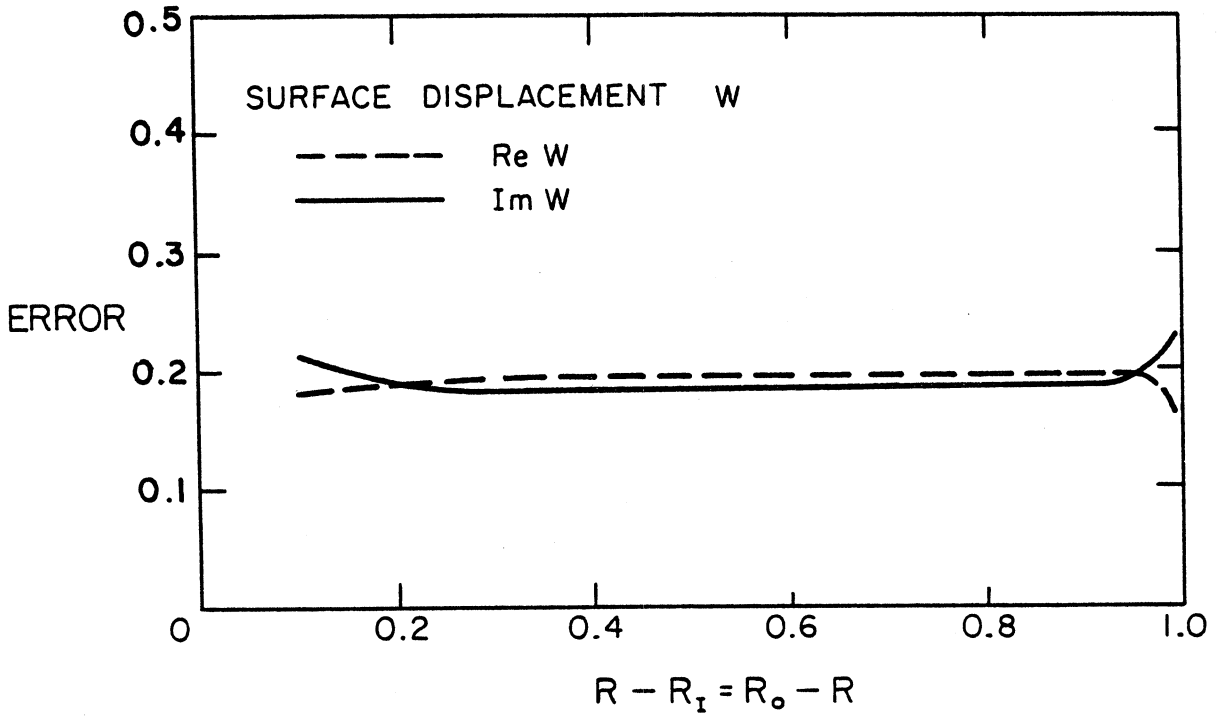

Fig. 11. Relative Error of Surface Displacement Field: Horizontal Incidence of a Plane SH-Wave Upon a Semi-Cylindrical Alluvial Valley Embedded in a Half-Space.
($y=0$, $-2R \leq x \leq 2R$ at 46 equallly spaced points; $\omega=0.79s^{-1}$, $R=1$, $\beta_1=\mu_1=1$, $\mu_2=0.167$, $\beta_2=0.5$, $M=L=11$, $N=23$).

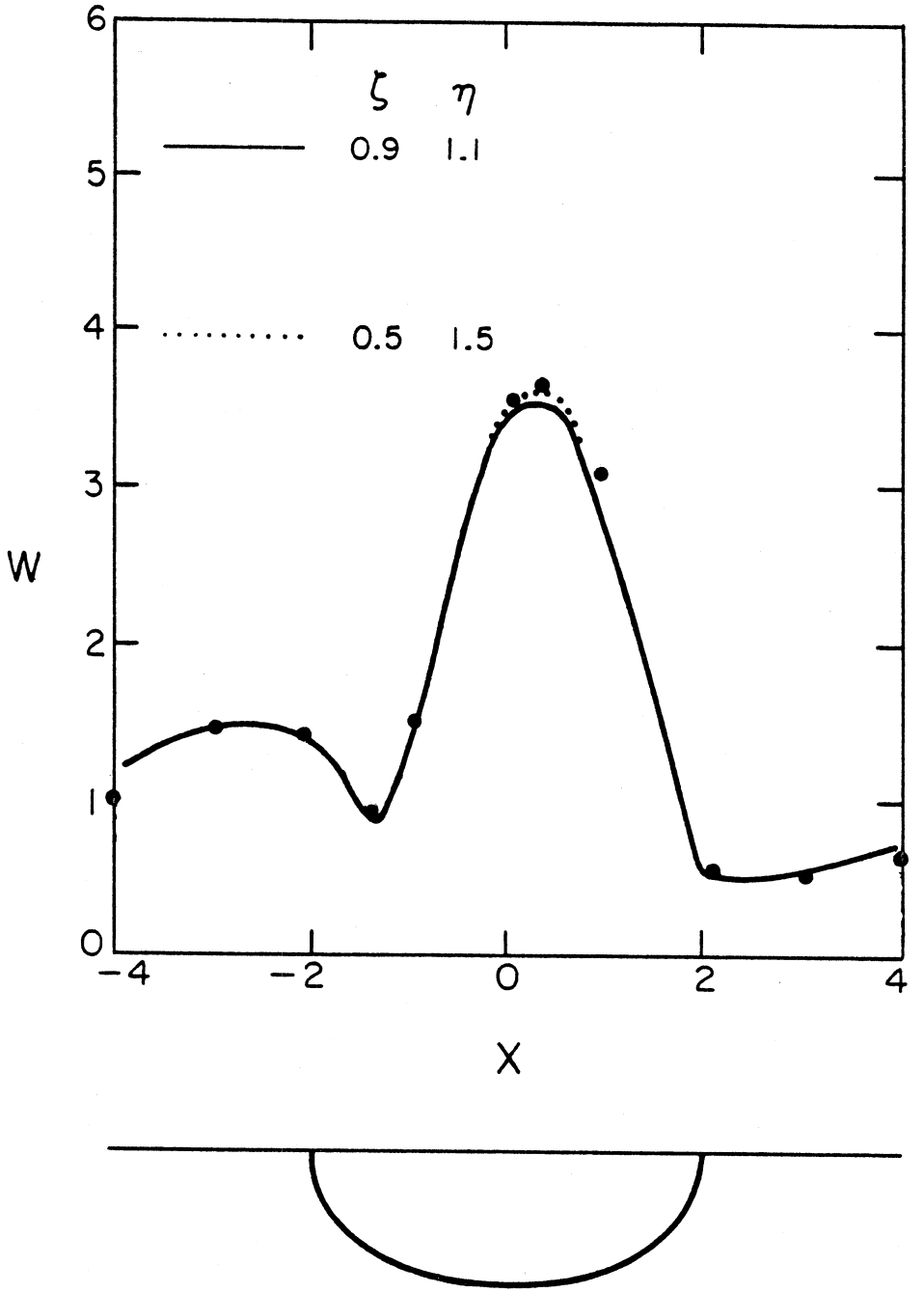

Fig. 12 Surface Displacement Amplitude for Antiplane Strain Model of Semi-Elliptical Alluvial Valley Embedded into a Half-Space. Exact Solution-Nonconnected Solid Circles; Source Method Solution - Different Types of Lines.

(ω=0.79 s^{-1}, θ_o=30°, R_1=2, R_2=1.4, μ_1=β_1=1, μ_2=0.167, β_2=0.5, N=23, M=11, L=11)

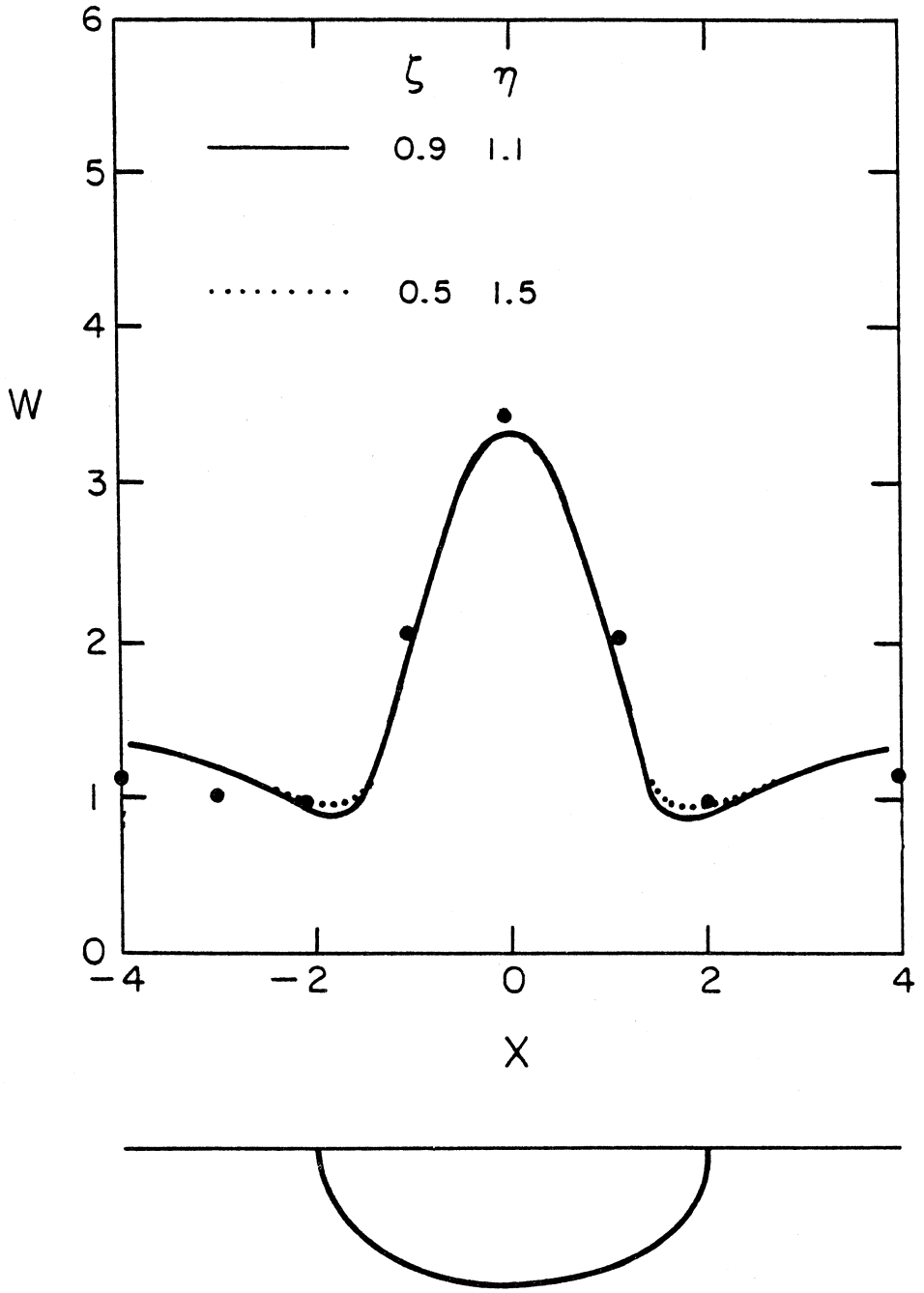

Fig. 13 Surface Displacement Amplitude for Antiplane Strain Model of Semi-Elliptical Alluvial Valley Embedded into a Half-Space. Exact Solution-Nonconnected Solid Circles; Source Method Solution - Different Types of Lines.
(ω=0.79 s^{-1}, θ_o=0°, R_1=2, R_2=1.4, μ_1=β_1=1, μ_2=0.167, β_2=0.5, N=23, M=11, L=11)

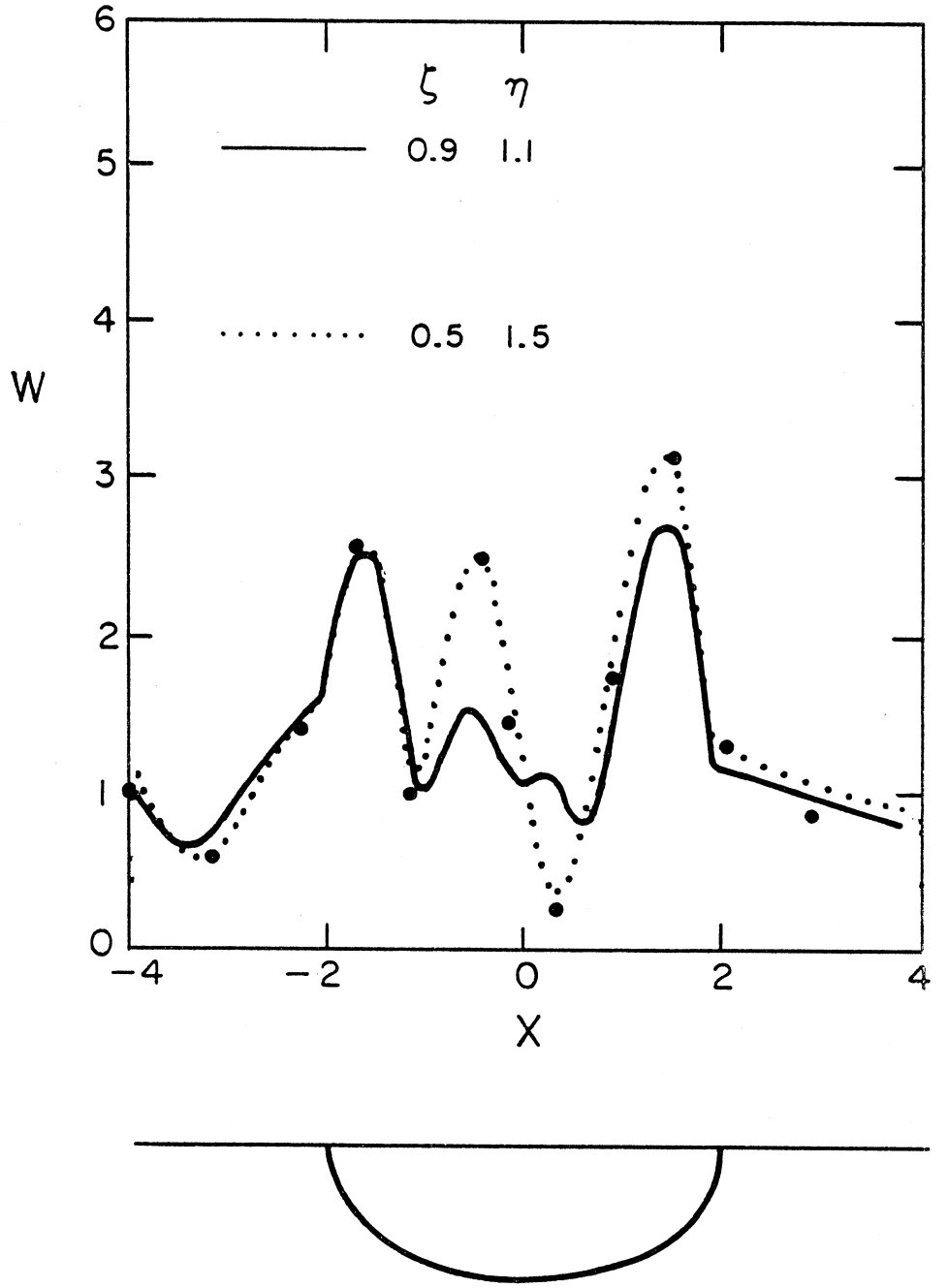

Fig. 14 Surface Displacement Amplitude for Antiplane Strain Model of Semi-Elliptical Alluvial Valley Embedded Into a Half-Space. Exact Solution-Nonconnected Solid Circles; Source Method Solution - Different Types of Lines.
(ω=1.57 s^{-1}, θ_o=30°, R_1=2, R_2=1.4, μ_1=β_1=1, μ_2=0.167, β_2=0.5, N=23, M=11, L=11)

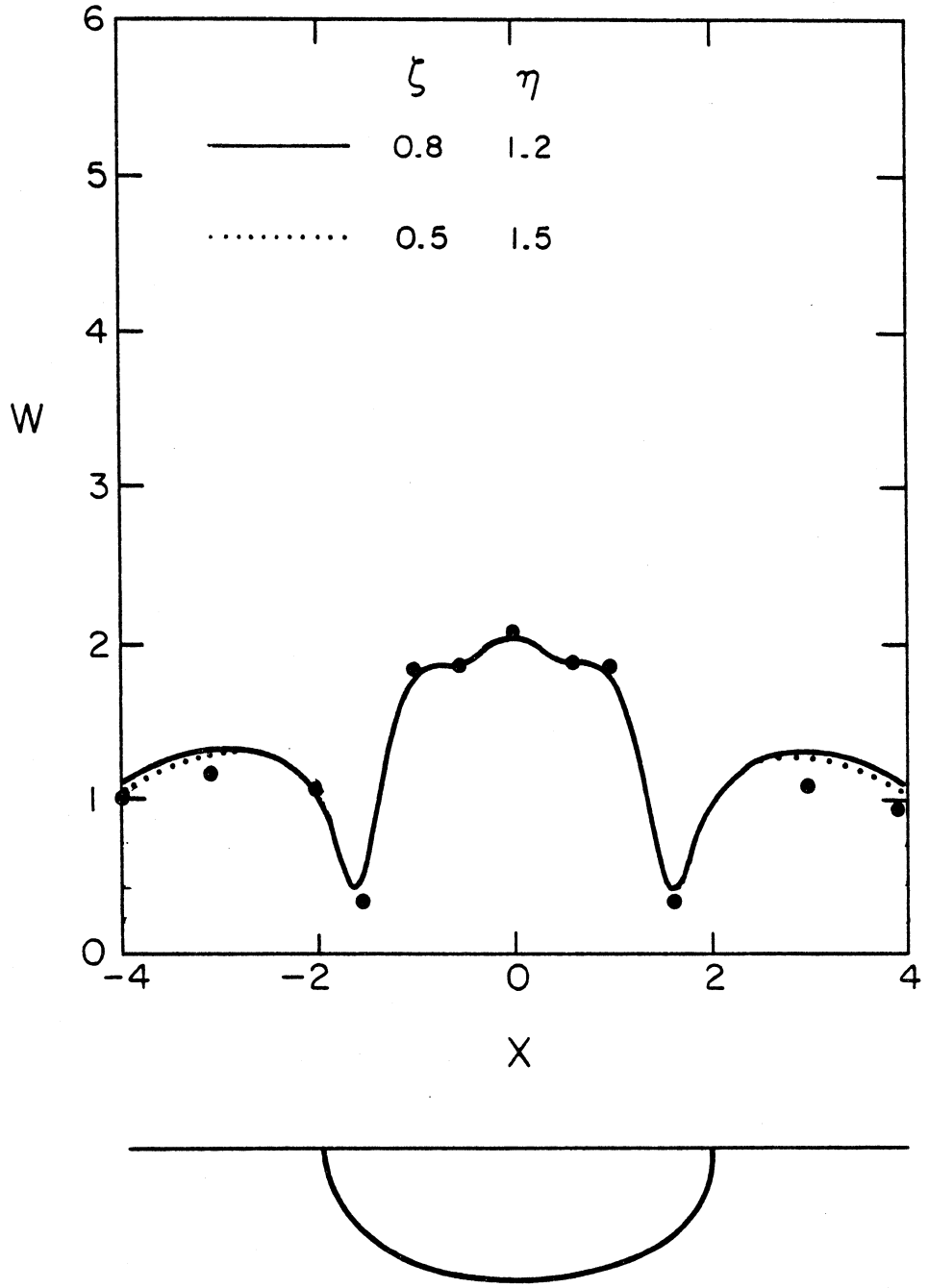

Fig. 15 Surface Displacement Amplitude for Antiplane Strain Model of Semi-Elliptical Alluvial Valley Embedded Into a Half-Space. Exact Solution-Nonconnected Solid Circles; Source Method Solution - Different Types of Lines.
(ω=1.57 s^{-1}, θ_o=0°, R_1=2, R_2=1.4, μ_1=β_1=1, μ_2=0.167, β_2=0.5, N=23, M=11, L=11)

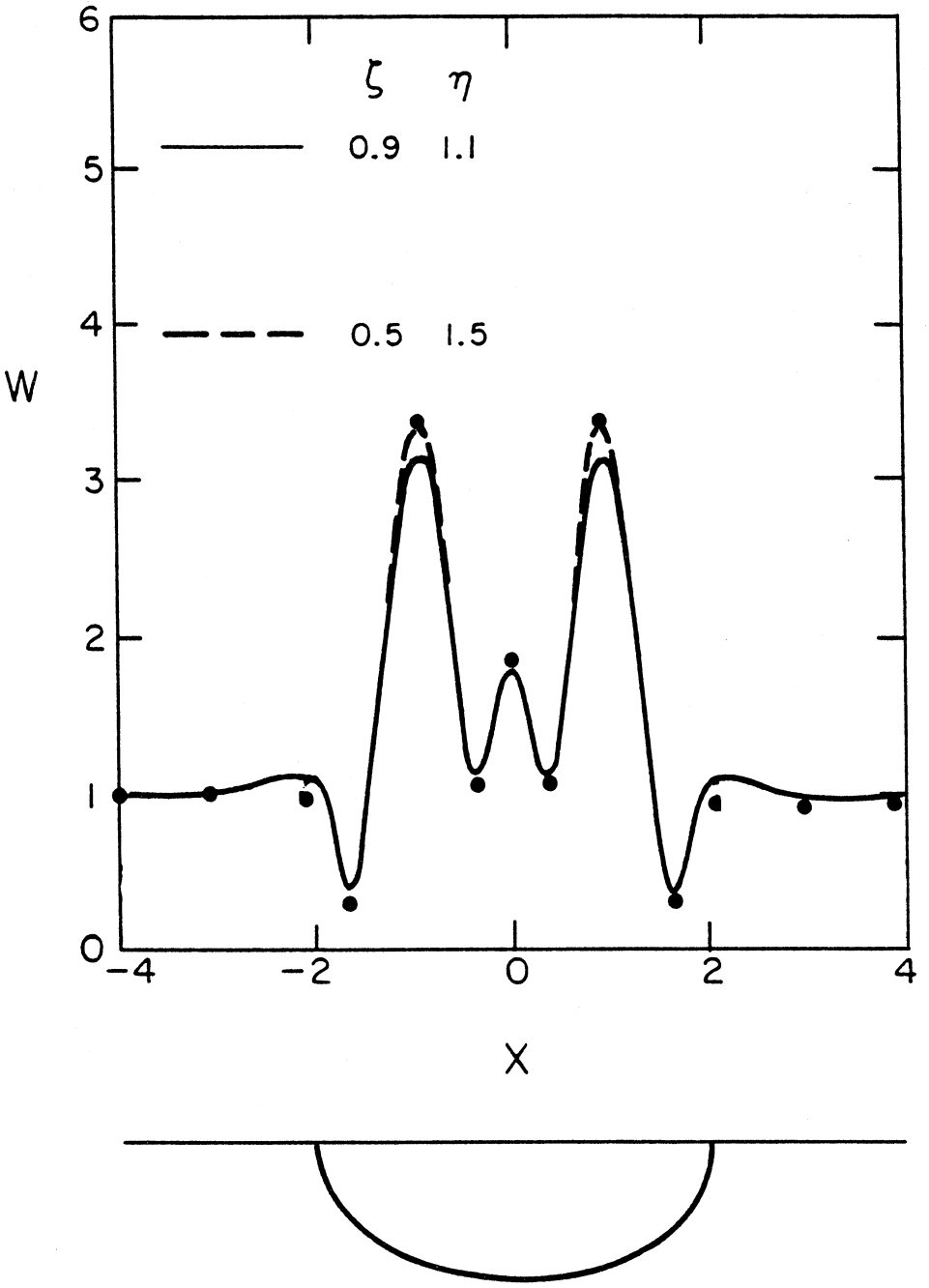

Fig. 16 Surface Displacement Amplitude for Antiplane Strain Model of Semi-Elliptical Alluvial Valley Embedded Into a Half-Space. Exact Solution-Nonconnected Solid Circles; Source Method Solution - Different Types of Lines.
(ω=2.36 s^{-1}, θ_o=0°, R_1=2, R_2=1.4, μ_1=β_1=1, μ_2=0.167, β_2=0.5, N=23, M=11, L=11).

This concludes the analysis of scattering of the plane SH-waves by an alluvial valley using the source method. Next model to be considered is the plane-strain one. First, the theoretical basis of the source method for the plane stain model is presented in detail. Then, the accuracy of the method is investigated by using the exact solution for a full-space problem. Finally, diffraction of plane P, SV and Rayleigh waves by a semi-elliptical alluvial valley is presented.

Plane Strain Model:

An outline of the source method formulation of the plane strain model is presented next. The equation of motion for a steady-state wave propagation is given by

$$\nabla^2 \begin{Bmatrix} \phi_j \\ \psi_j \end{Bmatrix} + \begin{Bmatrix} h_j^2 \phi_j \\ k_j^2 \psi_j \end{Bmatrix} = 0 \quad ; \quad j = 1, 2, \tag{17.1}$$

where ϕ and ψ represent the pressure and shear wave potentials, respectively, with corresponding wave numbers h and k. The velocity of P waves is denoted by α_j, j = 1, 2, and of the S waves by β_j, j = 1, 2. The components of the displacement vector $\underset{\sim}{u} = u\underset{\sim}{i} + v\underset{\sim}{j}$ are related to the potentials ϕ and ψ by (Achenbach, 1973)

$$\begin{aligned} u_j &= \frac{\partial \phi_j}{\partial x} + \frac{\partial \psi_j}{\partial y} \quad , j = 1, 2 \\ v_j &= \frac{\partial \phi_j}{\partial y} - \frac{\partial \psi_j}{\partial x} \quad . \end{aligned} \tag{17.2}$$

For a given incident wave, the total displacement field is specified through

$$u_1 = u^i + u_1^s \tag{18.1}$$

$$v_1 = v^i + v_1^s \tag{18.2}$$

$$u_2 = u_2^s \tag{18.3}$$

$$v_2 = v_2^s \quad , \tag{18.4}$$

where the superscript s denotes the scattered wave field. The boundary conditions are specified by (see Figure 1)

$$\sigma_{xy_j} = 0 \quad , \qquad y=0 \text{ and } \underset{\sim}{r} \in \mathcal{D}_j \quad , \; j=1,2, \tag{19.1}$$

$$\sigma_{yy_j} = 0 \quad , \tag{19.2}$$

Perfect bonding along the C gives

$$u^i + u_1^s = u_2^s \tag{20.1}$$

$$v^i + v_1^s = v_2^s \tag{20.2}$$

$$\text{for } \underset{\sim}{r} \in C$$

$$\sigma_{nn}^i + \sigma_{nn_1}^s = \sigma_{nn_2}^s \tag{20.3}$$

$$\sigma_{nt}^i + \sigma_{nt_1}^s = \sigma_{nt_2}^s \quad , \tag{20.4}$$

with σ_{nn} and σ_{nt} denoting the normal and shear stress, respectively. It is assumed that the scattered field is expressed in terms of single layer potentials

$$\phi_j^s = \int_{C_j} g_j^{\phi}(\underset{\sim}{r}_o)\phi_j(\underset{\sim}{r} \mid \underset{\sim}{r}_o)dS_o \tag{21.1}$$

$$j=1,2,$$

$$\psi_j^s = \int_{C_j} g_j^{\psi}(\underset{\sim}{r}_o)\psi_j(\underset{\sim}{r} \mid \underset{\sim}{r}_o)dS_o \quad . \tag{21.2}$$

The curves C_1 and C_2 are defined in the half-space, inside and outside of the interface C, respectively (Figure 2). The density functions g_j^{ϕ} and g_j^{ψ}, j=1,2, are yet to be determined. The Green's functions $\phi_j(\underset{\sim}{r} \mid \underset{\sim}{r}_o)$ and $\psi_j(\underset{\sim}{r},\underset{\sim}{r}_o)$ must satisfy the equation

$$\nabla^2 \begin{Bmatrix} \phi_j(\underset{\sim}{r} \mid \underset{\sim}{r}_o) \\ \\ \psi_j(\underset{\sim}{r} \mid \underset{\sim}{r}_o) \end{Bmatrix} + \begin{Bmatrix} h_j^2 \phi_j(\underset{\sim}{r} \mid \underset{\sim}{r}_o) \\ \\ k_j^2 \psi_j(\underset{\sim}{r} \mid \underset{\sim}{r}_o) \end{Bmatrix} = -\delta(|\underset{\sim}{r} - \underset{\sim}{r}_o|) \tag{22}$$

and should satisfy the boundary conditions

$$\sigma_{xy_j}(\underset{\sim}{r} \mid \underset{\sim}{r}_o) = 0 \tag{23.1}$$

$$y=0 \text{ and } r_j \varepsilon \mathcal{D}_j \quad , \; j=1,2,$$

$$\sigma_{yy_j}(\underset{\sim}{r} \mid \underset{\sim}{r}_o) = 0. \tag{23.2}$$

The explicit solution for the Green's functions is given in Appendix A. If it is assumed that the density functions are of the form

$$g_1^{\phi}(\underset{\sim}{r}_o) = \sum_{n=1}^{M} a_m \delta(|\underset{\sim}{r}_o - \underset{\sim}{r}_m|) \quad , \quad \underset{\sim}{r}_m \varepsilon C_1 \tag{24.1}$$

$$g_1^{\psi}(\underset{\sim}{r}_o) = \sum_{m=1}^{M} b_m \delta(|\underset{\sim}{r}_o - \underset{\sim}{r}_m|) \quad , \quad \underset{\sim}{r}_m \varepsilon C_1 \tag{24.2}$$

$$g_2^{\phi}(\underset{\sim}{r}_o) = \sum_{\ell=1}^{L} c_\ell \delta(|\underset{\sim}{r}_o - \underset{\sim}{r}_\ell|) \quad , \quad \underset{\sim}{r}_\ell \varepsilon C_2 \tag{24.3}$$

$$g_2^{\psi}(\underset{\sim}{r}_o) = \sum_{\ell=1}^{L} d_\ell \delta(|\underset{\sim}{r}_o - \underset{\sim}{r}_\ell|) \quad , \quad \underset{\sim}{r}_\ell \varepsilon C_2 , \tag{24.4}$$

the scattered wave field then becomes

$$\phi_1^s(\underset{\sim}{r}) = \sum_{m=1}^{M} a_m \phi_1(\underset{\sim}{r} \mid \underset{\sim}{r}_m) \quad , \quad \underset{\sim}{r}_m \varepsilon C_1 \tag{25.1}$$

$$\psi_1^s(\underset{\sim}{r}) = \sum_{m=1}^{M} b_m \psi_1(\underset{\sim}{r} \mid \underset{\sim}{r}_m) \qquad , \quad \underset{\sim}{r}_m \varepsilon C_1 \tag{25.2}$$

$$\phi_2^s(\underset{\sim}{r}) = \sum_{\ell=1}^{L} c_\ell \phi_2(\underset{\sim}{r} \mid \underset{\sim}{r}_\ell) \qquad , \quad \underset{\sim}{r}_\ell \varepsilon C_2 \tag{25.3}$$

$$\psi_2^s(\underset{\sim}{r}) = \sum_{\ell=1}^{L} d_\ell \psi_2(\underset{\sim}{r} \mid \underset{\sim}{r}_\ell) \qquad , \quad \underset{\sim}{r}_\ell \varepsilon C_2 \, . \tag{25.4}$$

Substituting the scattered wave field (25) into the continuity condition (2) at N observation points along C, the following result is derived

$$\underset{\sim\sim}{G}\underset{\sim}{z} = \underset{\sim}{f} \qquad , \quad \underset{\sim}{r} \varepsilon C \, . \tag{26.1}$$

The $\underset{\sim}{f}$ and $\underset{\sim}{z}$ are vectors of order [4N x 1] and [2(M+L) x 1], while $\underset{\sim}{G}$ is known 4N x 2(M+L) matrix, defined by

$$\underset{\sim}{G} \equiv -\begin{bmatrix} \underset{\sim}{U}^{\phi 1} & \underset{\sim}{U}^{\psi 1} & -\underset{\sim}{U}^{\phi 2} & -\underset{\sim}{U}^{\psi 2} \\ \underset{\sim}{V}^{\phi 1} & \underset{\sim}{V}^{\psi 1} & -\underset{\sim}{V}^{\phi 2} & -\underset{\sim}{V}^{\psi 2} \\ \underset{\sim}{\Sigma}_{nn}^{\phi 1} & \underset{\sim}{\Sigma}_{nn}^{\psi 1} & -\underset{\sim}{\Sigma}_{nn}^{\phi 2} & -\underset{\sim}{\Sigma}_{nn}^{\psi 2} \\ \underset{\sim}{\Sigma}_{nt}^{\phi 1} & \underset{\sim}{\Sigma}_{nt}^{\psi 1} & -\underset{\sim}{\Sigma}_{nt}^{\phi 2} & -\underset{\sim}{\Sigma}_{nt}^{\psi 2} \end{bmatrix} \tag{26.2}$$

with

$$\underset{\sim}{z}^T = [a_1, a_2, \ldots, a_M; \; b_1, b_2, \ldots, b_M; \; c_1, c_2, \ldots, c_L; \; d_1, d_2, \ldots, d_L] \tag{26.3}$$

$$\underset{\sim}{f}^T = [-\underset{\sim}{u}^{inc}, -\underset{\sim}{v}^{inc}, -\underset{\sim}{\sigma}_{nn}^{inc}, -\underset{\sim}{\sigma}_{nt}^{inc}] \tag{26.4}$$

$$\underset{\sim}{u}^{inc} \equiv [u^{inc}(\underset{\sim}{r}_i)] \qquad i=1,\ldots,N \tag{26.5}$$

$$\underset{\sim}{v}^{inc} \equiv [v^{inc}(\underset{\sim}{r}_i)] \tag{26.6}$$

$$\underset{\sim}{\sigma}^{inc}_{nn} \equiv \left[\sigma^{inc}_{nn}(\underset{\sim}{r}_i)\right] \tag{26.7}$$

$$\underset{\sim}{\sigma}^{inc}_{nt} \equiv \left[\sigma^{inc}_{nt}(\underset{\sim}{r}_i)\right] \tag{26.8}$$

$$\underset{\sim}{U}^{\phi^S_1} \equiv \left[u^{\phi^S_1}(\underset{\sim}{r}_i \mid \underset{\sim}{r}_j)\right] \qquad i=1,\ldots,N;\ j=1,\ldots,M;\ \ell=1,\ldots,L$$

$$\underset{\sim}{U}^{\psi^S_1} \equiv \left[u^{\psi^S_1}(\underset{\sim}{r}_i \mid \underset{\sim}{r}_j)\right]$$

$$\underset{\sim}{U}^{\phi^S_2} \equiv \left[u^{\phi^S_2}(\underset{\sim}{r}_i \mid \underset{\sim}{r}_\ell)\right]$$

$$\underset{\sim}{U}^{\psi^S_2} \equiv \left[u^{\psi^S_2}(\underset{\sim}{r}_i \mid \underset{\sim}{r}_\ell)\right]$$

$$\underset{\sim}{V}^{\phi^S_1} \equiv \left[v^{\phi^S_1}(\underset{\sim}{r}_i \mid \underset{\sim}{r}_j)\right]$$

$$\underset{\sim}{V}^{\psi^S_1} \equiv \left[v^{\psi^S_1}(\underset{\sim}{r}_i \mid \underset{\sim}{r}_j)\right]$$

$$\underset{\sim}{V}^{\phi^S_2} \equiv \left[v^{\phi^S_2}(\underset{\sim}{r}_i \mid \underset{\sim}{r}_\ell)\right] \tag{26.9}$$

$$\underset{\sim}{V}^{\psi^S_2} \equiv \left[v^{\psi^S_2}(\underset{\sim}{r}_i \mid \underset{\sim}{r}_\ell)\right]$$

$$\underset{\sim}{\Sigma}^{\phi^S_1}_{nn} \equiv \left[\sigma^{\phi^S_1}_{nn}(\underset{\sim}{r}_i \mid \underset{\sim}{r}_j)\right]$$

$$\underset{\sim}{\Sigma}^{\psi^S_1}_{nn} \equiv \left[\sigma^{\psi^S_1}_{nn}(\underset{\sim}{r}_i \mid \underset{\sim}{r}_j)\right]$$

$$\underset{\sim}{\Sigma}^{\phi^S_2}_{nn} \equiv \left[\sigma^{\phi^S_2}_{nn}(\underset{\sim}{r}_i \mid \underset{\sim}{r}_\ell)\right]$$

$$\underset{\sim}{\Sigma}^{\psi^S_2}_{nn} \equiv \left[\sigma^{\psi^S_2}_{nn}(\underset{\sim}{r}_i \mid \underset{\sim}{r}_\ell)\right]$$

$$
\begin{aligned}
\underset{\sim}{\Sigma}^{\phi_1^s}_{nt} &\equiv \left[\sigma^{\phi_1^s}_{nt}(\underset{\sim}{r}_i \mid \underset{\sim}{r}_j)\right] \\
\underset{\sim}{\Sigma}^{\psi_1^s}_{nt} &\equiv \left[\sigma^{\psi_1^s}_{nt}(\underset{\sim}{r}_i \mid \underset{\sim}{r}_j)\right] \\
\underset{\sim}{\Sigma}^{\phi_2^s}_{nt} &\equiv \left[\sigma^{\phi_2^s}_{nt}(\underset{\sim}{r}_i \mid \underset{\sim}{r}_\ell)\right] \\
\underset{\sim}{\Sigma}^{\psi_2^s}_{nt} &\equiv \left[\sigma^{\psi_2^s}_{nt}(\underset{\sim}{r}_i \mid \underset{\sim}{r}_\ell)\right] .
\end{aligned}
\tag{26.9}
$$

In other words, the matrix $\underset{\sim}{G}$ incorporates displacement and stress field information, due to Green's functions ϕ_j, and ψ_j, j=1,2,; vector $\underset{\sim}{f}$ represents the displacement and stress field due to incident waves, and vector $\underset{\sim}{z}$ consists of the unknown coefficients (source intensities). Solving (26.1) in the least square sense, it follows that

$$
\underset{\sim}{z} = (\underset{\sim}{G}^* \underset{\sim}{G})^{-1} \underset{\sim}{G}^* \underset{\sim}{f} . \tag{27}
$$

Once the expansion coefficients are known, the scattered wave field is determined at any point of the media through the use of (25).

At this point, a systematic error analysis is done to determine the accuracy of the method for this model, based on few exact solutions which are available for simple geometries (e.g., Pao and Mow, 1973). The choice of sources and their distribution is studied to determine in what way they influence the accuracy of the method.

Scattering and Diffraction of the Plane P-Wave by an Elastic Cylindrical Inclusion

The geometry of the problem is depicted by Figure 17. An elastic cylinder embedded in an elastic full space is subjected to an incident plane P-wave:

$$\phi^i = e^{-ih_1 x} , \tag{28}$$

where the factor $e^{+i\omega t}$ is being understood.

All the equations stated for the half-space model remain formally the same, except for the stress free boundary conditions (19) and (23) which are missing in the full space problem. Therefore, the Green's functions (22) are specified by (Pao and Mow, 1973), as

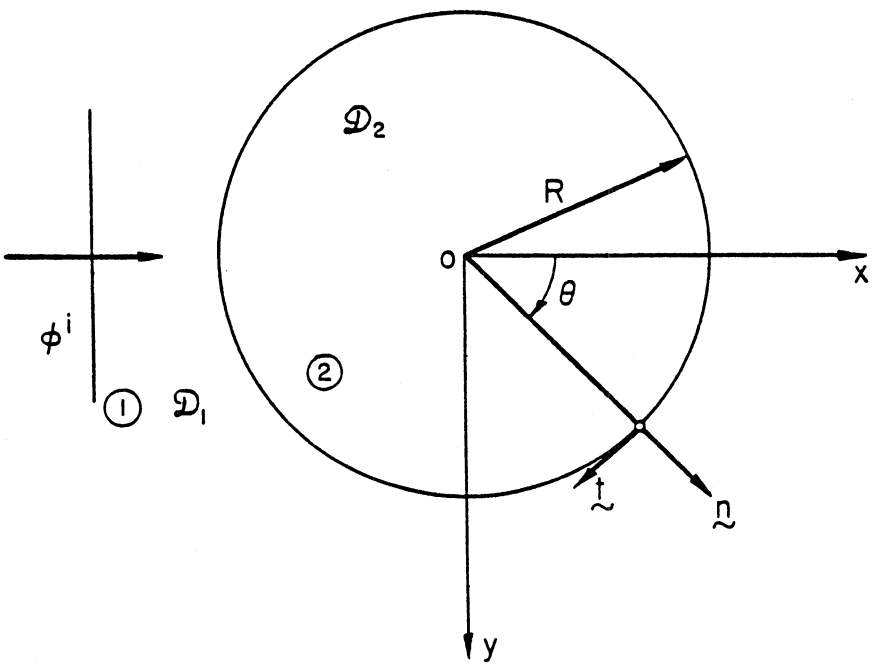

Figure 17

$$\phi_j(\underset{\sim}{r} \mid \underset{\sim}{r}_s) = H_o^{(2)}(h_j|\underset{\sim}{r} - \underset{\sim}{r}_s|) \tag{29.1}$$

$$\psi_j(\underset{\sim}{r} \mid \underset{\sim}{r}_s) = H_o^{(2)}(k_j|\underset{\sim}{r} - \underset{\sim}{r}_s|) \ .$$

Assuming the scattered wave field to be of the form (25) the corresponding displacement and stress fields can be correlated explicitly according to Appendix A. In other words the elements of the equation (26) are known and one can proceed with the numerical evaluation of the results.

Exact Solution

The exact solution for the total wave field is given by (Pao and Mow, 1973) for an incident plane P-wave

$$\phi_1 = \phi^i + \phi_1^s \tag{30.1}$$

$$\psi_1 = \psi_1^s \tag{30.2}$$

$$\phi_2 = \phi_2^s \tag{30.3}$$

$$\psi_2 = \psi_2^s \ , \tag{30.4}$$

where the scattered wave field is defined by

$$\phi_1^s = \sum_{n=0}^{\infty} A_n H_n^{(2)}(h_1 r)\cos n\theta \quad ; \qquad \underset{\sim}{r} \in \mathcal{D}_1 \tag{31.1}$$

$$\psi_1^s = \sum_{n=0}^{\infty} B_n H_n^{(2)}(k_1 r)\sin n\theta \quad ; \tag{31.2}$$

$$\phi_2^s = \sum_{n=0}^{\infty} C_n J_n(h_2 r)\cos n\theta \quad ; \qquad \underset{\sim}{r} \in \mathcal{D}_1 \tag{31.3}$$

$$\psi_2^s = \sum_{n=0}^{\infty} D_n J_n(k_2 r)\sin n\theta \ . \tag{31.4}$$

The continuity of the stress and displacement fields implies the expansion coefficients through

$$\left[A_n, B_n, C_n, D_n\right]^T = \underset{\sim}{B}^{-1}\underset{\sim}{b} \quad , \qquad n=0,1,2,\ldots, \tag{32.1}$$

where the elements of the matrix $\underset{\sim}{B}$ and the vector $\underset{\sim}{b}$ are defined to be

$$B_{11} = h_1 H_n^{(2)\prime}(h_1R) \quad ; \qquad B_{12} = \frac{n}{R} H_n^{(2)}(k_1R)$$

$$B_{13} = -h_2 J_n'(h_2R) \quad ; \qquad B_{14} = -\frac{n}{R} J_n(k_2R)$$

$$B_{21} = -\frac{n}{R} H_n^{(2)}(h_1R) \quad ; \qquad B_{22} = -k_1 H_n^{(2)\prime}(k_1R)$$

$$B_{23} = \frac{n}{R} J_n(k_2R) \quad ; \qquad B_{24} = k_2 J_n'(k_2R)$$

$$B_{31} = -k_1^2 H_n^{(2)}(h_1R) - \frac{2}{R} h_1) H_n^{(2)'}(h_1R) + \frac{2}{R^2} n^2 H_n^{(2)}(h_1R) \quad ;$$

$$B_{32} = -\frac{2}{R^2} n H_n^{(2)}(k_1R) + \frac{2}{R} n\, k_1 H_n^{(2)\prime}(k_1R)$$

$$B_{33} = -\mu_2/\mu_1 \left\{-k_2^2 J_n(h_2R) - \frac{2}{R} h_2 J_n'(h_2R) + \frac{2}{R^2} n^2 J_n(h_2R)\right\}$$

$$B_{34} = -\mu_2/\mu_1 \left\{-\frac{2}{R^2} n J_n(k_2R) + \frac{2}{R} n k_2 J_n'(k_2R)\right\}$$

$$B_{41} = \frac{2}{R^2} n H_n^{(2)}(h_1R) - \frac{2}{R} n h_1 H_n^{(2)\prime}(h_1R)$$

$$B_{42} = -k_1^2 H_n^{(2)\prime\prime}(k_1R) + \frac{1}{R} k_1 H_n^{(2)\prime}(k_1R) - \frac{n^2}{R^2} H_n^{(2)}(k_1R)$$

$$B_{43} = -\mu_2/\mu_1 \left\{\frac{2}{R^2} n J_n(h_2R) - \frac{2}{R} n h_2 J_n'(h_2R)\right\}$$

$$B_{44} = -\mu_2/\mu_1 \left\{-k_2^2 J_n''(k_2R) + \frac{k_2}{R} J_n'(k_2R) - \frac{n}{R^2} J_n(k_2R)\right\} \tag{32.2}$$

$$b_1 = -h_1 \varepsilon_n (-1)^n J_n'(h_1 R) \quad ; \quad \varepsilon_n = \begin{cases} 1, & n = 0 \\ 2, & n = 1, 2, \ldots \end{cases}$$

$$b_2 = \frac{n}{R} \varepsilon_n (-i)^n J_n(h_1 R)$$

$$b_3 = -\varepsilon_n (-i)^n \{ -k_1^2 J_n(h_1 R) - \frac{2}{R} h_1 J_n'(h_1 R) + \frac{2}{R^2} n^2 J_n(h_1 R) \}$$

$$B_4 = \frac{2n}{R^2} \varepsilon_n (-i)^n \{ h_1 R J_n'(h_1 R) - J_n(h_1 R) \} \quad . \tag{32.3}$$

For the source method, the surfaces C_1 and C_2 (5) are chosen to be the semi-cylinders $r = R_I$ and $r = R_0$, respectively, with $0 < R_I < R < R_0 < \infty$. The sources and the observation points are equally spaced along the C_1, $_2$ and C, respectively. Initially, the number of sources along each surface is chosen to be six (M=L=6) and the number of observation points along the interface to be twelve (N=12). The scattered wave field is evaluated at N observation points along the interface by the exact and the source method. The results are then compared and the relative error evaluated through the error functional (15). To further simplify the error analysis an average error is introduced

$$E = [e\,(R_e\, Z) + e\,(I_m\, Z)] \,/\, 2, \tag{33}$$

where each of the terms e(Z) have been defined by (15).

For the circular frequency of the incident P-wave $\omega = 1.57 s^{-1}$ the relative error for the scattered field ϕ_1^s, ψ_1^s, ϕ_2^s, and ψ_2^s is shown by Figs. 18 and 19. These results indicate that the relative error is fairly constant for different locations of the sources. The exception is the wave potential ψ_2^s with the corresponding relative error being higher with respect to the error associated with the rest of the potentials. Indeed, throughout the numerical evaluation of the error results, it

was established that for the same number of inner and outer sources, the relative error for the scattered field inside the inclusion is higher in comparison with the error for the half-space field. In particular higher error has been associated with the shear wave potential ψ_2^s . This suggests that it might be necessary to take a larger number of the shear sources to model the ψ_2^s field more accurately.

Error results for the two fold increase of sources and observation points to twelve (M=L=12) and twenty-four (N=24) points, respectively are presented by Figs. 20 and 21. Granting that the frequency of the incident waves is substantially higher than that presented in the previous two figures, the accuracy of the source method result is better for larger number of sources. Although no claim of the uniformity of this process can be made at this point, the error analysis for the plane strain model appears to provide analogous results to the ones found in the study of the anti-plane strain model: approximate results are more accurate at the lower frequencies for a fixed number of sources. As the number of sources increases, the relative error becomes smaller.

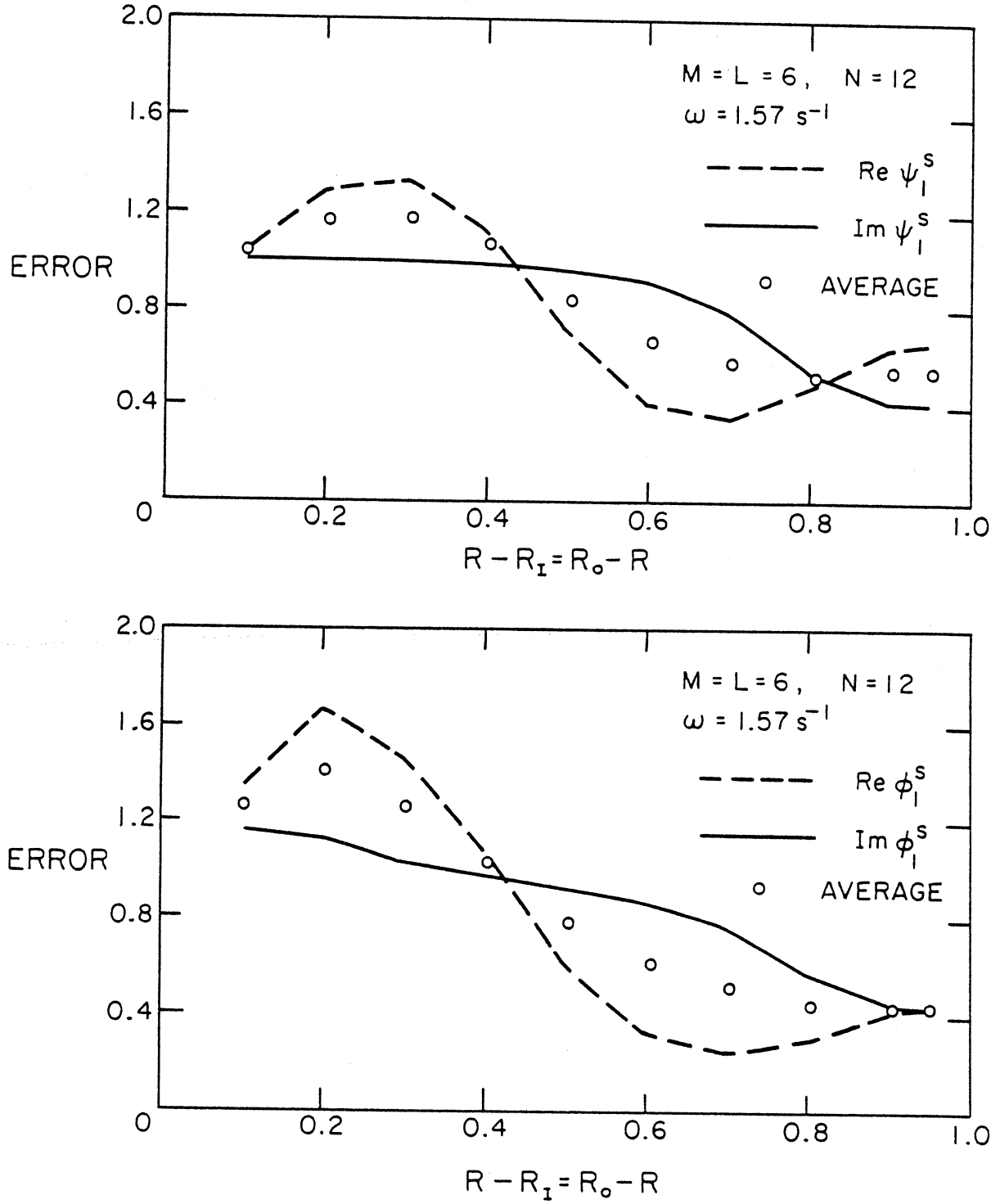

Fig. 18. Relative Error for Scattered Field Along the Interface: Horizontal Incidence of a Plane P-Wave Upon a Circular Inclusion in a Full-Space. (ω=1.57s^{-1}, R=μ_1=β_1=1, α_1=1.45, μ_2=β_2=0.6, α_2=0.9, M=L=6, N=12)

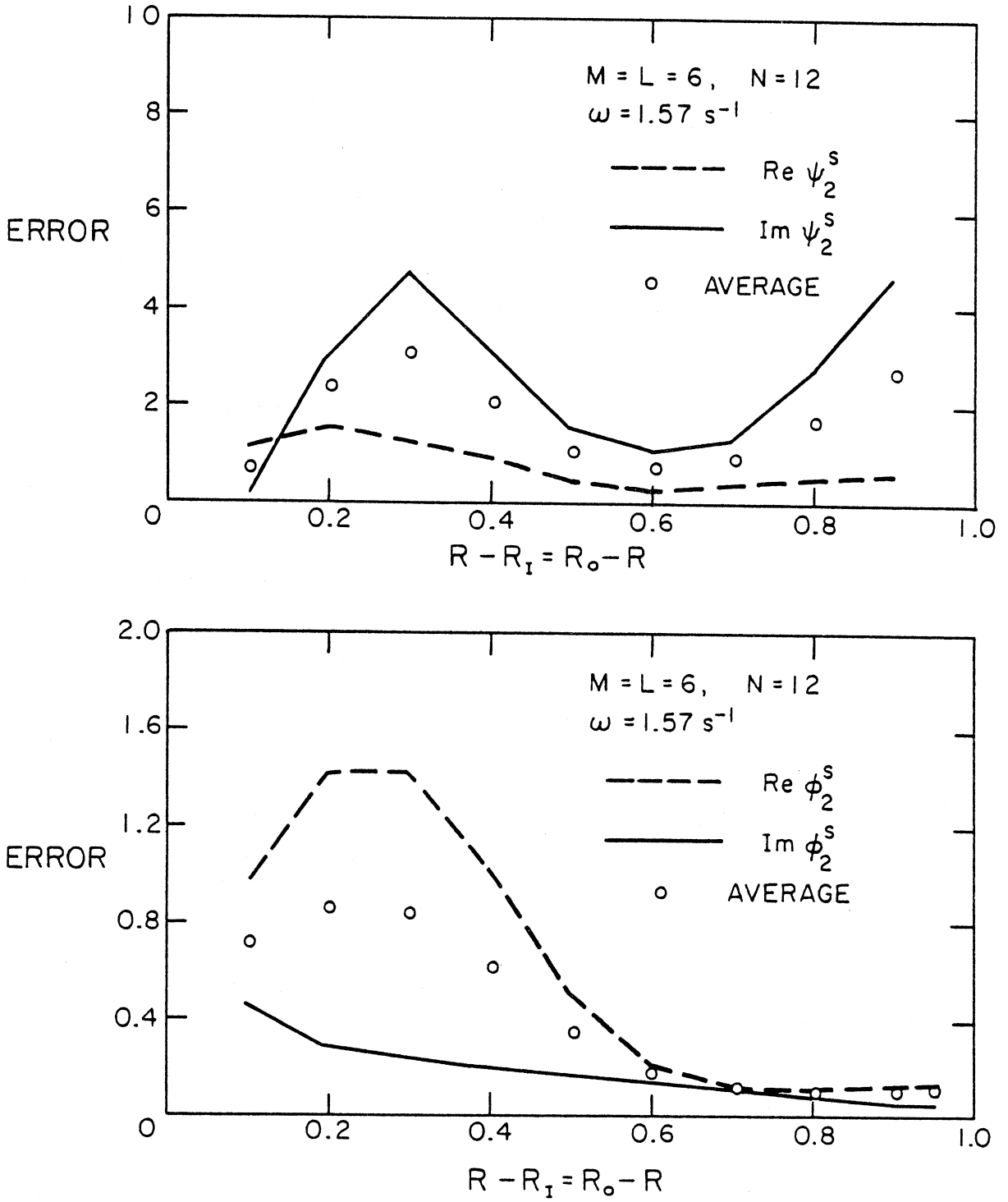

Fig. 19. Relative Error for Scattered Field Along the Interface: Horizontal Incidence of a Plane P-Wave Upon a Circular Inclusion in a Full-Space. (ω=1.57s^{-1}, R=μ_1=β_1=1, α_1=1.45, μ_2=β_2-0.6, α_2=0.9, M=L=6, N=12).

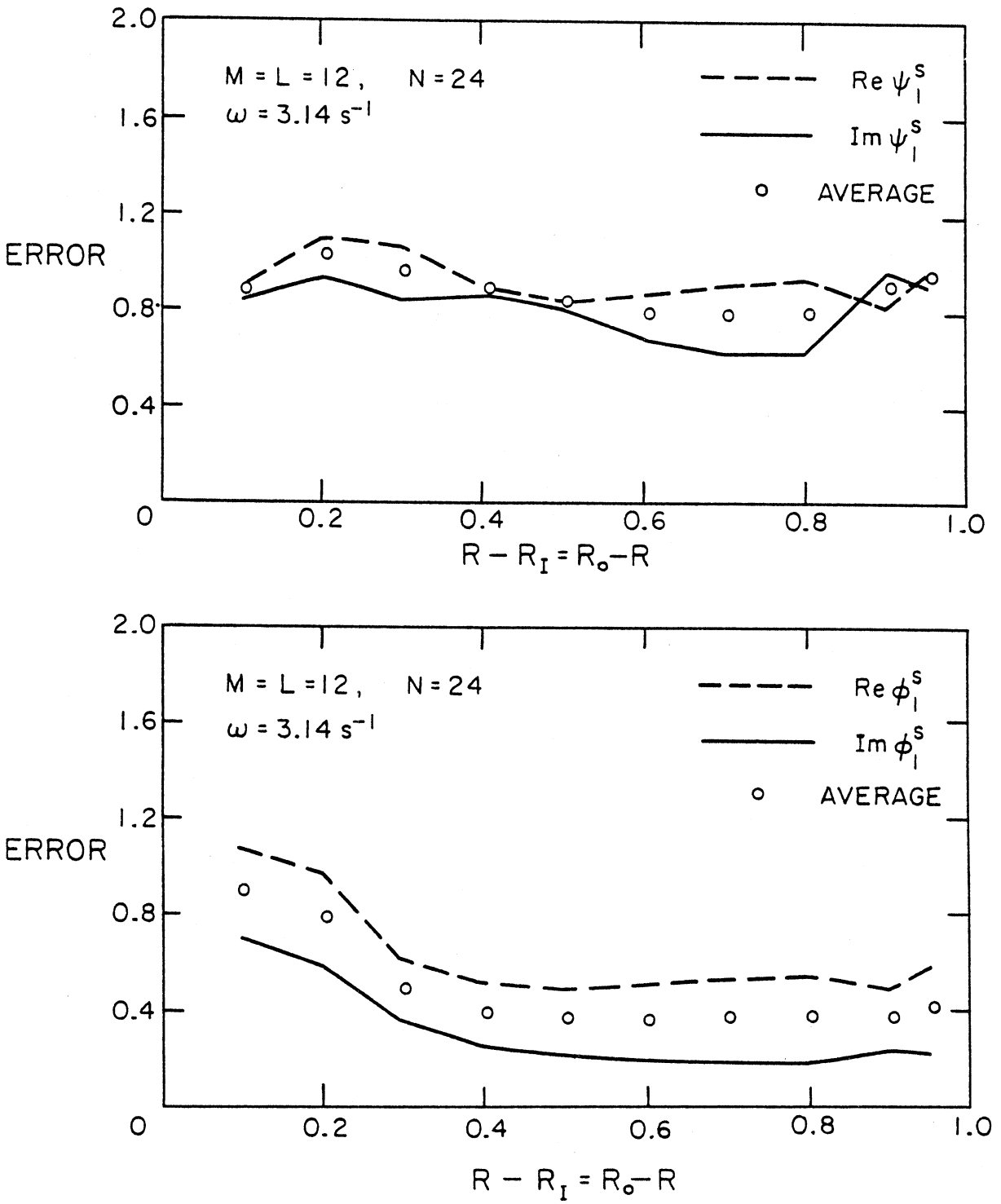

Fig. 20. Relative Error for Scattered Field Along the Interface: Horizontal Incidence of a Plane P-Wave Upon a Circular Inclusion in a Full-Space. (ω=3.14s^{-1}, R=μ_1=β_1=1, α_1=1.45, μ_2=β_2=0.6, α_2=0.9, M=L=12, N=24).

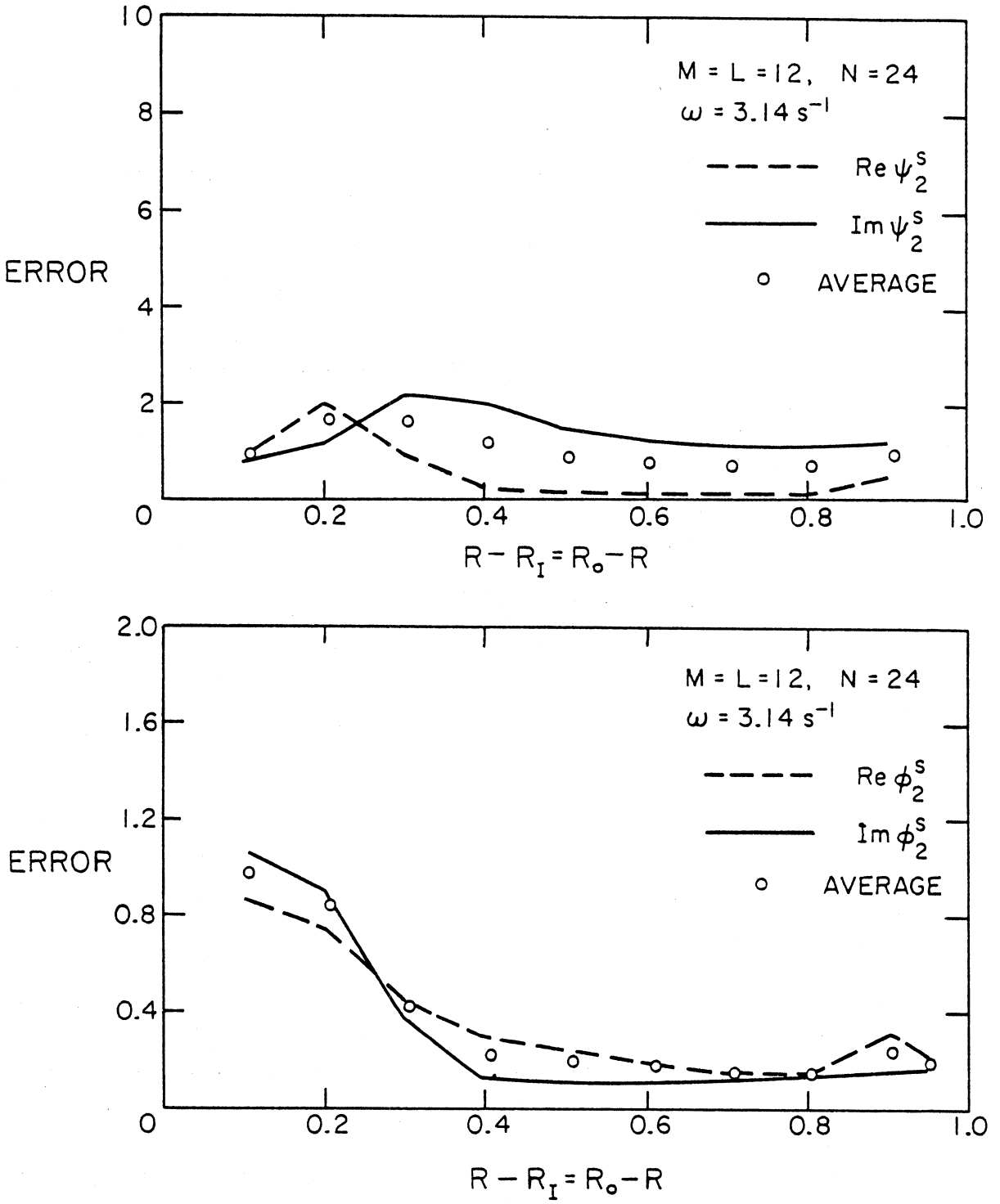

Fig. 21. Relative Error for Scattered Field Along the Interface: Horizontal Incidence of a Plane P-Wave Upon a Circular Inclusion in a Full-Space. (ω=3.14s^{-1}, R=μ_1=β_1=1, α_1=1.45, μ_2=β_2=0.6, α_2=0.9, M=L=12, N=24).

PLAIN STRAIN MODEL: HALF-SPACE PROBLEM

For the half-space problems the unknown scattered wave field (25) is evaluated through $\underset{\sim}{z} = (\underset{\sim}{G}^{*}\underset{\sim}{G})^{-1}\ \underset{\sim}{G}^{*}\underset{\sim}{f}$ (Eq. (27)) with a slight modification in the forcing term $\underset{\sim}{f}$. Initially, the forcing term $\underset{\sim}{f}$ defined by (26.4) incorporated the incident wave field only. For the half-space problems it is convenient to express the forcing term $\underset{\sim}{f}$ by

$$f^{T} = [-\underset{\sim}{u}^{ff},\ -\underset{\sim}{v}^{ff},\ -\underset{\sim}{\sigma}_{nn}^{ff},\ -\underset{\sim}{\sigma}_{nt}^{ff}] \tag{34.1}$$

$$\underset{\sim}{u}^{ff} = [u^{ff}(\underset{\sim}{r}_i)], \quad i = 1,\ldots, N \tag{34.2}$$

$$\underset{\sim}{v}^{ff} = [v^{ff}(\underset{\sim}{r}_i)] \tag{34.3}$$

$$\underset{\sim}{\sigma}_{nn}^{ff} = [\sigma_{nn}^{ff}(\underset{\sim}{r}_i)] \tag{34.4}$$

$$\underset{\sim}{\sigma}_{nn}^{ff} = [\sigma_{nt}^{ff}(\underset{\sim}{r}_i)] \tag{34.5}$$

where the superscript ff denotes the so called free-field. The free-field represents the sum of the incident and the reflected wave fields in the absence of the alluvial valley. The remaining elements of equation (27) remain formally the same as defined earlier.

The most difficult part in the plane strain problem is to evaluate the Green's functions (22) with corresponding boundary conditions (23) for the line source in the half-space. Following the papers by Lamb (1904) and Lapwood (1948), this problem is addressed in the Appendix A.

The resulting Green's functions are presented in a form which is con-

venient for numerical evaluation. Once the Green's functions are known it is possible to study the problems of diffraction of the plane P and SV waves as well as the surface Rayleigh waves by an elastic alluvial valley of arbitrary shape embedded into an elastic half-space.

DIFFRACTION OF PLANE P-WAVE BY A SEMI-ELLEPTICAL ALLUVIAL VALLEY

Alluvial valley is specified by

$$C: x = R_1 \cos\theta;\ y = R_2 \sin\theta \quad ; \quad 0 \leq \theta \leq \pi, \tag{35}$$

where the principal axis R_1 and R_2 are known. The sources are placed along the curves (surfaces)

$$C_1 : x = R_{1i} \cos\theta \quad ; \quad y = R_{2i} \sin\theta \ ; \quad 0 \leq \theta \leq \pi \ ;$$

$$C_2 : x = R_{1o} \cos\theta \quad ; \quad y = R_{2o} \sin\theta \ , \tag{36}$$

with $R_{1i} < R_{1o}$; $R_{2i} < R_{2o}$; and $R_1 > R_2$.

An incident plane longitudinal (P) wave strikes the valley and causes various waves to be scattered into elastic space. The incident wave is specified through

$$\phi^i(x,y) = (i/h)e^{-i[h(x\sin\theta_o - y\cos\theta_o) - \omega t]} \ , \tag{37}$$

where θ_o represents the angle of incidence and h is the wave number. The free field associated with incident plane P-wave is given in Appendix B.

The "observation" points along C are chosen to be at values of $\theta = \frac{\pi}{23} n$; n = 0, 1, 2, ..., 23. The source points are taken to be along C_1 and C_2 at $\theta = \frac{\pi}{11} n$; n = 0, 1, 2,...,11. For angle of incidence $\theta_o = 30^o$ and the frequency $\omega = 0.31s^{-1}$. The absolute value of dis-

placement field along the interface is presented by Fig.22.It can be seen from the figure that along the major part of the interface the predominant motion takes place in vertical direction.Significant displacement amplification effects occur at the surface of the half-space at both ends of the alluvial valley.Since no exact solution of the problem is available the question arises about the accuracy of the results derived by the source method.One way of checking the numerical results is to increase the number of sources and compare the difference between the two results.If the difference is getting smaller, it would seem reasonable to assume that the result may converge to the exact-one.Another approach would be to compare the present results with the ones obtained by some other approximate technique.For time being,the first method of checking the results has been used in this work.Sensitivity of the displacement field upon the number of sources has been done and the results presented hereafter do have certain degree of accuracy.However,the final error analysis is post-poned for later date.Therefore,the results shown here are of preliminary nature and no specific accuracy is assigned to them.

DIFFRACTION OF PLANE SV-WAVE BY A SEMI-ELLIPTICAL ALLUVIAL VALLEY

Alluvial valley is specified by Eq.(35),with source surfaces C_1 and C_2 being defined by (36).An incident plane SV-wave is given by

$$\psi^i = -(i/k)e^{-i[k(x\sin\theta_o - y\cos\theta_o) - \omega t]} \quad , \qquad (38)$$

where θ_o represents the angle of incidence and k is the wavenumber associated with equivoluminal waves.The free field corresponding to the incident SV wave (38) is given in Appendix B.The observation and the source points are chosen in the same manner as in the case of incident P wave.

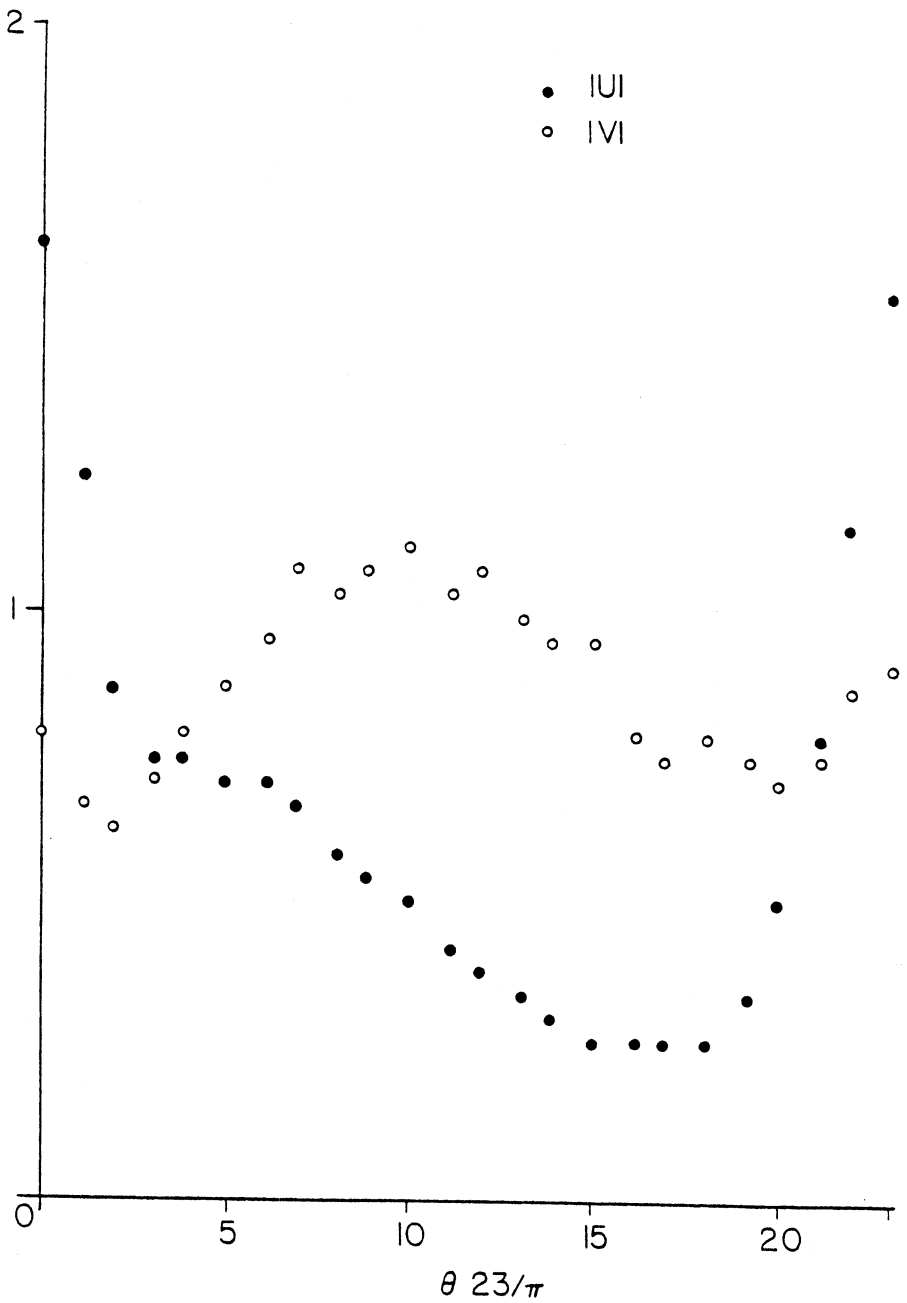

Fig. 22. Interface Displacement Field for Semi-Elliptical Inclusion. Incident P-Wave.
($\omega = 0.31 s^{-1}$, $\theta_o=30°$, $R_1=4$, $R_2=3$, $R_{1i}=3$, $R_{1o}=5$, $R_{2i}=2$, $R_{2o}=4$, $\mu_1=\beta_1=1$, $\alpha_1=2$, $\mu_2=\beta_2=0.8$, $\alpha_2=1.6$)

For angle of incidence of 30° and circular frequency 0.31 s^{-1} the absolute value of displacement field along the interface is depicted by Fig.23.It can be seen that along the major part of the interface the predominant motion takes place in horizontal direction.The largest displacement amplifications occur at the surface of the half-space at both ends of the alluvial valley.

Comparison of the results for incident P and SV waves reveals that,for the chosen set of physical parameters in the problem,the displacement amplification along the interface is larger for SV-waves then for P-waves.

DIFFRACTION OF RAYLEIGH WAVES BY A SEMI-ELLIPTICAL ALLUVIAL VALLEY

For the alluvial valley (35) and the source surfaces (36) the free field consists of Rayleigh waves specified in Appendix B by (B28-B34). The amplitude A is chosen to be equal unity.The observation and the source points are chosen to be the same as in the case of incident P and SV waves. For the circular frequency 0.31 s^{-1},the displacement field along the interface is shown by Fig.24.It is seen that incident Rayleigh wave produces rather uniform displacement field throughout the interface between the half-space and the alluvial valley with predominant motion taking place in vertical direction.Comparison of the results with the corresponding ones evaluated for incident P and SV waves indicate that the displacement amplification due to Rayleigh wave may be of great importance even along relatively deep interface. However,the maximum amplification effects are smaller for incident Rayleigh wave compared to amplifications due to P and SV waves.

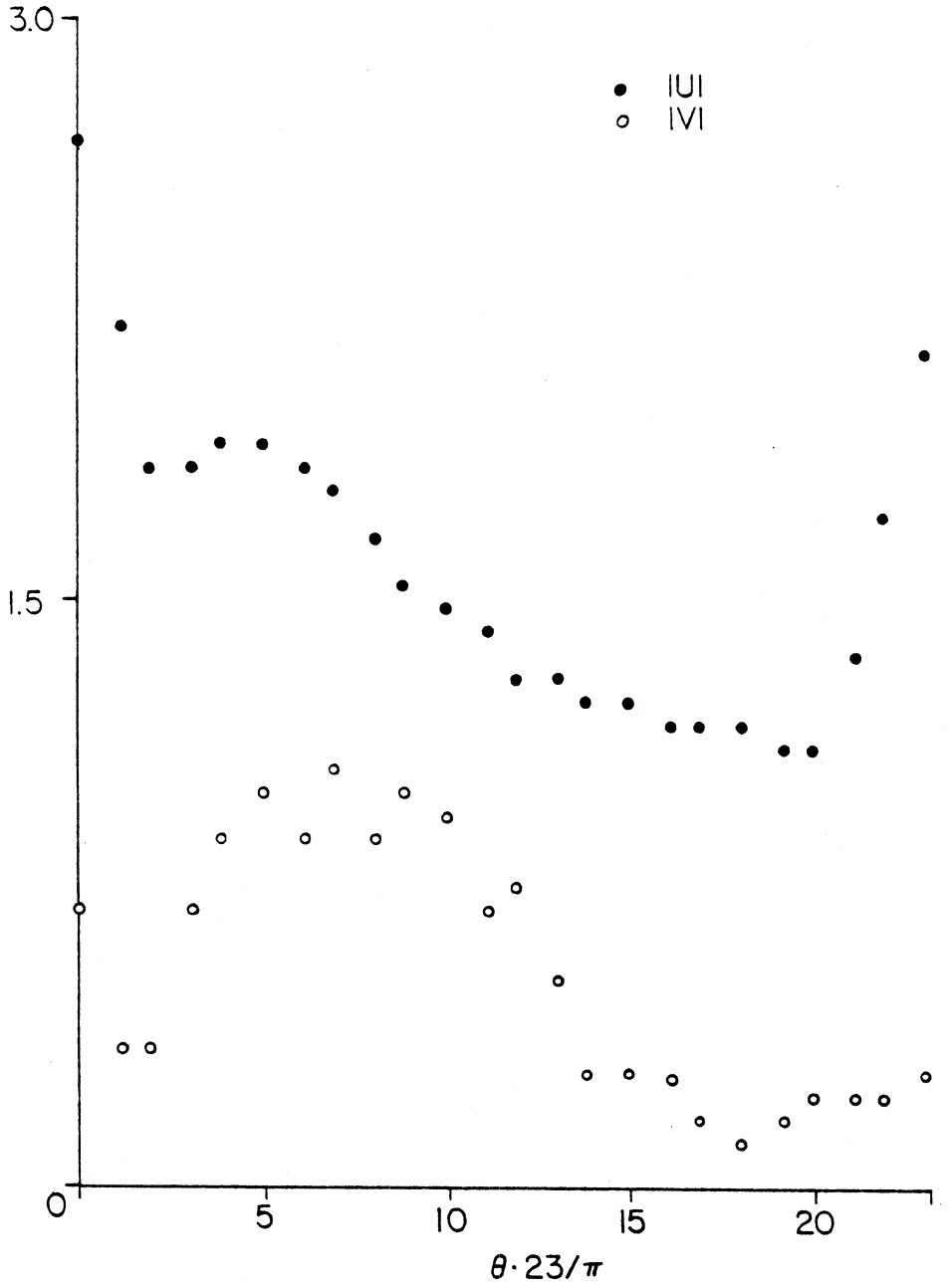

Fig. 23. Interface Displacement Field for Semi-Elliptical Inclusion. Incident SV-Wave.
(ω=0.31s^{-1}, θ_0=30°, R_1=4, R_2=3, R_{1i}=3, R_{1o}=5, R_{2i}=2, R_{2o}=4, $\mu_1=\beta_1$=1, α_1=2, $\mu_2=\beta_2$=0.8, α_2=1.6)

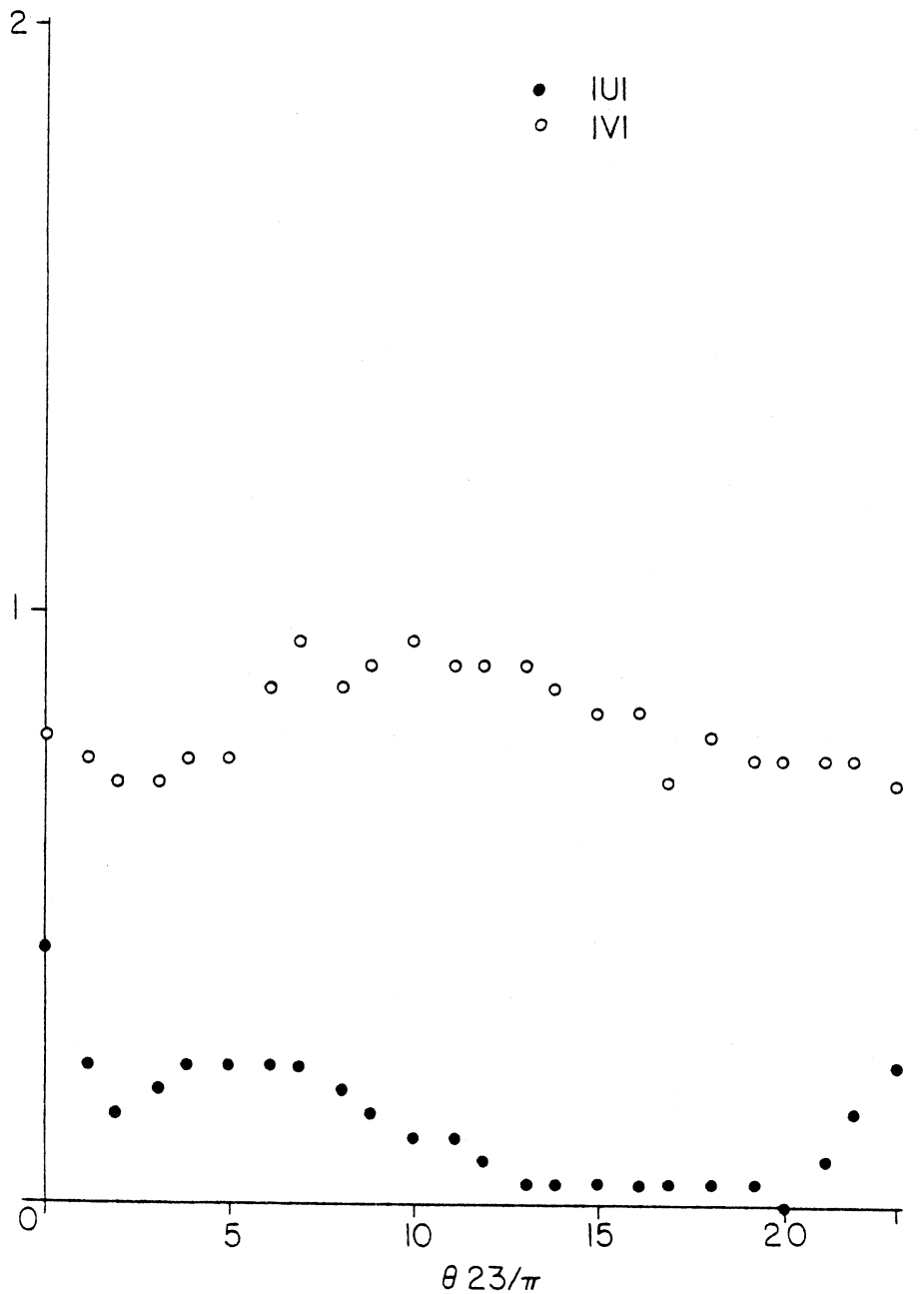

Fig. 24. Interface Displacement Field for Semi-Elliptical Inclusion. Incident Rayleigh Wave.
(ω=0.31s^{-1}, R_1=4, R_2=3, R_{1i}=3, R_{1o}=5, R_{2i}=2, R_{2o}=4, μ_1=β_1=1, α_1=2, μ_2=β_2=0.8, α_2=1.6)

SUMMARY AND CONCLUSIONS

Scattering of plane waves by an elastic inclusion of arbitrary shape embedded in an elastic half-space were considered by using the source method. Approximate results are compared with the existing exact solutions implying good agreement between the two for a wide range of physical parameters of the model under consideration.

Variation of location of the sources and their number provided some insight into the quality of approximation of the source method. These results can be summarized as follows:

1. The approximate results depend on the frequency (wavelength) of excitation. Lowering the frequency leads to smaller error in the scattered wave field for a fixed number of sources.
2. The number of sources influences significantly the quality of approximation. In general, larger number of sources leads to a smaller error in the results.
3. Due to singularities of the Green's functions as the "source" point approaches the "observation" point the sources should not be placed too close to the interface.

Although much more work remains to be done in acquiring complete understanding of the source method, these initial results do indicate the power and efficiency of the source method in problems of geophysics and earthquake engineering.

ACKNOWLEDGEMENTS

The author expresses gratitude to H.L. Wong for suggesting the method and to M.D. Trifunac for critical reading of the manuscript and numerous suggestions.

Criticism by F.E. Udwadia and discussions with J.E. Luco are greatly appreciated.

This research was supported in part by a grant from the United States Geological Survey and in part by a contract from the Nuclear Regulatory Commission.

REFERENCES

Achenbach, J.D. (1973). Wave Propagation in Elastic Solids, North-Holland, Amsterdam.

Aki, K., and K.L. Larner (1970). Surface Motion of a Layered Medium Having an Irregular Interface due to Incident Plane SH-Waves, J. Geophys. Res., 75, pp. 933-954.

Alterman, Z., and F.C. Karal (1968). Propagation of Elastic Waves in Layered Media by Finite Difference Method, Bull. Seism. Soc. Amer., 58, pp. 367-398.

Asano, S. (1966). Reflection and Refraction of Elastic Waves at a Corrugated Surface, Bull. Seism. Soc. Amer., 56, pp. 201-221.

Boore, D.M. (1969). Finite Difference Solutions to the Equations of Elastic Wave Propagation with Application to Love Waves Over Dipping Interfaces, Ph.D. Thesis, MIT, Cambridge, Mass.

Boore, D.M. (1972). A note on the Effect of Simple Topography on Seismic SH waves, Bull. Seism. Soc. Amer., 62, pp. 275-284.

Boore, D. M. (1973). The Effect of Simple Topography on Seismic Waves: Implications for the Accelerations Recorded at Pacoima Dam, San Fernando Valley, California, Bull. Seism. Soc. Amer., 62, 1608-1609.

Bouchon, M. (1973). Effect of Topography on Surface Motion, Bull. seism. Soc. Amer., 63, pp. 615-632.

Bouchon, M., and K. Aki (1977). Near Field of a Seismic Source in a Layered Medium with Irregular Interfaces, Geoph. J.R. astr. Soc., 50, 3, pp. 669-684.

Cherry, J.T. (1973). Calculation of Near Field Earthquake Ground Motion, System, Science and Software, Tech. Rep. No. SSS-R-73-1759, La Jolla, California.

Clebsch, A., (1865). Uber die Reflexion an einer Kugelfläsche, Crelle's Journal für die Reine und Angewandte Mathematik, 61, pp. 195.

Cole, D.M., D.D. Kosloff, and J.B. Minster (1978). A Numerical Boundary Integral Equation Method for Elastodynamics: I, Bull. Seism. Soc. Amer, 68, 5, pp. 1331-1357.

Copley, L.G. (1967). Integral Equation Method for Radiation from Vibrating Surfaces, J. Acoust. Soc. Amer., 41, pp. 807-816.

Dravinski, M., and S.A. Thau (1976a). Multiple Diffraction of Elastic Shear Waves by a Rigid Rectangular Foundation Embedded in an Elastic Half-Space, Journal of Applied Mechanics, ASME, 43, pp. 295-299.

Dravinski, M., and S.A. Thau (1976b). Multiple Diffractions of Elastic Waves by a Rigid Rectangular Foundation: Plane Strain Model, Journal of Applied Mechanics, ASME,43, pp. 291-294.

Dravinski, M., and F.E. Udwadia. "Scattering of Horizontally Polarized Shear Waves by a Periodic Boundary, " XV International Congress of Theoretical and Applied Mechanics, Toronto, Canada, 1980.

Duke, C.M. (1958). Bibliography of Effects of Soil Conditions on Earthquake Damage, Earthquake Engineering Research Institute, San Francisco.

Esteva, L. (1977). Microzoning: Models and Reality, Proc. World Conf. Earthquake Engr., 6th, New Delhi.

Ewing, W.M., W.S. Jardetzky, and F. Press, "Elastic Waves in Layered Media," McGraw-Hill, 1957.

Griffiths, D.W., and G.A. Bollinger (1979). The Effects of Appalachian Mountain Topography on Seismic Waves, Bull. Seism. Soc. Amer., 69, 4, pp. 1081-1105.

Grimaldi, F.M. (1665). Physico-Mathesis du Lumine, Coloribus et Iride, Bolognia.

Gutenberg, B. (1957). Effects of Ground on Earthquake Motion, Bull. Seism. Soc. Amer. 47, pp. 221-250.

Heise, U. (1978). Numerical Properties of Integral Equations on Which the Given Boundary Values and the Sought Solutions are Defined on Different Curves, J. Computers Struct., 8, pp. 199-205.

Hudson, D.E. (1972). Local Distribution of Strong Earthquake Ground Motions Bull. Seism. Soc. Amer., 62, pp. 1765-1786.

Ilan, A., L.J. Bond, and M. Spivak (1979). Interaction of a Compressional Impulse with a Slot Normal to the Surface of an Elastic Half-Space, Geoph. J.R. astr. Soc., 57, pp. 463-477.

Jennings, P.C. (editor)(1971). San Fernando Earthquake of February 9, 1971, EERL-71-02, Calif. Inst. of Tech., Pasadena.

Kanai, K., T. Tanaka, and T. Suzuki (1953). Relation Between the Earthquake Damage and the Nature of the Ground, Bull. Earthquake Res. Inst., Tokyo Univ., 31, pp. 57-62.

Kanai, K. (1957). The Requisite Conditions for Predominant Vibrations of Ground, Bull. Earthquake Res. Inst., Tokyo Univ., 35, p. 457.

Kanai, K., and T. Tanaka (1961). On Microtremors, VIII., Bull. Earthquake Res. Inst., Tokyo Univ., 39, pp. 97-115.

Lamb, H., "On the Propagation of Tremors over the Surface of an Elastic Solid", Phil. Trans. Royal Soc. London, A 359, Vol. 203, 1904.

Lapwood, E.R., "The Disturbance due to a Line Source in a Semi-Infinite Elastic Medium", Phil. Trans. Royal Soc. London, A841, Vol. 242, 1948.

Lee, V.W. (1978). Displacement Near a Three-Dimensional Hemispherical Canyon Subjected to Incident Plane Waves, Univ. of So. Calif., Dept. of Civil Engineering, Report No. 78-16.

Lysmer, J., and G. Waas (1972). Shear Waves in Plane Infinite Structures, J. Eng. Mech. Div., ASCE. EMI, 98, pp. 85-108.

Mal, A.K., and L. Knopoff (1965). Transmission of Rayleigh Waves Past a Step Change in Elevation, Bull. Seism. Soc. Amer., 55, pp. 319-334.

Maxwell, J.C. (1865). A Dynamical Theory of the Electromagnetic Field, Phil. Trans. Royal Soc. London, 155, p. 459.

Miklowitz, J. (1966). Elastic Wave Propagation, Reprinted from Applied Mechanics Surveys, Spartan Books, Washington, D.C.

McIvor, I. (1969). Two Dimensional Scattering of a Plane Compressional Wave by Surface Imperfection, Bull. Seism. Soc. Amer., 59, pp. 1359-1364.

Noble, B. (1969). Applied Linear Algebra, McGraw Hill, New Jersey.

Oshaki, Y. (1973). On Movements of a Rigid Body in Semi-Infinite Elastic Medium, Proc. Japanese Earthquake Engineering Symp., Tokyo, Japan.

Pao, Y.H., and C.C. Mow (1973). The Diffraction of Elastic Waves and Dynamic Stress Concentrations, Crane-Russak, New York.

Reimer, R.B., R.W. Clough, and J.M. Raphael (1974). Seismic Response of Pacoima Dam in the San Fernando Earthquake, Proc. 5th World Conf. Earthquake Engineering, Rome, 2, pp. 2362-2337.

Sabina, F.J., and J.R. Willis (1975). Scattering of SH-Waves by a Rough Half-Space of Arbitrary Shape, Geophysical Journal, Vol. 42, 685-703.

Sanchez-Sesma, F.J., and J.A. Esquivel (1979). Ground Motion on Alluvial Valleys Under the Incident Plane SH Waves, Bull. Seism. Soc. Amer., 69, 4, 1107-1120.

Sanchez-Sesma, F.J., and E. Rosenblueth (1979). Ground Motion at Canyons of Arbitrary Shapes Under Incident SH Waves, Earthquake Eng. and Struct. Dyn., 7,5, pp. 441-450.

Schlue, J.W. (1979). Love Wave Propagation in Three Dimensional Structures Using Finite Element Techniques, Bull. Seism. Soc. Amer., 69, 2, pp. 319-328.

Sezawa, K. (1927). Scattering of Elastic Waves and Some Allied Problems, Bulletin of Earthquake Research Institute, Tokyo Imperial University, 3, pp. 18.

Sills, L.B. (1978). Scattering of Horizontally-Polarized Shear Waves by Surface Irregularities, Geoph. J.R. astr. Soc., 54, 2, pp. 319-348.

Singh, S.K., and F.J. Sabina (1979). Ground Motion Amplification by Topographic Depressions for Incident P-Wave Under Acoustic Approximation, Bull., Seism. Amer., 67, 2, pp. 345-352.

Smith, W.D. (1974). The Application of Finite Element Analysis to Body Wave Propagation Problems, Tenth Int. Symp. Math. Geophysics, Cambridge, Ma.

Sozen, M.A., P.C. Jennings, R.B. Matthiesen, G.W. Housner and N.M. Newmark (1968). Engineering Report on the Caracas Earthquake of 29 July, 1967. National Academy of Sciences, Washington, D.C.

Trifunac, M.D. (1971). Surface Motion of a Semicylindrical Alluvial Valley for Incident Plane SH Waves, Bull. Seism. Soc. Amer., 61, pp. 1755-1770.

Trifunac, M.D. (1973). Scattering of Plane SH Waves by a Semicylindrical Canyon, Int. J. Earthquake Eng. and Struct. Dyn., 1, pp. 267-281.

Thau, S.A., and A. Umek (1973). Transient Response of a Buried Foundation to Antiplane Shear Waves, Journal of Applied Mechanics, ASME, 40, pp. 1061-1066.

Thau, S.A., and A. Umek (1974). Coupled Rocking and Translating Vibrations of Buried Foundation, J. Appl. Mech., ASME, 41, pp. 697-702.

Ursell, F. (1973). On the Exterior Problem of Acoustics, Proc. Cambridge Phil. Soc., 74, pp. 117-125.

Wong, H.L. (1979). Diffraction of P, SV and Rayleigh Waves by Surface Topograhies, Univ. of Southern California, Dept. of Civil Engineering, Report No. 79-05.

Wong, H.L, and M.D. Trifunac (1974a). Scattering of Plane SH Waves by a Semi-Elliptical Canyon, International Journal Earthquake Engineering and Struct. Dyn., 3, pp. 157-169.

Wong, H.L., and M.D. Trifunac (1974b). Surface Motion of a Semi-Elliptical Alluvial Valley for Incident Plane SH Waves, Bull. Seism. Soc. Amer., 64, pp. 1389-1408.

Wong, H.L., and P.C. Jennings (1975). Effect of Canyon Topography on Strong Ground Motion, Bull. Seism. Soc. Amer., 65, pp. 1239-1257.

Wong, H.L., and J.E. Luco (1976). Dynamic Response of Foundations of Arbitrary Shape, Earthquake Eng. and Struct. Dyn., 9.

Wong, H.L. (1975). Dynamic Soil-Structure Interaction, EERL Report 75-01, Calif. Inst. of Tech., Pasadena.

Wong, H.L., M.D. Trifunac and B.D. Westermo (1977). Effects of Surface and Subsurface Irregularities on the amplitudes of Monochromatic Waves, Bull. Seism. Soc. Amer., 67, 2, pp. 353-368.

APPENDIX A

DILATATIONAL LINE SOURCE FOR A HALF-SPACE

Consider a half space $|x|<\infty$, $y \geq 0$ subjected to a dilationational line source at a point (0,f). The wave potential of the source in an infinite solid at (o,f) is given by

$$\phi^s = H_0^{(2)}(hr) \; ; \; \psi^s = 0 \; ; \quad r^2 = x^2 + (y - f)^2 \quad , \tag{A1}$$

where $H_0^{(2)}$ is the Hankel function of order zero and of the second kind, h is the wave number of the longitudinal waves and the factor $e^{+i\omega t}$ is understood. The boundary of the half space is stress free, i.e.

$$\sigma_{yy}(x,o) = 0 \tag{A2}$$

$$\sigma_{xy}(x,o) = 0 \tag{A3}$$

In order to solve for the half-space problem, the superposition of the potentials of the full-space problems is used. Therefore, an equal source to the one given by (A1) is placed at (0,-f). Thus the potential of the sources is given by

$$\phi^s = H_0^{(2)}(hr) + H_0^{(2)}(hr') \; ; \; \psi^s = 0 \; ; \; r' = \sqrt{x^2 + (y + f)^2}. \tag{A4}$$

It is easy to check that the waves specified by A4 satisfy the boundary condition (A3) i.e. $\sigma_{xy}^s(x,o) = 0$ but the normal stress $\sigma_{yy}^s(x,o)$ is different from zero and it must be "removed" in order to solve the half-space problem by superposition of the full space problems. The wave potentials (A4) can be represented in more convinient form (see for example Lapwood, 1948)

$$\phi^s = \frac{4i}{\pi}\int_0^\infty \frac{e^{-\alpha f}}{\alpha}\cosh\alpha y\cos\zeta x\,d\zeta x\,d\zeta\ ;\ \psi^s = 0;\ \alpha^2 \equiv \zeta^2 - h^2;\ y < f, \quad (A5)$$

where the following integral representation for the Hankel functions has been used

$$H_0^{(2)}(h\sqrt{x^2 + y^2}\ ) = \frac{2i}{\pi}\int_0^\infty e^{-\alpha y}\cos\zeta x\,\frac{d\zeta}{\alpha}\ ;\ y > 0. \quad (A6)$$

The wave field ϕ^R and ψ^R is added to the (A5) in order to satisfy the boundary conditions (A2,3) exactly, i.e.

$$\phi(x,y) = \phi^s(x,y) + \phi^R(x,y) \quad (A7)$$

$$\psi(x,y) = \psi^R(x,y)\ . \quad (A8)$$

Additional field is assumed to be of the form

$$\phi^R = \frac{4i}{\pi}\int_0^\infty (A\cos\zeta x + B\sin\zeta x)e^{-\alpha y}d\zeta \quad (A9)$$

$$\psi^R = \frac{4i}{\pi}\int_0^\infty (C\cos\zeta x + D\sin\zeta x)e^{-\beta y}d\zeta\ ; \quad (A10)$$

$$\beta^2 \equiv \zeta^2 - k^2\ ,$$

where k is the wave number associated with the transverse waves. The unknown A,B,C, and D are determined from the boundary conditions (A2,3) to be

$$B = C = 0 \quad A = -\frac{(2\zeta^2 - k^2)^2 e^{-\alpha f}}{\alpha\, F(\zeta)} \qquad D = \frac{2\zeta(2\zeta^2 - k^2)e^{-\alpha f}}{F(\zeta)}\ .$$

$$F(\zeta) = (2\zeta^2 - k^2)^2 - 4\zeta^2\alpha\beta\ . \quad (A11)$$

Then from (A7,8) it follows that the wave potentials in the half space due a longitudinal line source at (o,f), which satisfy the stress free boundary conditions $\sigma_{yy}(x,o) = \sigma_{xy}(x,o) = 0$, are given by

$$\phi(x,y) = H_0^{(2)}(hr) + H_0^{(2)}(hr') - \frac{4i}{\pi}\int_0^\infty \frac{(2\zeta^2 - k^2)^2}{\alpha F(\zeta)} e^{-\alpha(y+f)}\cos\zeta x\, d\zeta$$

$$= \frac{4i}{\pi}\left\{\int_0^\infty \frac{e^{-\alpha f}}{\alpha}\cosh\alpha y\cos\zeta x\, d\zeta - \int_0^\infty \frac{(2\xi^2 - k^2)^2}{\alpha F(\zeta)} e^{-\alpha(y+f)}\cos\zeta x\, d\zeta\right\}$$

$$= H_0^{(2)}(hr) - H_0^{(2)}(hr') - \frac{16i}{\pi}\int_0^\infty \frac{\zeta^2\beta}{F(\zeta)} e^{-\alpha(y+f)}\cos\zeta x\, d\zeta$$

$$= \frac{4i}{\pi}\left\{\int_0^\infty \frac{e^{-\alpha f}}{\alpha}\sinh\alpha y\cos\zeta x\, d\zeta - 4\int_0^\infty \frac{\zeta^2\beta}{F(\zeta)} e^{-\alpha(y+f)}\cos\zeta x\, d\zeta\right\}$$

$$\psi(x,y) = \frac{8i}{\pi}\int_0^\infty \frac{\zeta(2\zeta^2 - k^2)}{F(\zeta)} e^{-\alpha f - \beta y}\sin\zeta x\, d\zeta. \qquad \text{(A12)}$$

The displacement and the stress fields are calculated to be

$$u^\phi = -hx\left[\frac{H_1^{(2)}(hr)}{r} - \frac{H_1^{(2)}(hr')}{r'}\right] + \frac{16i}{\pi}\int_0^\infty \frac{\xi^3\beta}{F(\xi)} e^{-\alpha(y+f)}\sin\xi x\, d\xi$$

$$- \frac{8i}{\pi}\int_0^\infty \frac{\beta\xi(2\xi^2 - k^2)}{F(\xi)} e^{-\alpha f - \beta y}\sin\xi x\, d\xi \qquad \text{(A13)}$$

$$v^\phi = -h\left[\frac{y-f}{r} H_1^{(2)}(hr) + \frac{y+f}{r'} H_1^{(2)}(hr')\right] + \frac{4i}{\pi}\int_0^\infty \frac{(2\xi^2 - k^2)^2}{F(\xi)}$$

$$e^{-\alpha(y+f)}\cos\xi x\, d\xi$$

$$- \frac{8i}{\pi}\int_0^\infty \frac{\xi^2(2\xi^2 - k^2)}{F(\xi)} e^{-\alpha f - \beta y}\cos\xi x\, d\xi \qquad \text{(A14)}$$

$$\sigma_{xx}^\phi/\mu = 2h\left[\frac{1}{r} - 2\frac{(y-f)^2}{r^3}\right] H_1^{(2)}(hr) + \left[2h^2\frac{(y-f)^2}{r^2} - k^2\right] H_0^{(2)}(hr)$$

$$-2h\left[\frac{1}{r'} - 2\frac{(y+f)^2}{r'^3}\right] H_1^{(2)}(hr') - \left[2h^2\frac{(y+f)^2}{r'^2} - k^2\right] H_0^{(2)}(hr')$$

$$+ \frac{16i}{\pi} \int_0^\infty \frac{\xi^2 \beta}{F(\xi)} (k^2 + 2\alpha^2)\, e^{-\alpha(y+f)} \cos\xi x\, d\xi$$

$$- \frac{16i}{\pi} \int_0^\infty \frac{\beta\xi^2(2\xi^2 - k^2)}{F(\xi)} e^{-\alpha f - \beta y} \cos\xi x\, d\xi \qquad \text{(A15)}$$

$$\sigma_{xy}^{\phi}/\mu = \frac{4hx(y-f)}{r^3} H_1^{(2)}(hr) - \frac{2h^2x(y-f)}{r^2} H_0^{(2)}(hr)$$

$$+ \frac{4hx(y+f)}{r'^3} H_1^{(2)}(hr') - \frac{2h^2x(y+f)}{r'^2} H_0^{(2)}(hr')$$

$$- \frac{8i}{\pi} \int_0^\infty \frac{\xi(2\xi^2 - k^2)^2}{F(\xi)} e^{-\alpha(y+f)} \sin\xi x\, d\xi$$

$$+ \frac{8i}{\pi} \int_0^\infty \frac{\xi(2\xi^2 - k^2)^2}{F(\xi)} e^{-\alpha f - \beta y} \sin\xi x\, d\xi \qquad \text{(A16)}$$

$$\sigma_{yy}^{\phi}/\mu = 2h\left[\frac{1}{r} - \frac{2x^2}{r^3}\right] H_1^{(2)}(hr) + \left[\frac{2h^2x^2}{r^2} - k^2\right] H_0^{(2)}(hr)$$

$$- 2h\left[\frac{1}{r'} - \frac{2x^2}{r'^3}\right] H_1^{(2)}(hr') - \left[\frac{2h^2x^2}{r'^2} - k^2\right] H_0^{(2)}(hr')$$

$$- \frac{16i}{\pi} \int_0^\infty \frac{\xi^2\beta(2\xi^2 - k^2)}{F(\xi)} e^{-\alpha(y+f)} \cos\xi x\, d\xi$$

$$+ \frac{16i}{\pi} \int_0^\infty \frac{\xi^2\beta(2\xi^2 - k^2)}{F(\xi)} e^{-\alpha f - \beta y} \cos\xi x\, d\xi \qquad \text{(A17)}$$

EVALUATION OF IMPROPER INTEGRALS

The displacement and the stress fields (A13 - A17) contain improper integrals which are evaluated by using the contour integrations in complex plane. The integrals are of the form (Lapwood, 1948)

$$I_1 = \int_0^\infty G(\zeta)\cos\zeta x d\zeta \; ; \quad I_2 = \int_0^\infty \zeta G(\zeta)\sin\zeta x d\zeta \; , \tag{A18}$$

where G is an even function of ζ which is considered to be complex in general. Branch points of the integral occur at $\zeta = \pm k$ and $\zeta = \pm h$ (recall $\alpha = \sqrt{\zeta^2 - h^2}$, $\beta = \sqrt{\zeta^2 - k^2}$) and the isolated singularity is at $\zeta = \kappa$, where κ is assumed to be solution of $F(\kappa) = 0$ (see (A11)). The branch cuts are chosen in such a fashion that along the integration path $\mathrm{Re}\,\alpha \geq 0$ and $\mathrm{Re}\,\beta \geq 0$, which physically correspond to bounded displacement and stress fields at infinity. Denoting $\zeta = \xi + i\eta$ and $\omega = s - ic$ the condition $\mathrm{Re}\,\alpha = 0$ implies

$$\xi\eta = -\frac{sc}{c_L^2} \quad \text{and} \quad \xi^2 - \eta^2 < \frac{s^2 - c^2}{c_L^2} \; , \tag{A19}$$

where c_L denotes the velocity of the longitudinal waves. Similarly, $\mathrm{Re}\,\beta = 0$ implies

$$\xi\eta = -\frac{sc}{c_T^2} \quad \text{and} \quad \xi^2 - \eta^2 < \frac{s^2 - c^2}{c_T^2} \; , \tag{A20}$$

with c_T being the velocity of the transverse waves.

Therefore, for $\mathrm{Re}\,\omega > 0$ conditions (A19,20) define the branch cuts in the complex ξ-plane as parts of hyperbolae depicted by dashed lines in fig. A1.

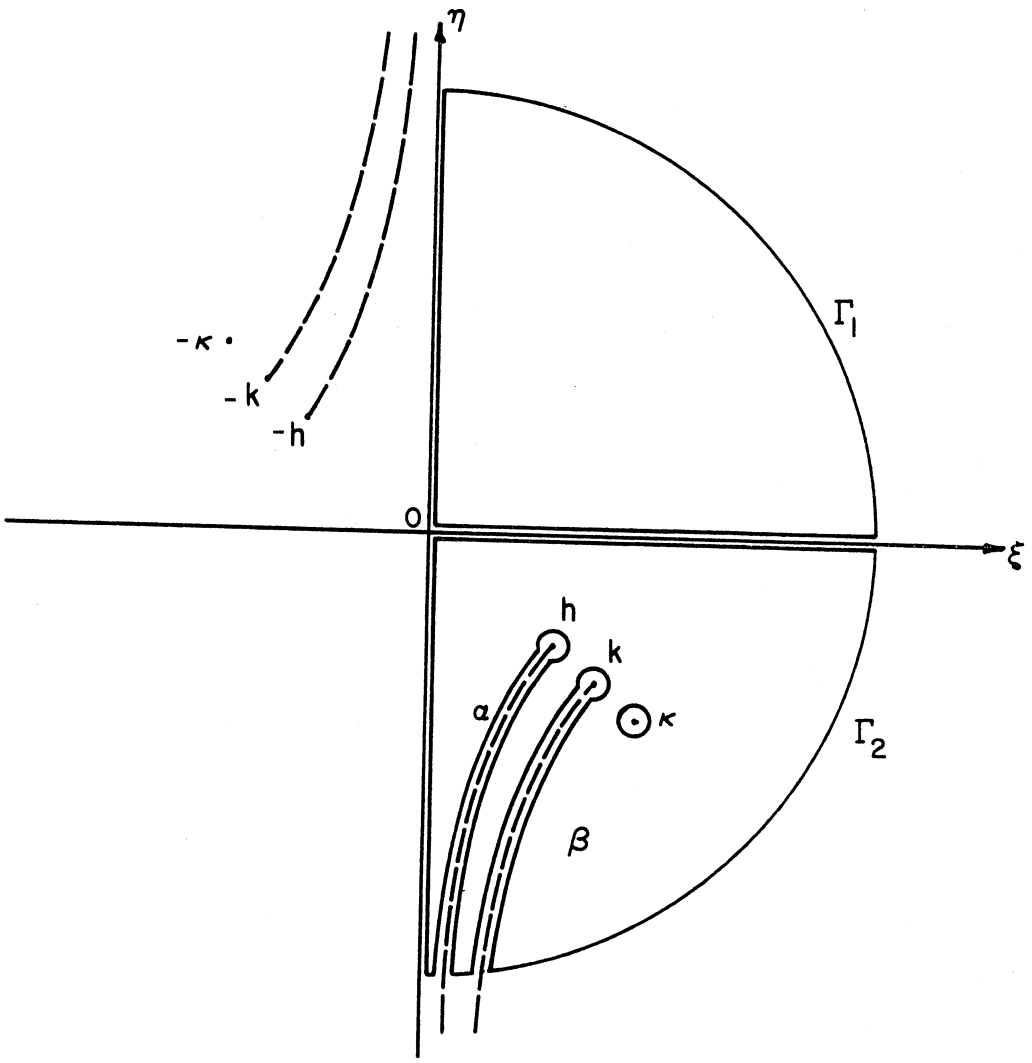

Fig. A1 The Contour of Integration

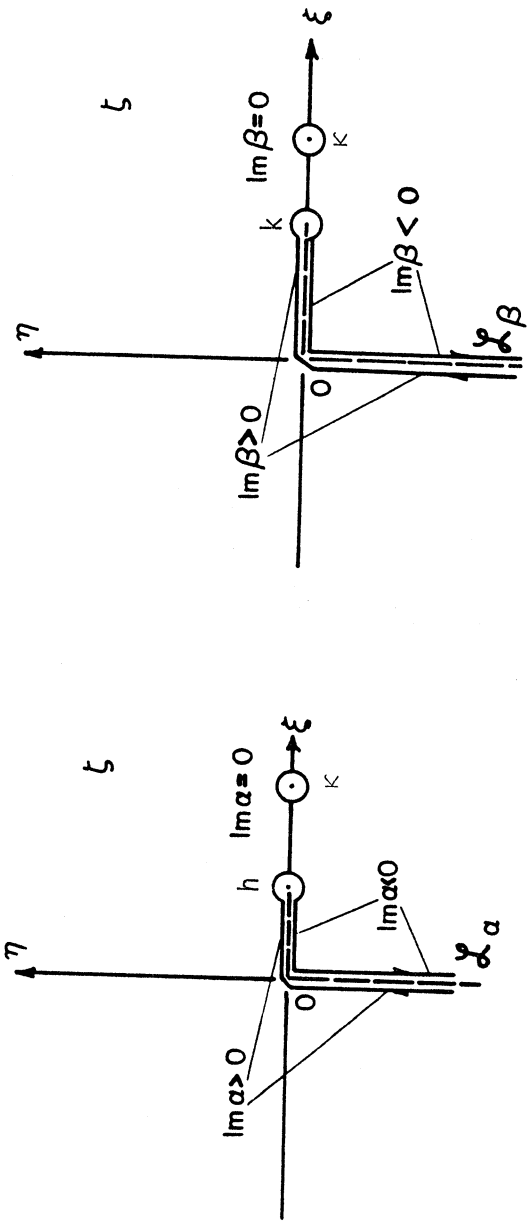

Fig. A2 The Degenerate Contours of Integration $\mathscr{L}_\alpha$ and $\mathscr{L}_\beta$.

DEFORMATION OF INTEGRATION PATH

The integrals (A18) can be written in the following form

$$I_1 = \frac{1}{2}\left[\int_0^\infty G(\zeta)\, e^{i\zeta x}\, d\zeta + \int_0^\infty G(\zeta) e^{-i\zeta x}\, d\zeta\right] \qquad (A21)$$

$$I_2 = \frac{1}{2i}\left[\int_0^\infty \zeta G(\zeta)\, e^{i\zeta x}\, d\zeta - \int_0^\infty \zeta G(\zeta) e^{-i\zeta x}\, d\zeta\right] . \qquad (A22)$$

By choosing the contours Γ_1 and Γ_2 for integrals involving $e^{i\xi x}$ and $e^{-i\xi x}$ respectively the following result is derived (Ewing et al, 1957)

$$I_1 = \frac{1}{2}\oint_{\mathscr{L}_\alpha + \mathscr{L}_\beta} G(\zeta) e^{-i\zeta x}\, d\zeta - 2\pi i \,\text{Res}\left\{\frac{1}{2} G(\zeta) e^{-i\zeta x}\ ;\ \kappa\right\} \qquad (A23)$$

$$I_2 = \frac{1}{2i}\oint_{\mathscr{L}_\alpha + \mathscr{L}_\beta} \zeta G(\zeta) e^{-i\zeta x}\, d\zeta - 2\pi i \,\text{Res}\left\{\frac{1}{2i} \zeta G(\zeta) e^{-i\zeta x}\ ;\ \kappa\right\} \qquad (A24)$$

where $\mathscr{L}_\alpha$ and $\mathscr{L}_\beta$ are keyhole parts of the Γ_2-loop shown by Fig. A1, and the sense of integration is indicated. As ω tends in the limit to a real number, the paths of integration $\mathscr{L}_\alpha$ and $\mathscr{L}_\beta$ degenerate, as shown by Fig. A2.

Taking into account the sign of α and β along the path of integration the improper integrals of type (A23,24) can be evaluated in sych a form that no singularities of integrends occur along the range of integration. The integrals needed in evaluation of the displacement and stress fields (A13-A17) are summarized as follows:

Summary of integrals.

$$\alpha = \sqrt{\zeta^2 - h^2} \qquad \beta = \sqrt{\zeta^2 - k^2} \qquad F(\zeta) = (2\zeta^2 - k^2)^2 - 4\zeta^2 \alpha\beta$$

$$\bar{\alpha} = \sqrt{h^2 - \xi^2} \qquad \bar{\beta} = \sqrt{k^2 - \xi^2} \qquad F_o^h(\xi) = (2\xi^2 - k^2)^2 + 4\xi^2 \bar{\alpha}\bar{\beta}$$

$$\bar{\bar{\alpha}} = \sqrt{\eta^2 + h^2} \qquad \bar{\bar{\beta}} = \sqrt{\eta^2 + k^2} \qquad F_o^{\infty}(\eta) = (2\eta^2 + k^2)^2 - 4\eta^2\,\bar{\bar{\alpha}}\,\bar{\bar{\beta}}$$

$$\alpha_\kappa = \sqrt{\kappa^2 - h^2} \qquad \beta_\kappa = \sqrt{\kappa^2 - k^2} \qquad F_h^k(\xi) = (2\xi^2 - k^2)^4 + 16\xi^4\,\alpha^2\bar{\beta}^2$$

(A25)

#1

$$\int_o^{\infty} \frac{\zeta^3\beta}{F(\zeta)}\, e^{-\alpha(y+f)} \sin\zeta x\, d\zeta = -2\int_o^{\infty} \frac{\eta^3\bar{\bar{\beta}}\, e^{-\eta x}\cos[\bar{\bar{\alpha}}(y+f)]}{F_o^{\infty}(\eta)}\, d\eta +$$

$$2\int_o^{h} \frac{\xi^3\bar{\beta}\, e^{-i\xi x}\cos[\bar{\alpha}(y+f)]}{F_o^{h}(\xi)}\, d\xi + \int_h^{k} \frac{\xi^3\bar{\beta}(2\xi^2 - k^2)^2 e^{-\alpha(y+f)} e^{-i\xi x}}{F_h^{k}(\xi)}\, d\xi$$

$$- \frac{\pi.\kappa^3\beta_\kappa e^{-\alpha_\kappa(y+f)}\, e^{-i\kappa x}}{F'(\kappa)}$$

(A26)

#2

$$\int_o^{\infty} \frac{\zeta\beta}{F(\zeta)}\,(2\zeta^2 - k^2)\, e^{-\alpha f - \beta y} \sin\zeta x\, d\zeta = -2\int_o^{\infty} \frac{\eta\bar{\bar{\beta}}(2\eta^2 + k^2)e^{-\eta x}\cos[\bar{\bar{\alpha}}f + \bar{\bar{\beta}}y]d\eta}{F_o^{\infty}(\eta)}$$

$$+ 2\int_o^{h} \frac{\xi\bar{\beta}(2\xi^2 - k^2)}{F_o^{h}(\xi)}\, e^{-i\xi x}\cos[\bar{\alpha}f + \bar{\beta}y]d\xi + \int_h^{k} \frac{\xi\bar{\beta}(2\xi^2 - k^2)}{F_h^{k}(\xi)}\, e^{-\alpha f}.e^{-i\xi x}$$

$$[(2\xi^2 - k^2)^2\cos\bar{\beta}y + 4\xi^2\alpha\bar{\beta}\sin\bar{\beta}y]d\xi$$

$$- \pi \cdot \frac{\kappa\beta_\kappa(2\kappa^2 - k^2)}{F'(\kappa)}\, e^{-\alpha_\kappa f - \beta_\kappa y}.e^{-i\kappa x}$$

(A27)

#3

$$\int_o^{\infty} \frac{(2\xi^2 - k^2)^2}{F(\zeta)}\, e^{-\alpha(y+f)} \cos\zeta x\, d\zeta = 2\int_o^{\infty} \frac{(2\eta^2 + k^2)^2}{F_o^{\infty}(\eta)}\, e^{-\eta x}.\sin[\bar{\bar{\alpha}}(y+f)]d\eta$$

$$-2i\int_0^h \frac{(2\xi^2-k^2)^2}{F_o^h(\xi)} e^{-i\xi x}\sin[\overline{\alpha}(y+f)]d\xi + i\int_h^k \frac{(2\xi^2-k^2)^2\cdot 4\xi^2\cdot\alpha\cdot\overline{\beta}e^{-\alpha(y+f)}}{F_h^k(\xi)} e^{-i\xi x}\, d\xi$$

$$-\pi i \frac{(2\kappa^2-k^2)^2\, e^{-\alpha_\kappa(y+f)}}{F'(\kappa)} e^{-i\kappa x} \qquad \text{(A28)}$$

#4

$$\int_0^\infty \frac{\zeta^2(2\zeta^2-k^2)}{F(\zeta)} e^{-\alpha f-\beta y}\cos\zeta x\, d\zeta = 2\int_0^\infty \frac{\eta^2(2\eta^2+k^2)e^{-\eta x}\sin(\overline{\overline{\alpha}}f+\overline{\overline{\beta}}y)}{F_o^\infty(\eta)}\, d\eta$$

$$-2i\int_0^h \frac{\xi^2(2\xi^2-k^2)}{F_o^h(\xi)} e^{-i\xi x}\cdot\sin(\overline{\alpha}f+\overline{\beta}y)d\xi - i\int_h^k \frac{\xi^2(2\xi^2-k^2)}{F_h^k(\xi)} e^{-\alpha f}\cdot e^{-i\xi x}\cdot$$

$$[(2\xi^2-k^2)^2\sin\overline{\beta}y - 4\xi^2\alpha\overline{\beta}\cos\overline{\beta}y]d\xi - \pi i\frac{\kappa^2(2\kappa^2-k^2)}{F'(\kappa)} e^{-\alpha_\kappa f-\beta_\kappa y} e^{-i\kappa x}$$

(A29)

#5

$$\int_0^\infty \frac{\zeta^2\beta}{F(\zeta)} e^{-\alpha(f+y)}(k^2+2\alpha^2)\cos\zeta x\, d\zeta = 2\int_0^\infty \frac{\eta^2\overline{\overline{\beta}}[k^2-2(\eta^2+h^2)]}{F_o^\infty(\eta)}\cos[\overline{\overline{\alpha}}(y+f)]e^{-\eta x}\, d\eta$$

$$+2i\int_0^h \frac{\xi^2\overline{\beta}[k^2+2(\xi^2-h^2)]}{F_o^h(\xi)}\cos[\overline{\alpha}(f+y)]e^{-i\xi x}d\xi + i\int_h^k \frac{\xi^2(2\xi^2-k^2)^2\overline{\beta}[k^2+2(\xi^2-h^2)]}{F_h^k(\xi)}$$

$$\cdot e^{-\alpha(f+y)} e^{-i\xi x}d\xi$$

$$-\pi i \frac{\kappa^2\beta_\kappa e^{-\alpha_\kappa(f+y)}\cdot[k^2+2(\kappa^2-h^2)]}{F'(\kappa)} e^{-i\kappa x} \qquad \text{(A30)}$$

#6

$$\int_0^\infty \frac{\zeta^2\beta(2\zeta^2-k^2)}{F(\zeta)} e^{-\alpha f-\beta y}\cos\zeta x\,d\zeta=-2\int_0^\infty \frac{\eta^2\bar{\bar{\beta}}(2\eta^2+k^2)}{F_o^\infty(\eta)}\cos(\bar{\bar{\alpha}}f+\bar{\bar{\beta}}y)e^{-\eta x}\,d\eta$$

$$+2i\int_0^h \frac{\xi^2\bar{\beta}(2\xi^2-k^2)\cos(\bar{\alpha}f+\bar{\beta}y)e^{-i\xi x}}{F_o^h(\xi)}\,d\xi$$

$$+i\int_n^k \frac{\xi^2\bar{\beta}(2\xi^2-k^2)e^{-\alpha f}}{F_h^k(\xi)}[(2\xi^2-k^2)^2\cos\bar{\beta}y+4\xi^2\alpha\bar{\beta}\sin\bar{\beta}y]e^{-i\xi x}\,d\xi$$

$$-\pi i\frac{\kappa^2\beta_\kappa(2\kappa^2-k^2)e^{-\alpha_\kappa f-\beta_\kappa y}}{F'(\kappa)}e^{-i\kappa x} \qquad (A31)$$

#7

$$\int_0^\infty \frac{\zeta(2\zeta^2-k^2)^2}{F(\zeta)} e^{-\alpha(y+f)}\sin\zeta x\,d\zeta = -2\int_0^\infty \frac{\eta(2\eta^2+k^2)^2e^{-\eta x}\sin\bar{\bar{\alpha}}(y+f)}{F_o^\infty(\eta)}d\eta$$

$$-2\int_0^h \frac{\xi(2\xi^2-k^2)^2e^{-i\xi x}}{F_o^h(\xi)}\sin\bar{\alpha}(y+f)\,d\xi+4\int_h^k \frac{\xi^3(2\xi^2-k^2)^2}{F_h^k(\xi)}e^{-\alpha(y+f)}\alpha\bar{\beta}\,e^{-i\xi x}\,d\xi$$

$$-\pi\frac{\kappa(2\kappa^2-k^2)^2e^{-\alpha_\kappa(y+f)}}{F'(\kappa)}e^{-i\kappa x} \qquad (A32)$$

#8

$$\int_0^\infty \frac{\zeta(2\zeta^2-k^2)^2}{F(\zeta)} e^{-\alpha f-\beta y}\sin\zeta x\,d\zeta =$$

$$=-2\int_0^\infty \frac{\eta(2\eta^2+k^2)^2e^{-\eta x}}{F_o^\infty(\eta)}\sin(\bar{\bar{\alpha}}f+\bar{\bar{\beta}}y)d\eta$$

$$-2\int_0^h \frac{\xi(2\xi^2 - k^2)^2\, e^{-i\xi x}}{F_o^h(\xi)} \sin(\bar{\alpha}f + \bar{\beta}y)d\xi$$

$$-\int_h^k \frac{\xi(2\xi^2 - k^2)^2}{F_h^k(\xi)} e^{-\alpha f} \cdot e^{-i\xi x}[(2\xi^2-k^2)^2\sin\bar{\beta}y - 4\xi^2\alpha\bar{\beta}\cos\bar{\beta}y]d\xi$$

$$-\pi \frac{\kappa(2\kappa^2 - k^2)^2}{F'(\kappa)} e^{-\alpha_\kappa f - \beta_\kappa y} e^{-i\kappa x} \qquad \text{(A33)}$$

#9

$$\int_0^\infty \frac{\zeta^2\beta(2\zeta^2 - k^2)}{F(\zeta)} e^{-\alpha(y + f)} \cos\zeta x d\zeta =$$

$$= -2\int_0^\infty \frac{\eta^2\bar{\bar{\beta}}(2\eta^2 + k^2)e^{-\eta x}}{F_o^\infty(\eta)} \cos\{\bar{\bar{\alpha}}(y + f)\}d\eta$$

$$+ 2i\int_0^h \frac{\xi^2\bar{\beta}(2\xi^2 - k^2)\, e^{-i\xi x}}{F_o^h(\xi)} \cos\{\bar{\alpha}(y + f)\}d\xi$$

$$+ i\int_h^k \frac{\xi^2\bar{\beta}(2\xi^2 - k^2)^3\, e^{-i\xi x}}{F_h^k(\xi)} e^{-\alpha(y + f)} d\xi$$

$$-\pi i \frac{\kappa^2\beta_\kappa(2\kappa^2 - k^2)}{F'(\kappa)} e^{-\alpha_\kappa(y + f)} \cdot e^{-i\kappa x} \qquad \text{(A34)}$$

#10

$$\int_0^\infty \frac{\zeta^2\beta(2\zeta^2 - k^2)}{F(\zeta)} e^{-\alpha f - \beta y} \cos\zeta x d\zeta =$$

$$= -2 \int_0^\infty \frac{\eta^2\bar{\bar{\beta}}(2\eta^2 + k^2)\, e^{-\eta x}}{F_o^\infty(\eta)} \cos\{\bar{\bar{\alpha}} f + \bar{\bar{\beta}} y\} d\eta$$

$$+ 2i \int_0^h \frac{\xi^2\bar{\beta}(2\xi^2 - k^2)\, e^{-i\xi x}}{F_o^h(\xi)} \cos\{\bar{\alpha} f + \bar{\beta} y\} d\xi$$

$$+ i \int_h^k \frac{\xi^2\bar{\beta}(2\xi^2 - k^2)\, e^{-\alpha f}\, e^{-i\xi x}}{F_h^k(\xi)} \{(2\xi^2 - k^2)^2 \cos\bar{\beta} y + 4\xi^2\alpha\bar{\beta}\sin\bar{\beta} y\} d\xi$$

$$-\pi i \frac{\kappa^2\beta_\kappa(2\kappa^2 - k^2)}{F'(\kappa)} e^{-\alpha_\kappa f - \beta_\kappa y} e^{-i\kappa x} \qquad \text{(A35)}$$

Introduction of integrals (A26 - A35) into (A13 - A17) allows numerical evaluation of the Green's functions for the longitudinal line source in the half space. Generalizations for the line source at an arbitrary point (x_s, y_s) can be easily achieved by replacing f with y_s and x by $\pm|x - x_s|$.

The Green's functions (A13 - A22) are in agreement with results derived differently by Wong (1979), however, he evaluated the improper integrals in quite different fashion than in this work.

EQUIVOLUMINAL LINE SOURCE FOR A HALF-SPACE

The half space $|x| < \infty$, $y \geq o$ is subjected to a shear line source at a point (o,f). By following the same procedure as in the case of a dilatational line source the wave potentials, which satisfy the stress free boundary conditions $\sigma_{yy}(x,o) = \sigma_{xy}(x,o) = 0$, are derived to be

$$\phi = \frac{-8i}{\pi} \int_0^\infty \frac{\zeta(2\zeta^2 - k^2)}{F(\zeta)} e^{-\alpha y - \beta f} \sin \zeta x d\zeta \tag{A36}$$

$$\psi = H_o^{(2)}(kr) + H_o^{(2)}(kr') - \frac{4i}{\pi} \int_0^\infty \frac{(2\zeta^2 - k^2)^2}{\beta F(\zeta)} e^{-\beta(y+f)} \cos \zeta x d\zeta$$

$$= H_o^{(2)}(kr) - H_o^{(2)}(kr') - \frac{16i}{\pi} \int_0^\infty \frac{\zeta^2 \alpha}{F(\zeta)} e^{-\beta(y+f)} \cos \zeta x d\zeta, \tag{A37}$$

where

$$\alpha^2 = \zeta^2 - h^2 \; ; \; \beta^2 = \zeta^2 - k^2 \; ; \; F(\zeta) = (2\zeta^2 - k^2)^2 - 4\zeta^2 \alpha\beta$$

$$r = \sqrt{x^2 + (y-f)^2} \quad , \quad r' = \sqrt{x^2 + (y+f)^2} \tag{A38}$$

Corresponding displacement and stress fields are calculated to be

$$u^\psi = \frac{-8i}{\pi} \int_0^\infty \frac{\zeta^2(2\zeta^2 - k^2)}{F(\zeta)} e^{-\alpha y - \beta f} \cos \zeta x d\zeta$$

$$- k\left[H_1^{(2)}(kr) \cdot \frac{y-f}{r} + H_1^{(2)}(kr') \frac{y+f}{r'}\right]$$

$$+ \frac{4i}{\pi} \int_0^\infty \frac{(2\zeta^2 - k^2)^2}{F(\zeta)} e^{-\beta(y+f)} \cos \zeta x d\zeta \; . \tag{A39}$$

$$v^\psi = \frac{8i}{\pi} \int_0^\infty \frac{\alpha\zeta(2\zeta^2 - k^2)}{F(\zeta)} e^{-\alpha y - \beta f} \sin \zeta x d\zeta$$

$$+ kx\left[\frac{H_1^{(2)}(kr)}{r} - \frac{H_1^{(2)}(kr')}{r'}\right] - \frac{16i}{\pi} \int_0^\infty \frac{\alpha\zeta^3}{F(\zeta)} e^{-\beta(y+f)} \sin \zeta x d\zeta \tag{A40}$$

$$\sigma_{xx}^{\psi}/\mu = \frac{8i}{\pi}\int_0^{\infty}\frac{\zeta(2\zeta^2-k^2)(k^2+2\alpha^2)}{F(\zeta)}e^{-\alpha y-\beta f}\sin\zeta x\,d\zeta$$

$$\frac{4kx(y-f)}{r^3}H_1^{(2)}(kr)-\frac{2k^2x(y-f)}{r^2}H_0^{2}(kr)$$

$$+\frac{4kx(y+f)}{r'^3}H_1^{(2)}(kr')-\frac{2k^2x(y+f)}{r'^2}H_0^{(2)}(kr')$$

$$-\frac{8i}{\pi}\int_0^{\infty}\frac{\xi(2\zeta^2-k^2)^2}{F(\zeta)}e^{-\beta(y+f)}\sin\zeta x\,d\zeta \qquad (A41)$$

$$\sigma_{xy}^{\psi}/\mu = \frac{16i}{\pi}\int_0^{\infty}\frac{\alpha\zeta^2(2\zeta^2-k^2)}{F(\zeta)}e^{-\alpha y-\beta f}\cos\zeta x\,d\zeta$$

$$+(1-\frac{2x^2}{r^2})\left[\frac{2k}{r}H_1^{(2)}(kr)-k^2H_0^{(2)}(kr)\right]$$

$$-(1-\frac{2x^2}{r'^2})\left[\frac{2k}{r'}H_1^{(2)}(kr')-k^2H_0^{(2)}(kr')\right]$$

$$-\frac{16i}{\pi}\int_0^{\infty}\frac{\alpha\zeta^2(2\zeta^2-k^2)}{F(\zeta)}e^{-\beta(y+f)}\cos\zeta x\,d\zeta. \qquad (A42)$$

$$\sigma_{yy}^{\psi}/\mu = -\frac{8i}{\pi}\int_0^{\infty}\frac{\zeta(2\zeta^2-k^2)^2}{F(\zeta)}e^{-\alpha y-\beta f}\sin\zeta x\,d\zeta$$

$$-\frac{4kx(y-f)}{r^3}H_1^{(2)}(kr)+\frac{2k^2x(y-f)}{r^2}H_0^{(2)}(kr)$$

$$-\frac{4kx(y+f)}{r'^3}H_1^{(2)}(kr')+\frac{2k^2x(y+f)}{r'^2}H_0^{(2)}(kr')$$

$$+\frac{8i}{\pi}\int_0^{\infty}\frac{\zeta(2\zeta^2-k^2)^2}{F(\zeta)}e^{-\beta(y+f)}\sin\zeta x\,d\zeta. \qquad (A43)$$

The improper integrals in (A39-A43) are evaluated by contour inte-

gration as indicated by (A23-24). The summary of integrals is presented as follows:

$$\alpha = \sqrt{\zeta^2 - h^2} \qquad \beta = \sqrt{\zeta^2 - k^2} \qquad F(\zeta) = (2\zeta^2 - k^2)^2 - 4\zeta^2\alpha\beta$$

$$\bar{\alpha} = \sqrt{h^2 - \xi^2} \qquad \bar{\beta} = \sqrt{k^2 - \xi^2} \qquad F_o^h(\xi) = (2\xi^2 - k^2)^2 + 4\xi^2\bar{\alpha}\,\bar{\beta}$$

$$\bar{\bar{\alpha}} = \sqrt{\eta^2 + h^2} \qquad \bar{\bar{\beta}} = \sqrt{\eta^2 + k^2} \qquad F_o^\infty(\eta) = (2\eta^2 + k^2)^2 - 4\eta^2\,\bar{\bar{\alpha}}\,\bar{\bar{\beta}}$$

$$\alpha_\kappa = \sqrt{\kappa^2 - h^2} \qquad \beta_\kappa = \sqrt{\kappa^2 - k^2} \qquad F_h^k(\xi) = (2\xi^2 - k^2)^4 + 16\xi^4\,\xi^2\bar{\beta}^2$$

#I

$$\int_o^\infty \frac{\zeta^2(2\zeta^2 - k^2)}{F(\zeta)} e^{-\alpha y - \beta f} \cos \zeta x\, d\zeta = 2\int_o^\infty \frac{\eta^2(2\eta^2 + k^2)}{F_o^\infty(\eta)} e^{-\eta x} \sin(\bar{\bar{\alpha}}y + \bar{\bar{\beta}}f)\, d\eta$$

$$-2i\int_o^h \frac{\xi^2(2\xi^2 - k^2)}{F_o^h(\xi)} e^{-i\xi x} \sin(\bar{\alpha}y + \bar{\beta}f)\, d\xi$$

$$+ i\int_h^k \frac{\xi^2(2\xi^2 - k^2)}{F_h^k(\xi)} e^{-\alpha y} e^{-i\xi x}[4\xi^2\alpha\bar{\beta}\cos\bar{\beta}f - (2\xi^2 - k^2)^2 \sin\bar{\beta}f]\, d\xi$$

$$-\pi i \frac{\kappa^2(2\kappa^2 - k^2)}{F'(\kappa)} e^{-\alpha_\kappa y - \beta_\kappa f} e^{-i\kappa x} \qquad \text{(A44)}$$

#II

$$\int_o^\infty \frac{(2\xi^2 - k^2)^2 e^{-\beta(y+f)}}{F(\zeta)} \cos \zeta x\, d\zeta = 2\int_o^\infty \frac{2\eta^2 + k^2)^2 e^{-\eta x}}{F_o^\infty(\eta)} \sin \bar{\bar{\beta}}(y+f)\, d\eta$$

$$-2i\int_o^h \frac{(2\xi^2 - k^2)^2}{F_o^h(\xi)} e^{-i\xi x} \sin\bar{\beta}(y+f)\, d\xi$$

$$+ i\int_h^k \frac{(2\xi^2 - k^2)^2}{F_h^k(\xi)} e^{-i\xi x}[4\xi^2\alpha\,\bar{\beta}\cos\bar{\beta}(y+f) - (2\xi^2 - k^2)^2 \sin\bar{\beta}(y+f)]\, d\xi$$

$$-\pi i \frac{(2\kappa^2 - k^2)^2 e^{-\beta_\kappa (y+f)}}{F'(\kappa)} e^{-i\kappa x} \tag{A55}$$

#III

$$\int_0^\infty \frac{\zeta\alpha(2\zeta^2 - k^2)}{F(\zeta)} e^{-\alpha y - \beta f} \sin\zeta x d\zeta = -2\int_0^\infty \frac{\eta\bar{\bar{\alpha}}(2\eta^2+k^2)e^{-\eta x}}{F_o^{\infty}(\eta)} \cos(\bar{\bar{\alpha}}y + \bar{\bar{\beta}}f)d\eta$$

$$+ 2\int_0^h \frac{\xi\bar{\alpha}(2\xi^2 - k^2) e^{-i\xi x}}{F_o^{h}(\xi)} \cos(\bar{\alpha}y + \bar{\beta}f)d\xi - \int_h^k \frac{\xi\alpha(2\xi^2-k^2) e^{-\alpha y} e^{-i\xi x}}{F_h^{k}(\xi)}$$

$$[(2\xi^2 - k^2)^2 \sin\bar{\beta}f - 4\xi^2\alpha\bar{\beta}\cos\bar{\beta}f]d\xi$$

$$-\pi \frac{\kappa\alpha_\kappa(2\kappa^2 - k^2)}{F'(\kappa)} e^{-\alpha_\kappa y - \beta_\kappa f} e^{-i\kappa x} \tag{A56}$$

#IV

$$\int_0^\infty \frac{\alpha\zeta^3 e^{-\beta(y+f)}}{F(\zeta)} \sin\zeta x d\zeta = -2\int_0^\infty \frac{\eta^3\bar{\bar{\alpha}} e^{-\eta x}}{F_o^{\infty}(\eta)} \cos\bar{\bar{\beta}}(y+f)d\eta$$

$$+ 2\int_0^h \frac{\xi^3\bar{\alpha}\cos\bar{\beta}(y+f)e^{-i\xi x}}{F_o^{h}(\xi)} d\xi - \int_h^k \frac{\alpha\xi^3 e^{-i\xi x}}{F_h^{k}(\xi)}[(2\xi^2-k^2)^2\sin\bar{\beta}(y+f) - 4\xi^2\alpha\bar{\beta}\cos\bar{\beta}(y+f)d\xi]$$

$$-\pi \frac{\alpha_\kappa \kappa^3 e^{-\beta_\kappa (y+f)}}{F'(\kappa)} e^{-i\kappa x} \tag{A57}$$

#V

$$\int_0^\infty \frac{\zeta(2\zeta^2-k^2)(k^2+2\alpha^2)}{F(\zeta)} e^{-\alpha y - \beta f} \sin\zeta x d\zeta = 2\int_0^\infty \frac{\eta(2\eta^2+k^2)(k^2-2\bar{\bar{\alpha}}^2)}{F_o^{\infty}(\eta)} e^{-\eta x}\sin(\bar{\bar{\alpha}}y+\bar{\bar{\beta}}f)d\eta$$

$$-2\int_0^h \frac{\xi(2\xi^2-k^2)(k^2+2\alpha^2)}{F_o^{h}(\xi)} e^{-i\xi x}\sin(\bar{\alpha}y+\bar{\beta}f)d\xi + \int_h^k \frac{\xi(2\xi^2-k^2)(k^2+2\alpha^2)}{F_h^{k}(\xi)} e^{-\alpha y} e^{-i\xi x} \cdot$$

$$[4\xi^2\alpha\bar{\beta}\cos\bar{\beta}f - (2\xi^2-k^2)^2\sin\bar{\beta}f]d\xi$$

$$-\pi \frac{\kappa(2\kappa^2-k^2)(k^2+2\alpha_\kappa^2)}{F'(\kappa)} e^{-\alpha_\kappa y - \beta_\kappa f} e^{-i\kappa x}$$

#VI

$$\int_0^\infty \frac{\zeta(2\zeta^2-k^2)^2 e^{-\beta(y+f)}}{F(\zeta)} \sin\zeta x d\zeta = -2\int_0^\infty \frac{\eta(2\eta^2+k^2)^2 e^{-\eta x}}{F_o^{\infty}(\eta)} \sin\bar{\bar{\beta}}(y+f)d\eta$$

$$-2\int_0^h \frac{\xi(2\xi^2-k^2)^2}{F_o^{h}(\xi)} e^{-i\xi x}\sin\bar{\beta}(y+f)d\xi + \int_h^k \frac{\xi(2\xi^2-k^2)^2 e^{-i\xi x}}{F_h^{k}(\xi)} [4\xi^2\alpha\bar{\beta}\cos\bar{\beta}(y+f) - (2\xi^2-k^2)^2 \sin\bar{\beta}(y+f)]d\xi$$

$$-\pi \frac{\kappa(2\kappa^2-k^2)^2 e^{-\beta_\kappa(y+f)} e^{-i\kappa x}}{F'(\kappa)}$$

#VII

$$\int_0^\infty \frac{\zeta^2\alpha(2\zeta^2-k^2)}{F(\zeta)} e^{-\alpha y - \beta f}\cos\zeta x d\zeta = -2\int_0^\infty \frac{\eta^2\bar{\bar{\alpha}}(2\eta^2+k^2)}{F_o^{\infty}(\eta)} e^{-\eta x}\cos(\bar{\bar{\alpha}}y+\bar{\bar{\beta}}f)d\eta$$

$$+2i\int_0^h \frac{\xi^2\bar{\alpha}(2\xi^2-k^2)\, e^{-i\xi x}}{F_o^{h}(\xi)} \cos(\bar{\alpha}y + \bar{\beta}f)d\xi + i\int_h^k \frac{\xi^2\alpha(2\xi^2-k^2)e^{-\alpha y} e^{-i\xi x}}{F_h^{k}(\xi)} [4\xi^2\alpha\bar{\beta}\cos\bar{\beta}f - (2\xi^2-k^2)^2\sin\bar{\beta}f]d\xi$$

$$-\pi i \frac{\kappa^2\alpha_\kappa(2\kappa^2-k^2)e^{-\alpha_\kappa y - \beta_\kappa f}}{F'(\kappa)} e^{-i\kappa x}$$

#VIII

$$\int_0^\infty \frac{\zeta^2\alpha(2\zeta^2-k^2)}{F(\zeta)} e^{-\beta(y+f)}\cos\zeta x d\zeta = -2\int_0^\infty \frac{\eta^2\bar{\bar{\alpha}}(2\eta^2+k^2)e^{-\eta x}\cos\bar{\bar{\beta}}(y+f)d\eta}{F_o^{\infty}(\eta)}$$

$$+2i\int_0^h \frac{\xi^2\bar{\alpha}(2\xi^2-k^2)e^{-i\xi x}}{F_o^{h}(\xi)} \cos\bar{\beta}(y+f)d\xi + i\int_h^k \frac{\xi^2\alpha(2\xi^2-k^2)e^{-i\xi x}}{F_h^{k}(\xi)} [4\xi^2\alpha\bar{\beta}\cos\bar{\beta}(y+f) - (2\xi^2-k^2)^2\sin\bar{\beta}(y+f)]d\xi$$

$$-\pi i \frac{\kappa^2 \alpha_\kappa (2\kappa^2 - k^2)}{F'(\kappa)} e^{-\beta_\kappa (y+f)} e^{-i\kappa x}$$

#IX

$$\int_0^\infty \frac{\zeta(2\zeta^2-k^2)^2}{F(\zeta)} e^{-\alpha y - \beta f} \sin\zeta x d\zeta = -2\int_0^\infty \frac{\eta(2\eta^2+k^2)^2 e^{-\eta x}}{F_o^{\infty}(\eta)} \sin(\bar{\bar{\alpha}} y + \bar{\bar{\beta}} f) d\eta$$

$$-2\int_0^h \frac{\xi(2\xi^2-k^2)^2}{F_o^{h}(\xi)} e^{-i\xi x} \sin(\bar{\alpha} y + \bar{\beta} f) d\xi + \int_h^k \frac{\xi(2\xi^2-k^2)^2 e^{-\alpha y} e^{-i\xi x}}{F_h^{k}(\xi)} [4\xi^2 \alpha\bar{\beta} \cos \bar{\beta} f$$

$$-(2\xi^2-k^2)^2 \sin\bar{\beta} f] d\xi$$

$$-\pi \frac{\kappa(2\kappa^2-k^2)^2}{F'(\kappa)} e^{-\alpha_\kappa y - \beta_\kappa f} e^{-i\kappa x}$$

#X

$$\int_0^\infty \frac{\zeta(2\zeta^2-k^2)^2}{F(\zeta)} e^{-\beta(y+f)} \sin\zeta x d\zeta = -2\int_0^\infty \frac{\eta(2\eta^2+k^2)^2 e^{-\eta x}}{F_o^{\infty}(\eta)} \sin \bar{\bar{\beta}} (y+f) d\eta$$

$$-2\int_0^h \frac{\xi(2\xi^2-k^2)^2}{F_o^{h}(\xi)} e^{-i\xi x} \sin\bar{\beta}(y+f) d\xi + \int_h^k \frac{\xi(2\xi^2-k^2)^2 e^{-i\xi x}}{F_h^{k}(\xi)} [4\xi^2 \alpha\bar{\beta} \cos\bar{\beta} (y+f)$$

$$-(2\xi^2-k^2)^2 \sin\bar{\beta} (y+f)] d\xi$$

$$-\pi \frac{\kappa(2\kappa^2-k^2)^2 e^{-\beta_\kappa (y+f)}}{F'(\kappa)} e^{-i\kappa x}$$

APPENDIX B

For the sake of completeness the free field results are summarized next.

Incident Plane Longitudinal Wave

For incident P-wave geometry of the problem is depicted by Fig. B1 . Incident and reflected waves are calculated to be (Achenbach, 1973)

$$\phi^i = A_o\, e^{-i[h(x\sin\theta_o - y\cos\theta_o) - \omega t]} \tag{B1}$$

$$\phi^r = A_1\, e^{-i[h(x\sin\theta_o + y\cos\theta_o) - \omega t]} \tag{B2}$$

$$\psi^r = A_2\, e^{-i[k(x\sin\theta_2 + y\cos\theta_2) - \omega t]}\ , \tag{B3}$$

where

$$\sin\theta_2 = \frac{h}{k}\sin\theta_o. \tag{B4}$$

By scaling $A_o = \frac{i}{h}|P|$ the amplitudes of reflected field are evaluated to be

$$A_1 = \frac{\Delta_1}{\Delta} A_o \qquad A_2 = \frac{\Delta_2}{\Delta} A_o\ , \tag{B5}$$

where

$$\begin{aligned}
\Delta_1 &= -(2h^2\sin^2\theta_o - k^2)^2 + 4h^4\sin^3\theta_o\cos\theta_o \\
\Delta_2 &= -2h^2\sin 2\theta_o(2h^2\sin^2\theta_o - k^2) \\
\Delta &= (2h^2\sin^2\theta_o - k^2)^2 + 4h^4\sin^3\theta_o\cos\theta_o.
\end{aligned} \tag{B6}$$

Consequently, the free field is calculated to be

$$\phi^{ff} = \phi^i + \phi^r \tag{B7}$$

$$\psi^{ff} = \psi^{r} \tag{B8}$$

$$u^{ff} = -ih\sin\theta_o\{\phi^i(x,y) + \phi^r(x,y) + c\tan\theta_2\ \psi^r(x,y)\} \tag{B9}$$

$$v^{ff} = -ih\cos\theta_o\{\phi^i(x,y) - \phi^r(x,y) + ih\sin\theta_o\ \psi^r(x,y)\} \tag{B10}$$

$$\sigma^{ff}_{xx}/\mu = (2h^2\cos^2\theta_o - k^2)[\phi^i(x,y) + \phi^r(x,y)] - 2h^2\sin^2\theta_o c\tan\theta_2\ \psi^r(x,y) \tag{B11}$$

$$\sigma^{ff}_{xy}/\mu = h^2\sin 2\theta_o[\phi^i(x,y) + \phi^r(x,y)] + (2h^2\sin^2\theta_o - k^2)\ \psi^r(x,y) \tag{B12}$$

$$\sigma^{ff}_{yy}/\mu = (2h^2\sin^2\theta_o - k^2)\ [\phi^i(x,y) + \phi^r(x,y)] + 2h^2\sin^2\theta_o c\tan\theta_2\ \psi^r(x,y) \tag{B13}$$

Free Field for Incident Plane SV Wave

For incident plane SV-wave the geometry of the problem is depicted by Fig. B2. Incident and reflected waves are given by (Achenbach, 1973)

$$\psi^i = A_0\ e^{-i[k(x\sin\theta_o - y\cos\theta_o) - \omega t]} \tag{B14}$$

$$\phi^r = A_1\ e^{-i[h(x\sin\theta_1 + y\cos\theta_1) - \omega t]} \tag{B15}$$

$$\psi^r = A_2\ e^{-i[k(x\sin\theta_o + y\cos\theta_o) - \omega t]}, \tag{B16}$$

where

$$\sin\theta_1 = \frac{k}{h}\sin\theta_o \tag{B17}$$

$$A_1 = \frac{\Delta_1}{\Delta} A_o \qquad A_2 = \frac{\Delta_2}{\Delta} A_o\ , \quad A_0 = -\ i|S|/k \tag{B18}$$

$$\Delta_1 = 4k^4 \sin\theta_0 \cos\theta_0 \, (2\sin^2\theta_0 - 1)$$

$$\Delta_2 = k^4[4\sin^3\theta_0 \cos\theta_0 \, \tan\theta_1 - (2\sin^2\theta_0 - 1)^2] \tag{B19}$$

$$\Delta = k^4[4\sin^3\theta_0 \cos\theta_0 \, \tan\theta_1 + (2\sin^2\theta_0 - 1)^2].$$

Therefore, the free field is evaluated to be

$$\phi^{ff} = \phi^r \tag{B20}$$

$$\psi^{ff} = \psi^i + \psi^r \tag{B21}$$

$$u^{ff} = ik[-\sin\theta_0 \phi^r + \cos\theta_0(\psi^i - \psi^r)] \tag{B22}$$

$$v^{ff} = ik\sin\theta_0[-\tan\theta_1 \phi^r + \psi^i + \psi^r)] \tag{B23}$$

$$\sigma_{xx}^{ff}/\mu = k^2[(2\sin^2\theta_0 \, \tan^2\theta_1 - 1)\phi^r + 2\sin\theta_0\cos\theta_0(\psi^i - \psi^r)] \tag{B24}$$

$$\sigma_{xy}^{ff}/\mu = k^2[-2\sin^2\theta_0 \cdot \tan\theta_1 \phi^r + (2\sin^2\theta_0 - 1)(\psi^i + \psi^r)] \tag{B25}$$

$$\sigma_{yy}^{ff}/\mu = k^2[(2\sin^2\theta_0 - 1)\phi^r - 2\sin\theta_0\cos\theta_0 \, (\psi^i - \psi^r)]. \tag{B26}$$

Throughout the derivation the following relations between the wave potentials and stress field have been used

$$\sigma_{xx}/\mu = -k^2\phi - 2\frac{\partial^2\phi}{\partial y^2} + 2\frac{\partial^2\psi}{\partial x \partial y}$$

$$\sigma_{xy}/\mu = 2\frac{\partial^2\phi}{\partial x \partial y} - k^2\psi - 2\frac{\partial^2\psi}{\partial x^2} \tag{B27}$$

$$\sigma_{yy}/\mu = -k^2\phi - 2\frac{\partial^2\phi}{\partial x^2} - 2\frac{\partial^2\psi}{\partial x \partial y} \quad .$$

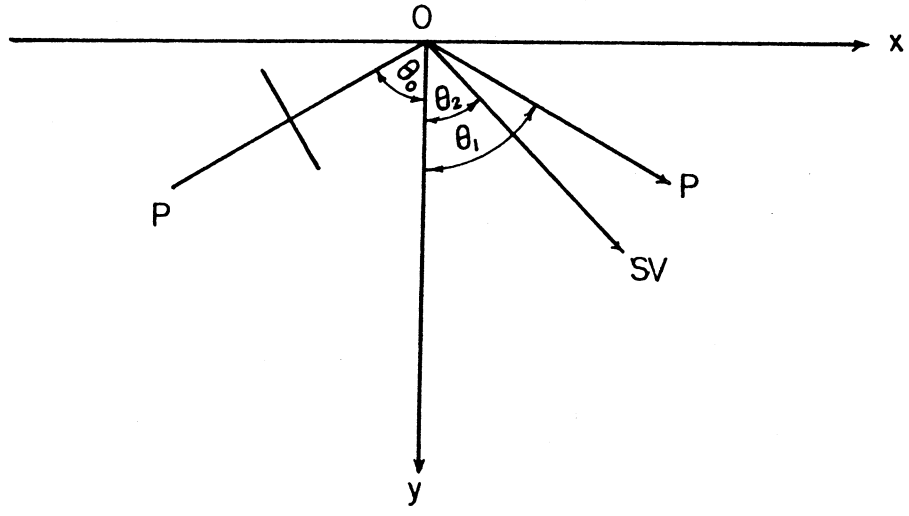

Fig. B1 Reflection of a Plane P-Wave at the Surface of a Half-Space.

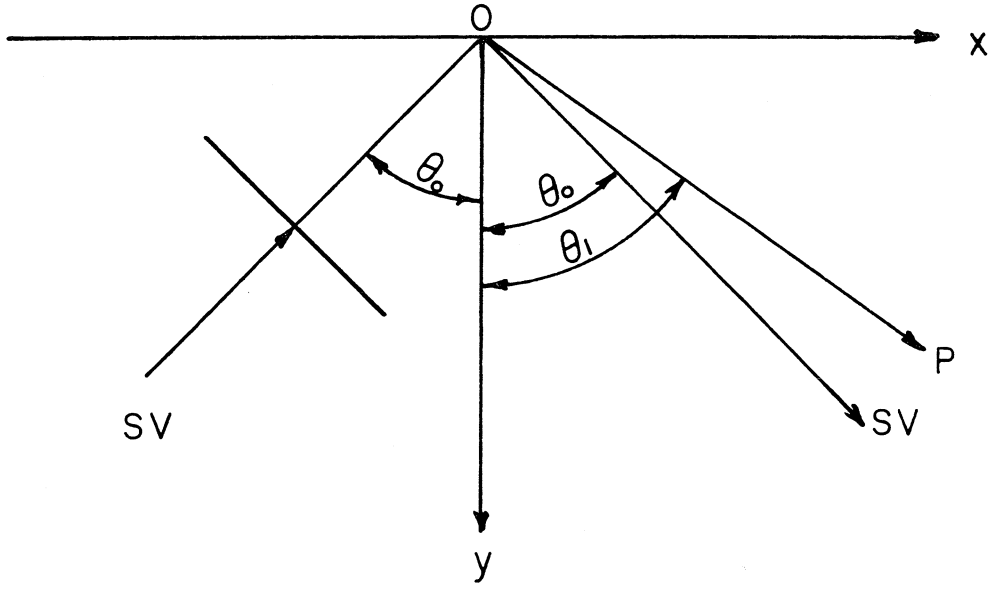

Fig. B2 Reflection of a Plane SV-Wave at the Surface of a Half-Space.

FREE FIELD FOR RAYLEIGH WAVES

For the Rayleigh waves in the half space $|x| < \infty$, $y \geq 0$ the displacement and the stress fields are derived to be (Achenbach, 1973)

$$u^{ff} = A\, e^{-i\kappa(x-ct)}\left[e^{-b_L y} - \frac{1}{2}\left(2 - \frac{c^2}{c_T^2}\right) e^{-b_T y}\right] \tag{B28}$$

$$v^{ff} = i\kappa A e^{-i\kappa(x-ct)}\left[-\frac{b_L}{\kappa^2}\, e^{-b_L y} + \frac{1}{2b_T}\left(2 - \frac{c^2}{c_T^2}\right) e^{-b_T y}\right] \tag{B29}$$

$$\sigma_{xx}^{ff}/\mu = i\kappa A e^{-i\kappa(x-ct)}\left\{\left[-\left(2 + \frac{c^2}{c_T^2}\right) + 2\frac{c^2}{c_L^2}\right] e^{-b_L y} + \left(2 - \frac{c^2}{c_T^2}\right) e^{-b_T y}\right\} \tag{B30}$$

$$\sigma_{xy}^{ff}/\mu = A\, e^{-i\kappa(x-ct)}\left[-2b_L\, e^{-b_L y} + \frac{\kappa^2\left(2 - \frac{c^2}{c_T^2}\right)^2}{2b_T} e^{-b_T y}\right] \tag{B31}$$

$$\sigma_{yy}^{ff}/\mu = i\kappa A\, e^{-i\kappa(x-ct)}\left(2 - \frac{c^2}{c_T^2}\right)\left(e^{-b_L y} - e^{-b_T y}\right) \quad , \tag{B32}$$

where

$$b_L = \kappa\left(1 - \frac{c^2}{c_L^2}\right)^{\frac{1}{2}} \; ; \qquad b_T = \kappa\left(1 - \frac{c^2}{c_T^2}\right)^{\frac{1}{2}} \quad . \tag{B33}$$

The velocity of the Rayleigh waves c satisfies the equation

$$\left(2 - \frac{c^2}{c_T^2}\right)^2 = 4\left(1 - \frac{c^2}{c_T^2}\right)^{\frac{1}{2}}\left(1 - \frac{c^2}{c_L^2}\right)^{\frac{1}{2}} \tag{B34}$$

Throughout the Appendices c_L and c_T denotes the velocity of dilatational and equivoluminal waves respectively. (In the main body of the paper the velocity of dilatational and potential waves is denoted by α and β respectively).